Department of Hydrology

Albert-Ludwigs-Universität Freiburg i. Br.

Master thesis

# Spatially heterogeneous water distribution within an agrivoltaic system and its significance for winter wheat

1st Examiner: apl. Prof. Dr. Jens Lange (University of Freiburg)

2nd Examiner: Jun.-Prof. Dr. Andreas Schweiger (University of Hohenheim)

Research supervisor: Prof. Dr. rer. nat. Ulrike Feistel (HTW Dresden)

Agnes Katharina Wilke (4950096)

Freiburg i. Br., October 2022

## Acknowledgement

This research was conducted in collaboration with the Fraunhofer Institute for Solar Energy Systems (ISE) in Freiburg, Germany.

# Contents

## List of Figures

## List of Tables

## Extended summary

Agrivoltaics combines agriculture and photovoltaics within the same area. It contributes to climate change mitigation and to climate adaption in agriculture by producing renewable energy and simultaneously protecting the crops with a modified microclimate. Crops were found to be exposed to heterogeneous abiotic conditions. The changes in microclimate and crop growth are due to the shading and shielding by the solar panels. Influencing factors are still not well enough understood to confidently pick suitable crops. Main attention has been given to the impact of light availability, while associated modified water fluxes still pose an unknown. To predict the crop growth in agrivoltaic systems (AV) however, the soil-plant-water continuum in an artificial setting requires further investigations. Especially the potential benefit in times of water deficit demands a differentiated inspection of the effect on the water status of the arable soil and cultivated plants during the growing season.

In this light, the AV with a clear height in Heggelbach, Baden-Wurttemberg (Germany), is analysed regarding its interception and throughfall of precipitation as drivers for heterogeneities illustrated by precipitation events during the growing season 2022. The plant water status of the cultivated winter wheat is derived from the soil water status and determined by the leaf water potential. Monitoring stretches from tillering to the end of grain filling.

At the AV in Heggelbach, the degree of heterogeneity in throughfall varies considerably and is related to the wind coming from the South and the interception depth. The area under a dripping edge of a solar panel shows a significant different volumetric water content in 30 - 60 cm soil depth compared to sheltered areas underneath solar panels. The differences in midday leaf water potential are higher within the AV than the difference between the agrivoltaic and the reference system. During the growing season in 2022, no water deficit stress was observed that affected the winter wheat during a crucial development stage.

Plant responses such as in the leaf water potential, the stomatal conductance or the root development reflect best the abiotic changes in an AV. A shift away from focusing on the microclimate and final yield towards plant processes and adaptions could support a better understanding of significant heterogeneities for certain crops. However, high spatial and temporal resolutions ideally on crop stand, plant, and leaf levels would be necessary to support models in capturing temporal lags in the water balance with the aim to provide a differentiated prediction on plant development more accurately.

**Keywords**: agrivoltaics, leaf water potential, soil water status, spatial heterogeneity, winter wheat, climate adaption, water deficit stress

## Zusammenfassung

Agri-Photovoltaik (Agri-PV) kombiniert Landwirtschaft und Photovoltaik (PV) auf derselben Fläche. Agri-PV trägt zum Klimaschutz und zur Klimaanpassung in der Landwirtschaft bei, indem sie erneuerbare Energie erzeugt, Kulturpflanzen schützt und das Mikroklima verändert. Es hat sich gezeigt, dass Kulturen in Agri-PV-Systemen heterogenen, abiotischen Bedingungen ausgesetzt sind. Veränderungen des Mikroklimas und des Pflanzenwachstums, sind auf die Beschattung und Abschirmung durch die PV-Module zurückzuführen. Die Einflussfaktoren sind noch nicht gut genug erforscht, um zuverlässig geeignete Kulturen für Agri-PV-Anlagen auszuwählen. Bisher lag der Fokus der Forschung auf der Lichtverfügbarkeit und nicht auf der Wasserverfügbarkeit. Zur Vorhersage des Pflanzenwachstums in Agri-PV-Systemen bedarf es weiterer Untersuchungen des Boden-Pflanze-Wasser-Kontinuums. Insbesondere der potenzielle Nutzen in Wassermangelzeiten erfordert eine differenzierte Betrachtung der Veränderungen im Wasserhaushalt des Ackerbodens und der Kulturpflanzen während der Vegetationsperiode.

Vor diesem Hintergrund wird die hoch aufgeständerte Agri-PV-Anlage in Heggelbach, Baden-Württemberg (Deutschland), hinsichtlich ihrer Interzeption und ihres Durchlasses von Niederschlägen anhand von mehreren Niederschlagsereignissen während der Vegetationsperiode 2022 analysiert. Dabei werden die potenziellen Ursachen für auftretende räumliche Heterogenität bewertet. Der Pflanzenwasserstatus des angebauten Winterweizens wird aus dem Bodenwasserstatus abgeleitet und mithilfe des Blattwasserpotenzials bestimmt. Das Monitoring erstreckt sich von der Bestockung bis zum Ende der Kornfüllung.

In der Agri-PV-Anlage in Heggelbach variiert der Durchlass vom Niederschlag stark und hängt mit dem Südwind und der Interzeption zusammen. Der Bereich unter der Abtropfkante eines PV-Moduls weist in 30 bis 60 cm Bodentiefe einen signifikant höheren volumetrischen Wassergehalt auf als die geschützten Bereiche unter den Modulen. Die Unterschiede im mittäglichen Blattwasserpotenzial sind innerhalb des Agri-PV-Systems höher als der Unterschied zur Referenzfläche. Es wurde kein Trockenstress beobachtet, der den Winterweizen in einem entscheidenden Entwicklungsstadium beeinträchtigt hätte.

Pflanzenreaktionen wie das Wasserpotenzial der Blätter, die stomatäre Leitfähigkeit oder die Wurzelentwicklung spiegeln am besten die abiotischen Veränderungen in einer Agi-PV-Anlage wider. Eine Verlagerung des Fokus von Mikroklima und finalem Ernteertrag hin zu pflanzlichen Anpassungsprozessen könnte zu einem besseren Verständnis der heterogenen Umweltbedingungen und ihre Auswirkungen auf bestimmte Kulturpflanzen beitragen. Um

Modelle besser bei der Erfassung von Verzögerungen im Wasserhaushalt in einer Agri-PV-Anlage zu unterstützen und die Pflanzenentwicklung differenzierter vorherzusagen, ist eine hohe räumliche und zeitliche Auflösung, idealerweise auf Flächen-, Pflanzen- und Blattebene, notwendig.

**Stichworte:** Agri-Photovoltaik, Blattwasserpotenzial, Bodenwasserstatus, räumliche Heterogenität, Winterweizen, Klimaanpassung, Trockenstress

# 1. Introduction

Agrivoltaic systems, enable the simultaneous production of food and energy on the same land area (Dupraz et al., 2011; Beck et al., 2012). The solar panels of elevated agrivoltaic systems shade (and may protect) the agricultural crops below, and thus alter the microclimate and associated environmental conditions for growth, such as increased soil moisture, decreased soil temperature and evapotranspiration (Marrou et al., 2013a; Armstrong et al., 2016; Barron-Gafford et al., 2019). In a world where agriculture is facing newly arising challenges as consequences of the rapid changes in climate, agrivoltaics could be a measure of climate adaption. In times of more frequently occurring extremes such as intense droughts, it could stabilise yield and play a role in securing our food (Beck et al., 2012; Marrou et al., 2013a; Armstrong et al., 2016; Elamri et al., 2018b; Amaducci et al., 2018; Barron-Gafford et al., 2019; Weselek et al., 2021a; Trommsdorff et al., 2021; IPCC, 2022). Simultaneously, it could be one measure of climate change mitigation by fostering the energy transition to renewables (Beck et al., 2012; Barron-Gafford et al., 2019; IPCC, 2022).

The agrivoltaic pilot system in Heggelbach (Baden-Wurttemberg, Germany), which is the here studied facility, with a capacity of 194.4 kW, demonstrated the positive effects of shading on the agricultural yield in the drought year 2018 (Trommsdorff et al., 2021; Weselek et al., 2021b). One reason could be the reduction of evapotranspiration losses due to shading within the system and hence a more reliable and, in comparison to the reference system higher crop productivity in dry periods. In rather wet years, crop production was reduced within the system (Marrou et al., 2013a; Amaducci et al., 2018; Elamri et al., 2018a; Weselek et al., 2021b; Weselek et al., 2021a). Additionally, the farmers cultivating in the mentioned agrivoltaic system, have raised concerns about the effect solar panels possibly have on the rainfed crops within the system.

## 1.1 Agrivoltaics

A review by Hernandez et al. (2014) considers conventional photovoltaics (PV) as a mitigating measure against climate change but looks at both reported positive and negative large-scale effects large solar parks may have on the environment; ecology, water and land use. They list “changes in microclimate and local hydrology” as a potential effect to be considered. In their review, the combined use of PV and agriculture is briefly mentioned as a niche that comes with co-benefits to land management and existing socioeconomic conflicts while meeting food and energy demands. Recently, Mamun et al. (2022) published a review that addresses agrivoltaics and its multi-facetted research efforts worldwide. If agrivoltaics was to be applied as an adaptive and mitigating solution in agriculture to climate change, it raises the crucial questions of how the combination would affect crops and which crops would be suitable (Hernandez et al., 2014; Armstrong et al., 2016; Wang et al., 2018).

### 1.1.1 Implications for the microclimate and crop development

The impact and relation of conventional ground-mounted solar parks on the microclimate and present vegetation has been investigated in several studies (Hernandez et al., 2014; Armstrong et al., 2016; Hassanpour Adeh et al., 2018). In these studies, it is distinguished between areas that are fully under the solar panel, partially under panels, and between panels in reference to the shade imposed by them. Changes in the microclimate due to shading are to be expected in air temperature, ground temperature, soil moisture, relative humidity, vapour pressure deficit, incident radiation and wind (Marrou et al., 2013b). The comparison of the microclimates between the defined areas, showed significant differences in mean relative humidity, wind speed, air temperature, vapour pressure deficit and radiation on a spatial scale (Armstrong et al., 2016; Hassanpour Adeh et al., 2018).

Similar effects on the microclimate specifically caused by agrivoltaics have been previously investigated, however more and user-related attention is required. Significant changes in meteorological conditions play an exceptional role for agricultural crops since they set the growth conditions for the cultivated plants (Dupraz et al., 2011; Armstrong et al., 2016, 2016; Weselek et al., 2019; Weselek et al., 2021a). Plant growth depends on abiotic factors such as light availability, temperature, water availability, and atmospheric water demand. Adding an agrivoltaic system changes the environmental conditions and thus the plants' growth rate (Wang et al., 2018). As agriculture seeks for optimal growth conditions, those changes can be of high relevance to agricultural crops (Hernandez et al., 2014; Armstrong et al., 2016, 2016; Trommsdorff et al., 2021). If well enough understood, they can be actively applied on a small scale to modify changing environmental conditions due to climate change to the benefit of the crops (Dupraz et al., 2011; Hernandez et al., 2014; Hassanpour Adeh et al., 2018). For example, Elamri et al. (2018a) observed a delay in ripening and thus harvest. A delay could potentially be harnessed as a crop management system, adapting to shifting seasonal patterns due to climate change (Elamri et al., 2018a; Barron-Gafford et al., 2019).

While agrivoltaics may act as an adaptive and mitigating measure in agriculture against climate change, but the altered microclimate also poses new challenges in the production of crops. Not only is the microclimate changed in comparison to an open field, but the solar panels cause spatially heterogeneous microclimatic changes at field level within the system. As a result, phenological development, and thus quality and quantity of crops could possibly differ between agrivoltaic and purely agricultural areas, as well as within the agrivoltaic system itself (Dupraz et al., 2011; Marrou et al., 2013a).

Most attention has been given to the reduced and fluctuating light availability since it is considered the main crop growth limiting factor at higher latitudes (Dupraz et al., 2011; Weselek et al., 2021a). Expected changes in the crop plant development would be represented in the crop growth rate, leaf area index (LAI) of the crop, nutrient content, chlorophyll content, nutritional value, and radiation interception efficiency (Beck et al., 2012; Trommsdorff et al., 2021).

So far, much effort has been put into the modelling of the change in light availability and spatial distribution on different temporal scales in order to predict crop growth within an agrivoltaic system. However, all studies to date lack further validation (Dupraz et al., 2011; Beck et al., 2012; Dinesh and Pearce, 2016; Armstrong et al., 2016; Chopard et al., 2021; Trommsdorff et al., 2021). Among these studies, Armstrong et al. (2016) focus on the impact of agrivoltaics on soil and air temperature on a diurnal and seasonal scale. From spring to autumn, soil temperature was lower under the solar panels and air temperature was lower during the day and higher at night. Daily minimum and maximum air temperatures were less extreme than at the control site. On a temporal scale, no significant difference was found in the daily average of air temperature, vapour pressure deficit, and absolute humidity. Marrou et al. (2013b) reported concurring results. Dupraz et al. (2011), who simulated relative global radiation and relative photosynthetically active radiation (%PAR) under solar panels, encourage in their conclusion to investigate the role of other microclimatic changes such as precipitation distribution and wind components.

In their developed model for crop growth within an agrivoltaic system, Elamri et al. (2018a) accounted for the variable precipitation distribution by simulating stomatal conductance in lettuce grown in an agrivoltaic system. They used stomatal conductance as proxy for water stress in response to the heterogeneous and reduced radiation (Elamri et al., 2018a; Elamri et al., 2018b). Fluctuating radiation can cause heterogeneity in soil moisture losses and in water availability for the crops. The combination of spatial and temporal heterogenous light and water availability could yield an undesired heterogeneous and or reduced biomass production. The extent to which that could happen, depends on location, agrivoltaic system, and vegetation or crop (Dupraz et al., 2011; Hassanpour Adeh et al., 2018).

### 1.1.2 Suitable crops and the placement of winter wheat

Researchers have given several recommendations as to which crops are suitable or less suitable for cultivation in an agrivoltaic system. General statements addressing the impairment in light availability, such as summer crops were more suitable for the cultivation in agrivoltaic systems than winter crops or crops with low root density but high net photosynthetic rate would have good pre-requirements, were made (Seidlova et al., 2009; Dupraz et al., 2011; Hassanpour Adeh et al., 2018). Rapid vegetative soil covering is also seen as an advantageous crop characteristic (Marrou et al., 2013a). Trommsdorff et al. (2021) have presented a categorisation of specific crops based on their shade tolerance as was suggested by Dupraz et al. (2011) and Beck et al. (2012). The assessment criterion was the simulated harvestable yield at up to 40 % light reduction. Three categories, 'plus', 'zero' and 'minus' group Germany's most common crops. However, Laub et al. (2022) did a more detailed meta regression, excluding studies based on simulations. With the aid of 58 experimental studies looking at the effect of different degrees of shading on the yield, 38 different crops, were classified based on their shade sensitivity over shade degrees.

In practice, after partially experiencing a detrimental effect on the of row crops in the agrivoltaic system in previous years, the farmer in Heggelbach decided to fully switch to grain crops in the agrivoltaic system in 2022. The reasoning behind it was the assumption that the dripping edge had negative effects on the row crops, especially in spring, when the bare soil might have been exposed to erosion under the dripping edge (Elamri et al., 2018b; Mamun et al., 2022). Figure 1 illustrates the impact. The higher risk of erosion could be reduced with grain crops (Fraunhofer Institute for Solar Energy Systems ISE, 2022).

Figure 1: Winter wheat in the agrivoltaic system in April 2022 (Photo by Anna Fath/University of Hohenheim)

Winter wheat (*Triticum aestivum* L.) has been assessed in its suitability as a grain crop within an agrivoltaic system in the context of the modified light availability. Several studies, mostly in the field of agroforestry, have found a positive correlation between light availability and wheat grain yield. They recognise the detrimental effect shading has on winter wheat, as it alters the functioning of chloroplasts, which consequently may reduce the net photosynthesis rate (Li et al., 2008; Li et al., 2010; Mu et al., 2010; Li et al., 2012; Yadav et al., 2018). In accordance, Beck et al. (2012) and Trommsdorff et al. (2021) have put winter wheat into the category 'minus', which means adverse effects predominate and a reduction in agricultural yield is to be expected. Indeed, Dupraz et al. (2011) simulated a wheat yield reduction of 19 % at a 57 % reduction in light availability but simultaneously derived that the light efficiency of wheat plants improved under the panels, supported by Marrou et al. (2013a). In contrast to the categories by Trommsdorff et al. (2021), Laub et al. (2022) classified $C_3$ cereals such as wheat as shade tolerant crops within agrivoltaic systems. However, the scope of their study did not allow them to consider the effect the interplay of shading and water availability could have on the crop.

### 1.1.3 Modified water balance in an artificial setting

The correlations between reduced radiation and both quantity and quality in harvest have been addressed in research (Sudmeyer and Speijers, 2007; Qiao et al., 2019). Of those studies, Sudmeyer and Speijers (2007) also studied the effects of intercepted rainfall on the growth of winter wheat plants and found it to be not sufficient of an explanatory variable. The impacts of an altered water regime on the yield of wheat, or crops in general, remains a triviality also in the research field of agrivoltaics. Most studies on spatial and temporal heterogeneity within agrivoltaic systems focus on the competition for the sun and illustrate this bias with the common attempt to zone the area based on the degree of intercepted light (Dupraz et al., 2011; Beck et al., 2012; Marrou et al., 2013b). Only few studies have addressed the microclimatic impacts in relation to the hydrological impacts of conventional ground-mounted photovoltaic systems, or for that matter the impacts of agrivoltaic systems on the cultivation due to altered water pathways, availability and distribution (Marrou et al., 2013a; Marrou et al., 2013b; Armstrong et al., 2016; Elamri et al., 2018a; Elamri et al., 2018b; Hassanpour Adeh et al., 2018). Elamri et al. (2018b) have stated that the heterogeneous distribution of precipitation is mainly driven by interception, which modifies its subsequent pathways. Interception is understood as the proportion of precipitation that is obstructed by a vegetative canopy and lost to evaporation. This concept can be transferred to the losses that arise due to the artificial construction of an agrivoltaic system that forms an impermeable roof (Levia and Germer, 2015; Elamri et al., 2018b). Throughfall is the proportion that is intercepted by the canopy but released for free fall, eventually dripping to the soil surface. (Jackson, 2000; Levia and Germer, 2015; Elamri et al., 2018b). In an agrivoltaic system a larger proportion of intercepted precipitation than in the traditional context, would fall from the tilted dripping edge off the panels as free throughfall. Stemflow is defined as the proportion of precipitation that is intercepted by the canopy and runs down along a plant's stem to the forest ground as a local water input. 'Stemflow' in an agrivoltaic system would run down the pillars of the sub-construction. The subdivision of precipitation into interception, stemflow and throughfall depends on the intercepting structure, meteorological circumstances, and the climate (Jackson, 2000; Guswa and Spence, 2012; Levia and Germer, 2015).

Within an agrivoltaic system throughfall may occur in form of driving rain, that is rain altering its vertical fall direction due to the influence of wind (Levia and Germer, 2015; Elamri et al., 2018b). When reaching the ground, the intercepted raindrops have a higher kinetic energy that may cause erosion and damage to young plants underneath the panels (Cook and McCuen, 2013; Elamri et al., 2018b). Erosion facilitated by the dripping edge of the agrivoltaic solar panels can be especially problematic at sloped agricultural fields and in the case of extreme events as they cause an increased surface runoff. Armstrong et al. (2016) and Weselek et al. (2021) observed the dripping edge resulting in higher water inputs under the panels. Elamri et al. (2017) suggested strategies to mitigate both the resulting risk for erosion and spatially heterogenous water input. In the case of spatial heterogeneity in soil moisture, Elamri et al. (2018a) and Armstrong et al. (2016) found it to be of limited significance as it is potentially made up for by a heterogeneous root system and lateral diffusion (Guswa and Spence, 2012). However, Hassanpour et al. (2018) found the soil water storage in areas under solar panels to be significantly higher than in the control area as the growing season progressed. Similarly, after irrigation Barron-Gafford et al. (2019) measured 15 % higher soil moisture levels in an agrivoltaic system than in a conventional agricultural system suggesting less evaporative losses. In both cases, ground-mounted solar panels were in use. Storage variations in soil were largest under the dripping edge where the highest throughfall, or effective rain was measured (Elamri et al., 2018a; Elamri et al., 2018b). Repeated heterogeneous patterns could promote more pronounced preferential flow patterns and undesired ponding (Elamri et al. 2018b). In this way, localised, concentrated and steady water inputs that would not exist in a conventional agricultural environment could create hot spots for percolation (Levia and Germer, 2015). Higher soil moisture values could be explained by overall lower evapotranspiration rates in the agrivoltaic system (Marrou et al., 2013a). However, Weselek et al. (2021) reported significantly lower levels of soil moisture in the agrivoltaic system in Heggelbach, which was unexpected and could not be further explained.

Evapotranspiration at an agricultural field depends on the crop, the degree of soil coverage with vegetation and meteorological circumstances such as the precipitation, solar irradiation, wind conditions, soil moisture, and the heat energy flux, which depend on the time of the year (Marrou et al., 2013a; Marrou et al., 2013b). The changes in evapotranspiration were best explained by a modified radiative balance in agrivoltaic systems, while the vapour pressure deficit and daily air temperature were not significantly different from the reference (Marrou et al., 2013b).

Marrou et al. (2013a) did a detailed statistical analysis of the changed water fluxes in an agrivoltaic system, considering different time periods of the vegetative year while also distinguishing between full shade, moderate shade, and full sun exposure. Significant and non-significant reductions of actual total evapotranspiration in full and moderate shade were found but were dependant on the crop and the season (Marrou et al., 2013a). This resulted from plants in shade conditions growing for an extended time under the conditions of PAR below saturating levels. The impact on the stomatal conductance led to decreased transpiration rates. At the same time, plants were less so exposed to higher levels of PAR than saturating levels. Due to the shifted time crops spend in light, a delayed induction time for photosynthesis activity is expected. This would lead to temporal lag effects in the water balance within the agrivoltaic system (Marrou et al., 2013a; Elamri et al., 2018a). The temporal and spatially heterogeneity and their interconnection are perceived as the greatest challenge in modelling affected crop growth in an agrivoltaic system. The altered stomatal conductance is perceived as key variable to improve modelling efforts, that generally still lacks validation, sensitivity, and uncertainty analysis. Also, a better understanding and inclusion of the soil water status in models would improve predictions made regarding surface runoff and ponding (Elamri et al., 2018a).

The change in evaporation in an agrivoltaic system was dependant on the vegetative soil coverage rate of the cultivated crop which determines possible evaporative losses through the bare soil. Overall, evaporation was more affected than transpiration in an agrivoltaic system (Zotarello et al.; Marrou et al., 2013a).
Marrou et al. (2013a) and Elamri et al. (2018a, 2018b) have so far been pioneers in the detailed research on the altered water distribution in an agrivoltaic system. However, both their research is within the context of irrigated agriculture, where the soil often is close to saturated. Stated water savings of 14 - 29 % due to reduced evaporative rates therefore do not necessarily hold true for rainfed agrivoltaic systems (Marrou et al., 2013a; Dinesh and Pearce, 2016).

### 1.1.4 Approaches to solve issues of heterogeneity

The technical design of the agrivoltaic structure plays a crucial role for approaches to solve the heterogeneity (Cook and McCuen, 2013; Marrou et al., 2013b; Armstrong et al., 2016; Elamri et al., 2018b). To begin with, agrivoltaic systems tend to have a Southeast (SE) and Southwest (SW) orientation instead of the conventional South (S) orientation. This addresses the issue of light heterogeneity (Beck et al., 2012). Where tracked solar panels are feasible, a temporal scheme of panel tilt could be adapted to the phenological light requirements of the crops. To account for the spatial heterogeneity in water fluxes, Elamri et al. (2018a, 2018b) also suggested a solar panel operation strategy that to some extent allows for mitigating variable throughfall. Their study used PV panels with adjustable tilt angles and found rain distribution to be most heterogeneous with flat panels (0° tilt angle) and least heterogeneous with panels either directly facing the wind or in the opposite direction. A time-variable tilt angle depending on wind direction was most effective at achieving a virtually uniform rainfall distribution (Elamri et al. 2017). In their model (see also 2.4.2), Elamri et al. (2017) also found the angle of rainfall incidence to be a key variable in the determination of rainfall distribution heterogeneity.

One way to prevent unexpected adverse impacts on crop growth due to heterogeneities, is modelling. While the fluctuating radiation within agrivoltaic systems can be modelled quite detailed over various temporal scales, the heterogeneity within an agrivoltaic system regarding water fluxes is not easily predictable. Modelled crop growth therefore tends to underestimate the influence of altered water fluxes. Observable variables that could support the simulations, are those that influence and describe the plant water availability within an agrivoltaic system (precipitation, soil moisture, runoff, drainage, water potential). The approach presented by Chopard et al. (2021) simulates daily predawn leaf water potential as the result of a modelled soil water balance. As plant-based indicator, it shall support agronomic decision making to optimise crop performance in agrivoltaic systems through controlling the degree of shading and irrigation. However, the novel model is constrained to a limited number of crops and requires validation.

## 1.2 Water stress in crops due to a water deficit

The soil's or plant's water status can define water stress in crops due to a water deficit, in the following referred to as water deficit stress (Lecoeur et al., 1992; Wery, 2005; Schopfer and Brennicke, 2010). A plants water status can be determined by measurements of either water contents or energy status of water in its cells (Turner, 1981). This includes the measurements of relative water content, and water, osmotic and turgor potentials, but also stomatal conductance and xylem (Lecoeur et al., 1992; Lecoeur et al., 1995). Soil water status is described similarly, with the aid of water potentials, or contents.

The use of soil water potential has its advantages when describing the edaphic water properties for a growing crop when compared to the relative water content. The difference in water potential in a segment of the soil-plant-atmosphere continuum (SPAC) controls the passive water transport from the soil, through the xylem tissue of plants, and into the atmosphere, as water follows the water potential gradient from a place of higher to lower potential levels (from less negative to more negative potentials) (Schopfer and Brennicke, 2010). In contrast, the relative soil water content, if not linked with the soil water retention characteristics, only describes the soil water state without immediate link to the plants. Given the known soil water retention characteristics, Passioura (1980) considered soil to be wet with a volumetric water content of $\theta > 0.2$. In winter wheat water stress can be induced at a soil moisture level of below

33 % of the field capacity (Plaut, 2005; Morgun et al., 2020). Unlike the water content, the significance of soil water potential for a plant is independent of soil texture characteristics influencing the soils capacity to retain water. Soil water potential has therefore been the preferred measure of soil water status in the context of water stress (Lecoeur et al., 1992; Lecoeur et al., 1995).

If observed in the rooting zone over time, soil water potential can be used to describe the soil drying process (Lecoeur et al., 1992). This is of particularly importance for agricultural purposes. In combination with the crops' growth stage, the soil water potential reveals when water stress occurs due to a water deficit, and as a consequence which plant processes will be affected (Wery, 2005; Marrou et al., 2013a). For example, Marrou et al. (2013a) defined the absence of water deficit stress for lettuce at a soil water potential less negative than - 0.02 MPa (≈ 2.3 pF) in 0.3 m soil depth. Lecoeur et al. (1992) studied chickpeas under different levels of water stress. Their control group was grown at a water potential of - 0.04 MPa (≈ 2.6 pF) in 0.3 m. They further distinguished moderate water stress by the speed the plants were exposed to a water deficit. On the one hand, moderate stress was defined for the flowering stage to be at - 0.06 MPa (≈ 2.8 pF). On the other hand, moderate water stress was induced by slowly drying the soil over the course of nine days to - 0.08 MPa (≈ 2.9 pF) (Lecoeur et al., 1992). In the case of winter wheat, Roohi et al. (2013) defined the water deficit stress to start at a soil water potential of - 1.2 MPa (≈ 4 pF).

Plant water potentials can also be used as a measure of water deficit stress in crops. Leaf water potential as a measure of water stress has been commonly used in a variety of settings (Lecoeur et al., 1992; Lecoeur et al., 1995; Schmidhalter, 1997; Donovan et al., 2001; Jiang et al., 2013). Thereby, it must be distinguished between measurements before sunrise and at midday.

Midday leaf water potential expresses the maximum water deficit stress during the day, which translates to the highest diurnal transpiration rate (Lecoeur et al., 1992). In contrast, predawn leaf water potential supposedly encompasses the lowest diurnal transpiration rate as the plant will have spent the maximum time in the dark with minimal stomatal activity. The gradient between predawn plant and soil water potential approximates zero at low transpiration rates, i.e., at very small water fluxes. Therefore, predawn leaf water potential of plants in wet soil has commonly been used as proxy for the soil water potential at the root zone which is dominated by the matric potential (Passioura, 1980). When the plant and its roots are at the predawn equilibrium with the soil, predawn leaf water potential represents not only plant water status but also soil water status (Donovan et al., 2001; Schopfer and Brennicke, 2010; Elamri et al., 2018a). However, this approximation within the soil-plant-atmosphere system becomes invalid at higher gradients when the soil has dried out. The relationship between the soil potential and the plant water potential is linear under wet soil conditions and becomes non-linear in dry circumstances (Passioura, 1980).

Predawn leaf water potential as a proxy for matric potential therefore always corresponds to the wettest root accessible soil. In spatially heterogenous soil moisture conditions, some roots may find themselves in dryer soil conditions, possibly causing an insufficient water supply to the plant overnight. This may lead to a predawn disequilibrium between the soil and the plant. In effect, the plant is experiencing more water stress and the predawn leaf water potential fails to reflect the soil water status and vice versa. However, to reach a predawn equilibrium, 20 % of the rooting volume growing in the wettest soil, could be enough. Additionally, discrepancies were found to be negligible for some crop species (Donovan et al., 2001).

The immediate response of a crop experiencing water stress involves the stomata. Stomatal conductance regulates the mechanism of transpiration. Water stress drives stomatal conductance insofar as it prompts the stomata to close when prevention of water loss is needed. The threshold value under which the stomata become responsive to water stress is species dependent and ranges from - 0.5 MPa to - 1.8 MPa. At the same time, diffusion of carbon dioxide into the plant is dependent on open stomata. Stomatal conductance is therefore coupled with the photosynthetic activity (Schopfer and Brennicke, 2010; Marrou et al., 2013a; Elamri et al., 2018a). Hence, water stress can impair crop processes responsible for biomass production (Wery, 2005). Water deficit stress at the permanent wilting point of a crop (typically pF 4.2) can cause the stomata to close with a delay, causing night transpiration and an additional loss of water (Schopfer and Brennicke, 2010). In the case of winter wheat, Jiang et al. (2013) found negative effects on the plant growth in response to a water deficit stress beginning at a plant water potential of - 1 MPa at predawn.

Depending on the growth stage of the crop during water stress, its observable response can be immediate, or one to two weeks delayed (Lecoeur et al., 1995). Generally, above-ground biomass is more impacted by water stress than yield (Wery, 2005). Through osmotic adjustments, entailing the active accumulation of ions in the cell vessels to reduce the plant water potential, affected plants can mitigate or postpone water loss through transpiration without impairing plant growth (Lecoeur et al., 1992). Osmoregulation induced by a controlled water deficit during tillering may even improve yield that is associated with a higher fertility of tillers (Lecoeur et al., 1992).

## 1.3 Development of winter wheat and their dependency on water availability

The sector of agriculture will face increasingly intense droughts in large regions of the world. Traditional staple food crops that are globally relevant and cultivated, such as common wheat (*Triticum aestivum* L.), play a critical role in the food security. The worldwide cultivation of common wheat, will have to adapt to an increasing demand due to population growth, and climate change challenges (Alghory and Yazar, 2019; Morgun et al., 2020).
Winter wheat, a $C_3$ plant belonging to the family of grasses, is the most important cereal in German agriculture and occupies an area of 2.9 million ha (Deutscher Bauernverband, 2022). The total water consumption of winter wheat throughout the life cycle is estimated to be between 430 mm and 470 mm (Zhang et al., 2003). Overall it uses 3.9 kg of water for the formation of 1 g of dry biomass (Schopfer and Brennicke, 2010). In more detail, the water requirements of winter wheat depend on the phenological development stage. That means, water, or the lack thereof, can have various effects on the development and yield, depending on the point in time (Zhang et al., 2003; Baser et al., 2004; Sun et al., 2006; Pinheiro and Chaves, 2011). As a winter crop, winter wheat is sown between September and October, and ripens earlier than other crops. The water availability in spring can therefore play a significant role for the final agricultural yield in late (Deutscher Bauernverband, 2022; tagesschau, 2022).

Yield and photosynthesis are positively correlated. The photosynthesis rate is influenced by the efficiency of respiration and assimilate partitioning. Water is one limiting factor for the performances of those processes and can be more relevant in certain development stages (Waraich and Ahmad, 2010). The impact of limited water also varies between cultivars, depending on their induced morphological response to compensate possible adverse impacts on productivity (Lipiec et al., 2013).

A standardised and coded terminology for the phenological development stages of cereals was introduced (Zadoks et al., 1974). It was then further developed by Meier (2001) and is now widely used internationally for mono- and dicotyledonous plants (Meier, 2001; Zhang et al., 2003; Sun et al., 2006; Waraich and Ahmad, 2010; Jiang et al., 2013; Morgun et al., 2020). The 'Biologische Bundesanstalt für Land- und Forstwirtschaft, Bundessortenamt und Chemische Industrie'-scale (BBCH-scale) as described by Meier (2001), divides the complete plant development cycle into 1-digit codes representing ten principal plant growth stages distinguishable by phenological changes. They are subdivided into secondary growth stages by a second digit comprising the beginning and end of each macro stage (Table 1). Their duration is mainly governed by the length of the days.

Germination and leaf development of winter wheat occur right after sowing in autumn. The next stage, tillering, can last several weeks before and or after dormancy in winter, depending on the weather conditions and the date of sowing. During tillering, several branches or shoots that will form stems and bear ears, emerge from the plant. The number of ears is a determinant for the final yield. In this development stage, the upward growth of the tillers requires the formation of a dense, lateral root system. This can only be achieved with an adequate level of soil moisture. Water availability during tillering is therefore decisive for the growth of roots and stems (Morgun et al., 2020). Thus, tillering is considered a sensitive development stage to water stress, as it may reduce the number of tillers and the potential yield (Trimble, 2005). However, excessive watering during tillering is ineffective since it causes redundant tillers to evolve that aspire nutrients but will not bear ears (Sun et al., 2006; Yadav et al., 2018). Tillering ends with the onset of stem elongation.

Stem elongation, also called jointing, is recognisable by the formation and elongation of internodes in the main stem (Lancashire et al., 1991). It concludes with the full development of the flag leaf. The fully expanded flag leaf is assumed to be the main contributor to grain yield owing to its rate of photosynthesis. Additionally, it is more impacted by water stress than the penultimate leaf (Olszewski et al., 2008; Schopfer and Brennicke, 2010; Morgun et al., 2020). Based on observations of the photosynthetic rate, Zhang et al. (2003) and Sun et al. (2006) identified the late phase of this stage and the subsequent booting stage to be most vulnerable to water stress. Morgun et al. (2020) treated winter wheat with a dry spell at a soil moisture level of 30 % of the field capacity during late stem elongation. This merely led to a reduced growth of the main shoot but a higher number of productive tillers compared to the control group, growing in optimal steady soil moisture conditions of 60 - 70 % of field capacity (Plaut, 2005). Another coping mechanism is a reduced expansion of the leaves (Lecoeur et al., 1995; Wery, 2005; Olszewski et al., 2008; Schopfer and Brennicke, 2010; Dupraz et al., 2011). In the pot experiment by Morgun et al. (2020), water supply was replenished after seven days. In the following, the decreased productivity of the main shoot was compensated by the productivity across all shoots (Plaut, 2005; Morgun et al., 2020). Hence, water stress is stated to have less of an effect on the overall productivity of winter wheat during the stage of stem elongation.

In the subsequent stage of booting, remaining harvestable vegetative plant parts are formed. The stage is recognisable by the further expansion of the previously formed flag leaf. In this and the previous stage, mature leaves serve as source of assimilates for expanding leaves. At the end of booting, the vegetative growth is largely completed, and the reproductive organs and roots become the primary sink of assimilates (Zadoks et al., 1974; Lancashire et al., 1991).

The stages after booting are mainly dedicated to the reproductive development. It starts with heading, during which the inflorescence emerges. With the end of heading and the start of anthesis, the inflorescence is fully visible. From heading to anthesis, most assimilates are invested into the formation of grains instead of vegetative plant parts. While previous vegetative development stages could address water stress with an adaptive growth strategy, the upcoming reproductive development steps dispose no such morphological mechanism to compensate for water deficit stress. Heading is therefore considered to be sensitive to insufficient water supply and water stress in this period may cause a delay of anthesis (Li et al., 2008; Dupraz et al., 2011).

Anthesis encompasses self-pollination with the aid of wind and the progression of flowering. It implies the complete formation of vegetative organs (Morgun et al., 2020). Both stems and roots have fully developed. In this stage, the leaf area index is maximised and the wheat plants' ability to regulate water uptake through stomatal closure cannot compensate for uncontrolled higher transpiration losses (Morgun et al., 2020). In a review condensing the advances in breeding drought tolerant wheat varieties they claim that at the stages of anthesis and just before (heading), water deficit stress has adverse effects on floret fertility and the quantity of grain yield (Lopes et al., 2014). Results of controlled pot experiments confirmed this (Morgun et al. 2020). The period from heading through anthesis is therefore suitable for evaluating drought tolerance among varieties of winter wheat (Lopes et al., 2014; Morgun et al., 2020). In contrast, Zhang et al. (2003) and Sun et al. (2006) found that anthesis is most vulnerable only after the previous stages of stem elongation and booting.

After anthesis, grain filling, follows. Finally, the stage of ripening begins when the grains are fully developed and ends with the full maturity of the grains for harvest.

In summary, water availability during and just before anthesis is supposed to have primary role for the development of the fruit and thus for the grain harvest. This is because the highest adverse impacts of grain yield from water stress were observed during these periods across multiple cultivars and locations. Water stress during the development of the fruit itself and stages thereafter, is considered less significant (Plaut, 2005; Sun et al., 2006; Waraich and

Ahmad, 2010; Dupraz et al., 2011; Alghory and Yazar, 2019). On this basis, Plaut (2005) expounds that water availability in the period between booting and early grain filling is crucial when the determinant parameter is final grain yield.

Disagreement on the greater importance of water supply between booting and early grain filling compared to tillering and stem elongation, may originate from the use of different productivity parameters without further differentiation. The determinants assess the vulnerability of wheat plants to water deficit stress in function of their development stages. Thus, when producing forage, all harvestable vegetative plant parts are of importance. The development of the whole plant until the end of booting, including the early production of biomass through lateral shoots, is relevant (Marrou et al., 2013b). When grain yield is of main interest, the parameters of choice would be restricted to the main shoot, such as mass of 1000 grains or ear productivity (Morgun et al., 2020).

Table 1: BBCH codes and their terminology (Meier, 2001)

| Code | Growing stage |
|---|---|
| 0 - 09 | Germination |
| 10 - 19 | Leaf development |
| 20 - 29 | Tillering |
| 30 - 39 | Stem elongation |
| 41 - 49 | Booting |
| 51 - 59 | Heading |
| 61 - 69 | Anthesis |
| 71 - 77 | Grain filling |
| 83 - 89 | Ripening |
| 92 - 99 | Dormancy |

## 1.4 Motivation and objective

Beneficial synergies from the diverse application of agrivoltaic systems within the water-energy-food nexus have recently been recognised by scientists across disciplines (Dinesh and Pearce, 2016; Armstrong et al., 2016; Amaducci et al., 2018; Elamri et al., 2018b; Barron-Gafford et al., 2019; Trommsdorff et al., 2021; Laub et al., 2022; IPCC, 2022). According to studies that have found reduced evapotranspiration and increased soil moisture under solar panels, one of these benefits consists in agricultural crops suffering less water deficit stress in agrivoltaic systems (Dupraz et al., 2011; Marrou et al., 2013a; Hassanpour Adeh et al., 2018; Barron-Gafford et al., 2019; Chopard et al., 2021). At the same time, heterogeneous microclimatic changes at field level within the agrivoltaic system have been identified as one of the challenges in the field of agrivoltaics since they could result in uncontrolled heterogeneities in the crops

(Dupraz et al., 2011; Marrou et al., 2013a). Research on the processes driving these heterogeneities have either focused on the light availability or were conducted in irrigated agrivoltaic systems (Marrou et al., 2013a; Dinesh and Pearce, 2016; Elamri et al., 2018a). On the one hand, because of the beneficial potential of agrivoltaics, and on the other hand, because of the lack in data regarding the water distribution and its effects, research in the context of the soil-plant-water continuum (SPAC) is needed (Armstrong et al., 2016).

In response, this work investigates the heterogeneity of a rainfed agrivoltaic system in terms of the water status with the attempt to zone areas in the agrivoltaic system based on the degree of intercepted rain, thereby representing the key pattern of rainfall distribution. Aim of this work is to quantify the spatial heterogeneity in water input, soil water status and plant water status of winter wheat. For the latter, leaf water potential is used as a proxy to evaluate differences in water deficit stress experienced by the plants during the growing season of 2022.

The overall objective of this work is to contribute to a better understanding of the heterogeneous soil and plant water status within an elevated, rainfed agrivoltaic system. It shall give a starting point from which to reasonably improve the design and modelling of agrivoltaic systems such that heterogeneous conditions and adverse impacts on the crop, rooted in the neglection of the altered water regime, can be avoided. In particular, the study's objectives are the following:

1. Demonstration of the spatial water distribution in the agrivoltaic system and comparison to a reference
2. Evaluation of the significance of heterogeneity in the water status within the agrivoltaic system

Heterogeneous rainfall and water availability are assumed to have caused observed adverse effects on the crops within the agrivoltaic system in Heggelbach (Baden-Wurttemberg, Germany). The questions at hand are of practical and utmost importance to the farmers concerned and will therefore be addressed as a case study at that site.

# 2 Methods

## 2.1 Site description

The study was carried out at the farm of the Hofgemeinschaft Heggelbach GbR/Heggelbach Süd GbR, which is situated in SW Germany, in the county of Sigmaringen, the municipality of Herdwangen-Schönach (47° 51' 2.257" N, 9° 8' 21.685" E). 95 ha of farmland are managed in a biodynamic manner. Following the guidelines of the German organic growers' association 'demeter' they have facilities for both crop cultivation and animal husbandry aiming for a closed circular economy on the level of an agricultural farm. Approx. 32 ha of farmland are occupied for growing forage grasses and field beans. Vegetables are grown on 20 ha and cereals on 30 ha (Krug, 2022).

On the arable field, 190 kg of common winter wheat (*Triticum aestivum* L.) of German 'B quality class' were sown on 27th October 2021. 5 kg of winter pea and 15 kg of mixed catch crops were sown under (Reyer, 2022). The study site with the agrivoltaic system is encircled on the left map of (Figure 2). The agrivoltaic system is located on a SW facing hill 645 m – 657 m a. s. l. with a slope of approx. 6.7°. Due to the proximity of Lake Constance the climate is maritime with a mean annual precipitation of 968 mm according to the closest weather station in Billafingen (N 47° 49' 58.08'', E 9° 7' 39.72'') operated by the Agricultural Technology Centre Augustenberg LTZ (Bundschuh et al., 2022). The weather station has been recording data since 2014 and is within a 2 km distance. March was repeatedly the driest month, while summer thunderstorms supplied excess water in the months of May to July. However, the weather in this hilly region is volatile and spatially variable. Therefore, the farmers of Heggelbach have set up a weather station in approx. 300 m distance and 50 m lower in altitude to the facility (N 47° 51' 0.7668'', E 9° 8' 15.747'') in March 2021 (Figure 5). As the private weather station has not yet recorded a full hydrological year, the right side of Figure 2 illustrates the climate conditions in the region based on Billafingen.

The arable soil texture present at the site is sandy loam and shall be verified within this work (Weselek et al., 2021a). A general soil analysis on 3rd May 2022 showed a slightly acidic average pH-value of 5.8.

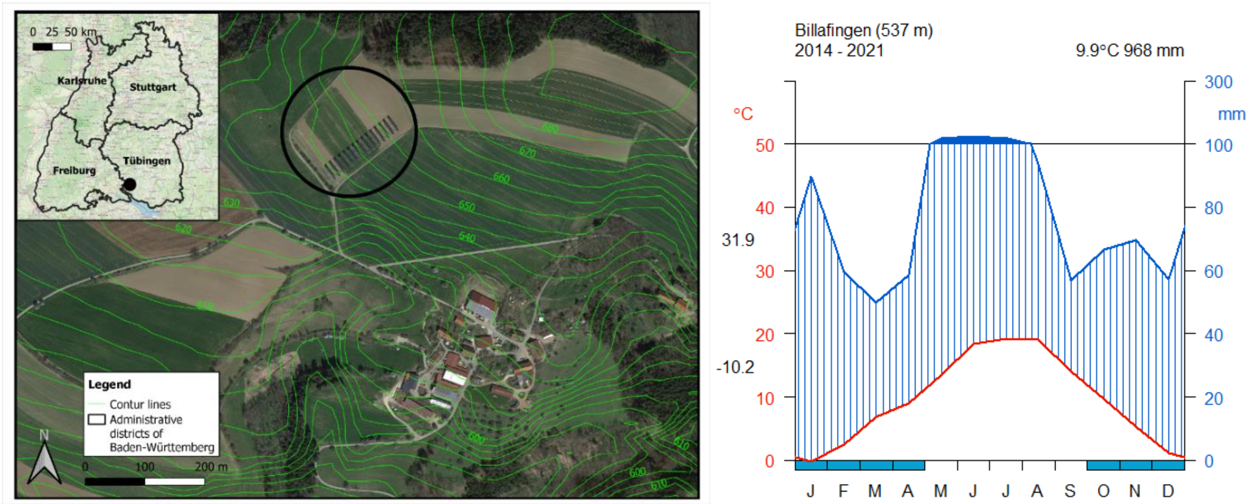


Figure 2: The study location; Left: Hofgemeinschaft Heggelbach GbR/Heggelbach Süd GbR in the administrative district of Tübingen, federal state of Baden-Wurttemberg (Germany); Right: Walter & Lieth climatic diagram of Billafingen (wetter-bw.de, 2022)

### 2.1.1 Agrivoltaic system

In accordance with the classification scheme of the preliminary standard DIN SPEC 91434, the agrivoltaic research facility in Heggelbach is classified as Category I, which is an agrivoltaic system with a clear height installation for annual and multi-year crops under the solar panels (DIN Deutsches Institut für Normung e. V., 2021). Due to its overhead clearance of 5 m and width clearance of approx. 18.4 m it is particularly well suited for the use of most agricultural machinery. In total, the facility extends over fifteen table rows of solar panels and covers an area of 25.3 m x 136.3 m (Trommsdorff et al., 2021).

The SW orientation of the facility with an azimuth of +52.5°, diverging from the conventional S orientation (azimuth = 0°) of ground-mounted PV, is adapted to the work and travel direction of machinery (Note the different conventional use of the azimuth angle Φin the sector of solar technology in contrast to the field of meteorology, where the reference direction N = 0° or 360°. The SW-orientation of the facility then corresponds to an azimuth of 232.5°). The row distance is considered to have the largest influence on both electrical and agricultural yield due to heterogeneous and reduced irradiation. In this case, at a row distance of 6.3 m a maximum of 20 % yield reduction was expected and approved by the farmer. One row consists of 24 x 2 modules above each other, resulting in a module width of 3.4 m (Trommsdorff et al., 2021). Apart from row distance, the type of solar panels is crucial for light management within the agrivoltaic system. Due to the high elevation of the solar panels, fixed 20° tilted bifacial solar panels where chosen (Table 2). These are able to increase electrical yield by using more diffuse and reflected irradiation from the crops on the ground on the back side of the solar cell (Trommsdorff et al., 2021).

As a preventive measure against compaction of the soil, mobile driveways for heavy trucks have been used during construction. Also, instead of a concrete foundation for the mounting structure, reversible steel rods have been installed in the soil (Trommsdorff et al., 2021). Despite these careful considerations in constructing the agrivoltaic system in Heggelbach, its influence on the water availability and distribution has been given little to no attention.

Table 2: Fixed geometric parameters of the agrivoltaic structure that are of relevance for the heterogeneity in both water and light distribution (Trommsdorff et al., 2021)

| Geometric parameters | |
|---|---|
| Tilting angle $\beta_{PV}$ | 20° |
| Azimuth Φ | 232.5° |
| Lower module height l | 5.5 m |
| Module length M | 3.52 m |
| Row distance B between pillars | 18.4 m |

### 2.1.2 Setup of the field experiment

To map the heterogeneity of the system, plant ecological and microclimatic measurements were taken with a high spatial resolution. Considering the extension of the agrivoltaic system and to avoid marginal effects, only the central 'corridor' was selected for the setup of the field experiment (47° 51' 13.27" N, 9° 8' 11.782" E). As suggested by Wang et al. (2018), this 'agrivoltaic unit' was chosen to represent the microclimatic characteristics of the whole agrivoltaic system. This is justified by the symmetric structure of the system. The chosen agrivoltaic unit of 18.4 m x 25.3 m is limited by strips of wild grass to the northeast (NE) and SW of it. The field experiment consisted of this unit in the agrivoltaic system (AV) and one area as a reference system (REF), as illustrated in Figure 3. AV was limited by the pillars of the agrivoltaic mounting structure and partially covered by three panel rows. In a 20 m distance to the northwest (NW), REF was situated with an almost identical experimental setup as seen in Figure 4. Differences in the setup for data collection will be pointed out.


Figure 3: The agrivoltaic (AV) and reference systems (REF) (Modified drone photo, BayWa r.e., 2016)

Following five areas in AV could be identified that were distinguishably affected during precipitation events (Figure 4):

- Area 1: The first area was the sheltered area under a solar panel.
- Area 2: The second area was the dripping edge of the middle panel row.
- Area 3: The third area was under the suspected dripping edge formed by the gap between the two panels that make a panel row.
- Area 4: The fourth area was the open space between the panel rows.
- Area 5: And the fifth area was the dripping edge of the upper panel row held up by pillars.

These five areas were represented by five plots of 1 m x 1 m in a transect in y-direction. Even though this allocation was repeated in three transects, it should be noted, that due to their changed position in x-direction these were no true repetitions. However, as they were representative of the defined areas, hereafter they will be summarised as area 1 - 5 when applicable. A total of fifteen plots were analysed in AV. The setup and the identifiers of the plots are illustrated in Figure 4.

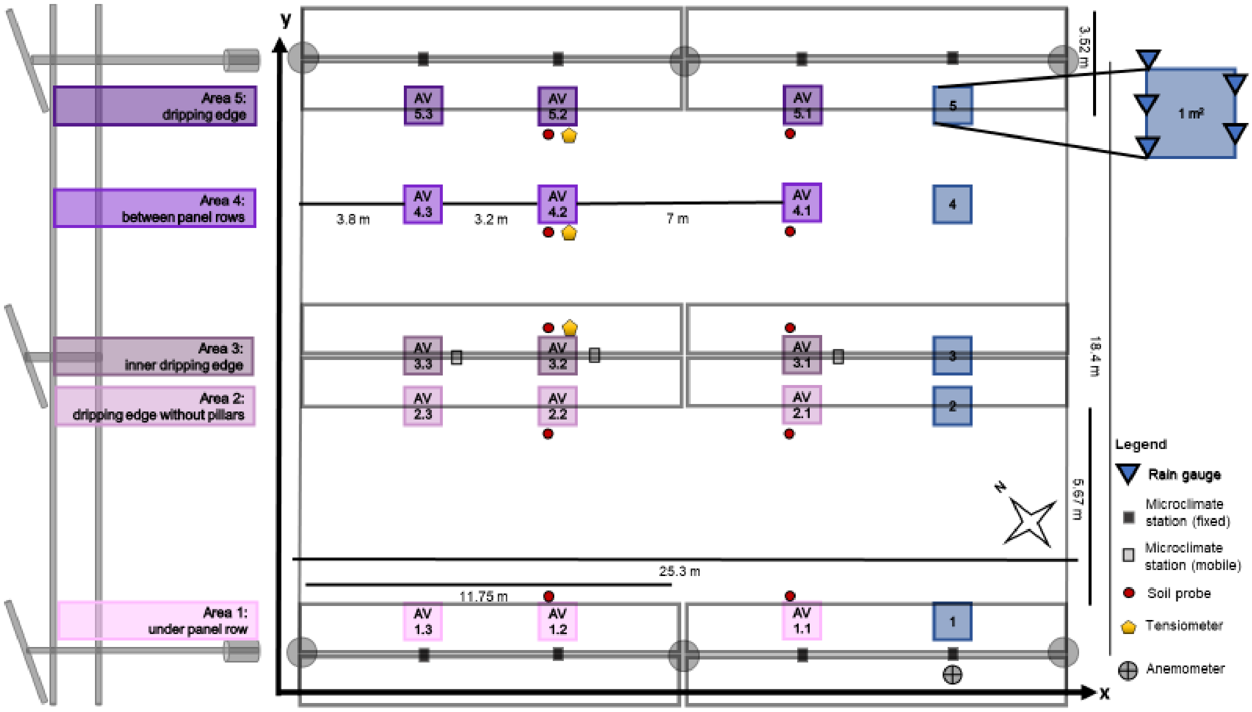


Figure 4: Layout of the experiment in the agrivoltaic system (not to scale); Lateral (left) and top plan view (right) (adapted from ©HILBER GmbH, 2016)

The dimension of the arable field extends further towards the NW than the agrivoltaic structure and the panel rows are oriented NW - SE (Figure 3). Thus, the working direction with heavy machines for sowing, weeding, fertilising, and harvesting follows the panel rows (SE - NW). Accordingly, fifteen plots of the same pattern of coordinates as in AV have been analysed in REF. While phenological measurements were taken within all 30 plots, soil samples and interim green cuttings were taken at a distance adjacent to the plots in x-direction. The purpose was to minimise the disturbance of the wheat plants growing within the plots.

## 2.2 Data collection

Data collection started on 10th May 2022, after the last agricultural activity on 29th April 2022 before the harvest (Reyer, 2022). Approximately every two weeks, a set of measurements on soil and plants was taken with three replicates. In concrete, soil, plant and precipitation measurements at the site were taken on five occasions from 10th to 12th May, from 22nd to 26th May, from 6th to 9th June, from 18th to 22nd June and from 2nd to 5th July (Table 3 and Table 4). On 25th and 26th July, the harvest was performed and soil samples for the creation of the pF-curve were collected. Plant ecological data collection was carried out on leaf and stand level.

### 2.2.1 Precipitation and wind

For a higher spatial resolution of the redistribution of precipitation in the agrivoltaic system, 25 rain gauges (70 mm; TFA Dostmann, Wertheim-Reichholzheim, Germany; ±0.5 mm) were positioned 1 m above the surface, just above the wheat canopy, in a transect of five plots (1 m x 1 m). These plots correspond to the areas that have previously been observed to be differently affected during precipitation events (Figure 4). Three additional rain gauges were put in REF. It was possible to take a total of 22 readings for partially accumulated precipitation. However, only eight rain events fulfilled the requirements of being observed parallel to wind measurements (Table 5). Collected data from the weather stations in Heggelbach (Figure 5) and Billafingen served as a comparison.

Two ultrasonic anemometers (ATMOS 22, METER Group Inc. USA; ± 0.3 m $s^{-1}$, ± 5°) were adjusted to the true-north and installed on the lower end of the transects for precipitation measurements to record wind speed, gust and direction for REF and AV 190 cm above the ground.

Figure 5: Precipitation measurements in Heggelbach; Left: 25 rain gauges in AV; Centre and right: Weather station with tipping bucket rain gauge in Heggelbach

### 2.2.2 Soil samples and measurements

Soil water retention characteristics describe the capability of the soil to hold or allow water to move within its pores. It is primarily defined by the soil texture, i.e., the grain size distribution and the soil structure, which is the proportion of air to bulk (bulk density). They determine the soil moisture which can be expressed in volumetric water content VWC [vol.-%] and in matric potential $\psi_M$ [cm or Pa]. As an important parameter to determine the water availability for plants, soil moisture is commonly seen as a parameter for optimisation of crop quality. Water or crop management systems that are adapted accordingly, increase the resilience of agriculture in regions where precipitation is declining and or becoming less predictable as precipitation patterns alter due to climate change (Trimble, 2005).

Thus, estimating the soil texture can give hints about the capacity of soil to hold water that is readily available for plants. For example, clay soils are capable to hold more water than sandy soils. Also, it requires more energy to remove the water from clay soils. The grain size distribution of the soil influences the soil water retention characteristics since different grain size fractions require different water tensions for the same change in soil moisture. One reason for these deviations is the increasing bond strength resulting from a reduction in pore radius (Trimble, 2005; Blume et al., 2011).

Soil texture at the site was estimated by applying the finger test to two depths (0 - 30 cm and 30 - 60 cm) at various locations of the field experiment following best practice set out by Blume et al. (2011). The finger test is a practical method that leads to an approximation of the grain size distribution in the field with an accuracy of 5 - 10 % for experienced users. For the finger test, soil is held in the hand and moistened until it no longer changes colour. The felt grain size indicates the sand content, the malleability indicates the clay content and dirt residues in the finger grooves indicate the silt content (Blume et al., 2011).
To additionally consider natural soil structure, 21 undisturbed soil ring samples with a volume of 100 $cm^3$ (area: 25 $cm^2$, height: 4 cm) were collected from the surface soil A horizon and the subsoil B horizon. The B horizon was recognisable by the distinctively compacted plough pan. Seventeen samples were collected at five plots in a transect of AV, with further four samples at plot REF 2.2. However, three repetitions of the same plot and horizon could not always be fulfilled due to time restraints (Table 11).

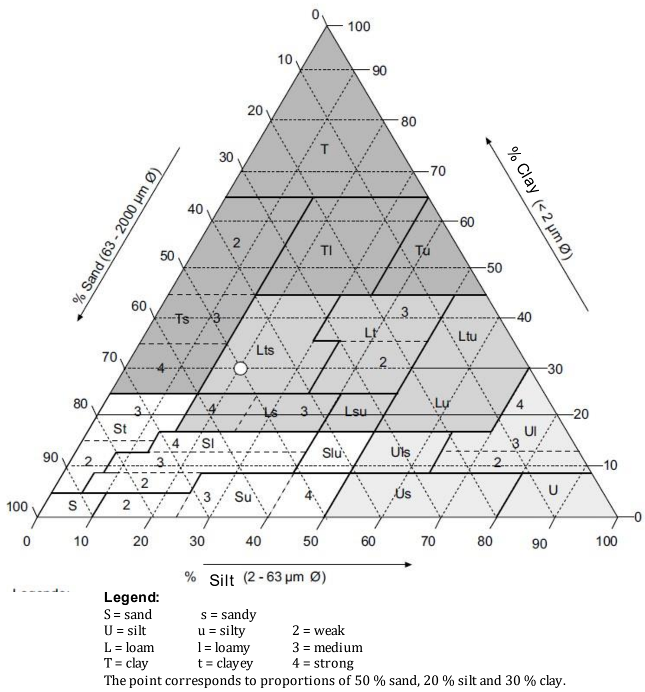


Figure 6: Soil texture triangle (adapted from Blume et al., 2011)

To document the soil moisture during the measurement campaign, a ‘Pürckhauer’ drill stick was used to collect destructive soil samples from two depths (0 - 30 cm, 30 - 60 cm) at every plot biweekly. Deeper soil samples of down to 90 cm were not practicable at the site, nor imperative since the active root system of winter wheat is mainly found to a depth of 60 cm, unless it is a variety adapted to dry conditions (Nakhforoosh et al., 2014; Audu et al., 2022).
Soil moisture $\theta_{VWC}$, measured in VWC [vol.-%], is defined by the quotient of the volume fraction of water $V_W$ within a given volume of dried soil $V_d$:

$$\theta_{VWC} = \frac{V_w}{V_d} \quad (1)$$

A standard direct gravimetric method has been applied to measure the VWC. In total, 120 fresh samples of known volume were collected and dried in the oven. By weighing the samples before and after drying, $\theta$ could be calculated according to Equation ( 1 ). The analyses were conducted in the laboratory of the Core Facility Hohenheim (University Hohenheim, Baden-Wurttemberg, Germany).

Furthermore, soil moisture $\theta_{TDR}$ was measured indirectly via the measurement of permittivity (or dielectric constant ε). The permittivity ε is measured with the principle of Time Domain Reflectory (TDR), using a sensor probe. The permittivity ε indicates the permeability of a material to electric fields. The general relationship between soil moisture and permittivity is described by the Topp equation (Topp et al., 1980):

$$\theta_{TDR} = 4.3 \text{ x } 10^{-6}\varepsilon^3 - 5.5\text{x } 10^{-4}\varepsilon^2 + 2.92 \text{ x } 10^{-2}\varepsilon - 5.3 \text{ x } 10^{-2} \qquad (2)$$

Fifteen TDR-sensors (5TM sensor, METER Group, Inc., Pullman, WA, USA; accuracy of ± 0.03 $m^3/m^3$) were installed in the field on 5th July. They were in two transects of AV (AV x.1 and AV x.2) and in one transect of REF (REF x.2). Due to the hard soil, water was applied while vertically inserting the sensors in the soil such that reported values reflect the integrated VWC in 20 - 30 cm depth (Blume et al., 2011; METER Group AG, 2019).
Soil moisture expressed in soil water potential $\psi_S$ describes the energy to be released or consumed (i.e., positive, or negative) when transferring a quantity of water from one point to a reference location. Soil water gradients determine the direction of water flow from higher to lower energy potentials. It refers to the energy of pure water at standard temperature and atmospheric pressure, at a reference height. Soil water is subject to the capillary, osmotic and gravitational forces in the pore space, which therefore control soil water potential. The total water potential $\psi_S$ is commonly divided into three potential components, the gravitational potential $\psi_G$, the osmotic potential $\psi_0$, and the matric potential $\psi_M$ (Blume et al., 2011).

The gravitational potential $\psi_G$ depends on the position in space. It is important for groundwater recharge and is defined as the product of gravitational acceleration g [cm $s^{-2}$] and the elevation of the soil water above reference height h [cm] (Weil and Brady, 2017).

The osmotic potential $\psi_0$ is caused by hygroscopic attraction forces by dissolved salts in the soil. At higher solute concentrations, the lower $\psi_0$ induces water to flow from lower to higher concentrations. This water movement is mainly facilitated by semi-permeable membranes that hinders solutes from moving, i.e., diffusion. The osmotic potential plays a minor role for water flows in the isolated soil and may therefore often be neglected. It is more relevant for the water pathways within the plant or in the water uptake by roots in the presence of solute accumulations in root vessels (Schopfer and Brennicke, 2010; Weil and Brady, 2017).

The matric potential $\psi_M$, also known as the water tension, depends on the adhesion, adsorption, and capillary forces on the polar surfaces of the fine pores that hold water in pore space. These forces are stronger when little water is present. Matric potential gradients cause rather slow water movements in the soil but have a key impact on soil moisture and the water supply of plant roots (Brady and Weil, 2002). Consequently, three tensiometers (TensioMark, ecoTech

Umwelt-Meßsysteme GmbH, Bonn, Germany; ± 30 hPa & 5 % Full Scale = 0.35 pF) continuously measuring the matric potential and soil temperature in 30 minute intervals were installed in AV 5.2, AV, 4.2 and AV 3.2 in approx. 20 cm depth on 18th June. Their locations were selected as representative positions in the agrivoltaic system: AV 5.2 represents a dripping edge, AV 4.2 compared to REF as it is situated between panel rows, and AV 3.2 represents the sheltered area (Marrou et al., 2013a).

The relationship between the VWC [vol.- %] and the matric potential $\psi_M$ is described by the soil water retention curve on a logarithmic scale [-log hPa]. It describes water transport in different soils and thus is one of the main controlling soil characteristic for plant water uptake (Schmidhalter, 1997). It is used to derive how much water is retained in the soil at certain pressure heads. To obtain the water retention curve of the soil at the site, the laboratory method has been applied. The 21 collected soil ring samples were saturated and subsequently stepwise drained at increasing pressures. At every inset of equilibrium, the samples of known volume were weighed. The first drainages at - 10 hPa (pF 1) and 60 hPa (pF 1.8) were performed at negative pressures. For that, the water-saturated soil ring samples were placed on a felt filter on a ceramic plate which was covered with a layer of water. A connected hanging water column caused the desired drainage level pressure. For the desorption at higher pressures (- 320 hPa and - 15 000 hPa, pF 2.5 and pF 4.2, respectively), the pressure plate method with excess pressure was applied (Fischer, 2010). Therefore, a pressure pot was used. In the case of the highest-pressure level only the finest pores retain water, such that the soil structure may be neglected. Hence, a soil slurry from air-dried sieved soil (≤ 2 mm) was used to accelerate the drying process (Cassel and Nielsen, 1986). The pF value is defined as log(-$\psi_M$). The linkage of the soil water potential and the previously introduced VWC is crucial to understand soil-plant-water interactions.

Table 3: Summary of all measurements; Manual measurements are marked with M, continuous with C.

| Type | Parameter | Device | Location AV | Location REF | C/M | Date | Interval |
|---|---|---|---|---|---|---|---|
| **Meteorology** | | | | | | | |
| | Precipitation | 28x Rain gauges (70 mm; TFA Dostmann, Wertheim-Reichholzheim, Germany; ±0.5 mm) | 25x in transect | 3x in transect | M | 22.05. - 26.07.22 | Occasionally, biweekly |
| | Wind direction<br>Wind speed<br>Wind gusts | ATMOS 22 Ultrasonic anemometer (METER Group Inc. USA; ± 0.3 m/s, ± 5°) | MC 17 | MC 21 | | since 08.06.22 | |
| | Air temperature<br>Relative Humidity<br>Atmospheric pressure | VP-4 sensor | MC 11, 12, 17, 18, 19, 20, 25, 26 | MC 15, 16, 21, 22, 23, 24, 29, 30 | C | since 2019 | 30 min |
| | PAR | QSO-S sensor | | | | | |
| | Air temperature<br>Relative Humidity | Tinytag Ultra 2 - TGU-4017 | centre (AV 3.1-3.3) | - | | since 10.05.22 | |
| **Weather station in Heggelbach** | Precipitation | Tipping bucket rain gauge (300 mm; TFA Dostmann, Wertheim-Reichholzheim, Germany; ±0.25 mm) | - | 47,8502130, 9,1370754 | C | since 07.09.21 | 60 min |
| | Wind direction<br>Wind speed<br>Wind gusts | Wind sensor | | | | Since 12.12.2020 | 7 min |
| | Air temperature<br>Relative Humidity | Temperature sensor | | | | | |
| | Soil temperature | Soil sensor | | | | | |

Table 4: Continuation of summary of all measurements; Manual measurements are marked with M, continuous are with C.

| Type | Parameter | Device | Location AV | Location REF | C/M | Date | Interval |
|---|---|---|---|---|---|---|---|
| **Plant** | Leaf water potential | Scholander pressure chamber (Model 1000 PMS Instruments) | plots | plots | M | 12.05.22, 25.05.22*, 08.06.22, 19.06.22, 03.07.22 | biweekly (5x) |
| | Yield | - | next to plots | next to plots | M | 25.07.22 | - |
| | BBCH | - | plots | plots | M | | biweekly (5x) |
| **Soil** | Matric potential (20 cm) | Tensiometer (TensioMark ecoTech) | plots | plots | C | 19.06.22 | 30 min |
| | Soil temperature (20 cm) | Tensiometer (TensioMark ecoTech) | plots | plots | C | 19.06.22 | 30 min |
| | Upper volumetric water content (15 cm) | TDR-probe (TRIME Pico64 IMKO) | plots | plots | | 08.06.22, 20.06.22 | - |
| | Volumetric water content (0-30 cm, 30 - 60 cm) | - | next to plots | next to plots | M | 11.05.22, 22.05.22, 06.06.22, 21.06.22 | biweekly (4x) |
| | $N_{min}$ (0-30 cm, 30 - 60 cm) | - | next to plots | next to plots | M | 11.05.22, 22.05.22, 06.06.22, 21.06.22 | biweekly (4x) |
| | Initial soil sample (pH, P, K, Mg, $N_{min}$) | - | randomised | randomised | | 26.04.22 | - |
| | Volumetric water content (20 - 30 cm) | 5TM sensor | AV x.1, AV x.2 | REF x.2 | C | 05.07.22 | 30 min |
| | Soil temperature (20 cm) | 5TM sensor | AV x.1, AV x.2 | REF x.2 | C | 05.07.22 | 30 min |

*No measurements of LWP due to rain on 25th May 2022 at predawn

### 2.2.3 Monitoring of wheat plants

On the base of the BBCH-scale as detailed in Meier (2001), the phenological development stages of the winter wheat plants were determined for the main stems of six randomly selected healthy plants in every plot biweekly (Meier, 2001).

Leaf water potential (LWP) and further plant physiological parameters could only be measured when no precipitation was occurring. For the LWP the pressure chamber technique was applied. A Scholander pressure bomb (Model 1000 Pressure Chamber Instrument, PMS Instrument Company; 0.5 %) was used to measure predawn (PD) and midday (MD) leaf water potentials on the same days, between 3 am and 6 am, and 10:30 am and 1:30 pm, respectively (six days of measurements of which one is without PD-measurements due to rain). In every plot the youngest fully expanded leaf of an intact wheat plant was cut off at one-third of the distance from the leaf base, with a sharp razor blade and immediately sealed in a plastic bag to avoid water losses through transpiration (Schmidhalter, 1997; Abdalla et al., 2022). By using only mature leaves, possible growth effects incorporated in the measurement could be avoided (Donovan et al., 2001). The youngest fully developed leaf was used for measurements, which corresponds to the penultimate leaf during the stem elongation stage, and the flag leaf from the heading stage onwards. In winter wheat, photosynthesis rates are highest in flag leaf and second leaf, such that their impairment can lead to a substantial reduction in biomass and in grain yield (Olszewski et al., 2008; Waraich and Ahmad, 2010; Morgun et al., 2020).

The leaves were inserted into the chamber of the pressure bomb and gradually pressurised with compressed nitrogen until xylem water was escaping at the cut surface, becoming visible with a magnifier glass. The pressure required until that point, corresponds to the water pressure within the leaf sample. The removal and insertion of the leaf into the pressure chamber was performed in less than sixty seconds to prevent dehydration of the leaves (Schmidhalter, 1997; Donovan et al., 2001; Knipfer et al., 2020).

Just like soil water status, plant water status expressed in plant water potential $\psi_P$ describes the energy consumed (i.e., negative potential) when water is passively transferred along an increasingly negative water potential gradient $\Delta\psi_P$ through the xylem vessels. The potential gradient in a plant system is the result of mainly three components acting simultaneously on the water, which are the solute or osmotic potential $\psi_O$, the hydrostatic pressure or turgor potential $\psi_T$ , and the gravitational potential $\psi_G$, (Schopfer and Brennicke, 2010): $\psi_p = \psi_G + \psi_T + \psi_O + \cdots$

## 2.4 Data processing

Data processing and analysis were carried out using the programming and statistics language R Version 4.1.3 (R Core Team, 2022) in the environment provided by RStudio Version 2022.07.0 (RStudio Team, 2022).

To provide a better understanding of the modified water fluxes in the agrivoltaic system, precipitation was quantified as throughfall and interception at several positions. The difference and heterogeneity among them were assessed to be related with possibly influencing factors.

The soil data was examined for homogeneity to exclude the confounding effect arising from variability in soil texture and structure. Key parameters of the soil for the growth of plants were derived and linked to the observed soil water status during the growing season to gain a first indication for water deficit stress.

Also, the leaf water potential measurements were analysed: Firstly, the difference and variability between REF and AV, as well as within AV were evaluated. Secondly, the leaf water potential measurements were linked to the phenological development to differentiate the possible influence of water stress during the growing season.

### 2.4.1 Evaluating the heterogeneity of water input into the agrivoltaic system

Precipitation and its subsequent pathways within an agrivoltaic system may be compared with precipitation over a forest canopy. It partitions into three water fluxes: stemflow, throughfall and interception. In this case, stemflow will be neglected as the pillars of the agrivoltaic mounting structure are only located in the peripheral area of the study site. Throughfall will be the major component. The tilt of the solar panels facilitates almost immediate free throughfall along the dripping edge (Elamri et al., 2018b). The measurements of throughfall will be used to estimate the areal precipitation input $\overline{\mathrm{P}}$ within the agrivoltaic system compared to the actual incident precipitation at REF. The difference between both will be termed the interception IC.

Since there are no continuous measurements of precipitation in the AV or REF, the study of its heterogeneous distribution was mainly event based. Thus, 22 manually measured precipitation events were compared with the corresponding hourly precipitation depths recorded at the farm's private weather station. Due to two events of distinctively higher rain intensity, a non-parametric correlation test was applied to compare the weather station in Heggelbach to the measurements taken at REF. Since the available data is only a short time series at the weather station and based on single events at REF, no correction of precipitation measurements was applied. Applying a sweeping monthly correction factor (7 - 9 % for this region between May and July) to specific locations is not recommended as they might overrule the particular measurement conditions of that station (Richter, 1995; Strub et al., 1999).

Eight of the 22 rain events were selected to estimate the areal precipitation in AV compared to the incident rainfall measured at REF. The arithmetical mean method with N = 25 rain gauges in AV was selected since the rain gauges were evenly distributed in AV and altitudes are negligible. The areal precipitation $\overline{P}$ [mm] was computed for each plot, area, and rain gauge position, with throughfall sum $TF_i$ [mm] of gauge i for the time interval of each event ( 3 ). Additionally, the cumulative throughfall sums of the events were calculated to get an idea of the variable spatial distribution from June to July exemplified by eight rain events.

$$\overline{P} = \frac{TF_1 + TF_2 + TF_3 + \dots + TF_n}{n} = \frac{1}{n}\sum_{1}^{n} TF_i \qquad (3)$$

Table 5: Precipitation events and their characteristics: Observations of precipitation without observations of wind are greyed out. Precipitation events for further analysis are bold.

| Obser-vation | Date | Duration [h] | I* [mm/h] | $P_{REF}$ [mm] | $P_{Station}$ [mm] | Comment |
|---|---|---|---|---|---|---|
| 1 | 23.05.22 | 1 | 8 | 8 | 8.5 | |
| 2 | 25.05.22 | 0.4 | 5 | 2 | 0 | |
| 3 | 25.05.22 | 0.3 | 1.7 | 0.5 | 0 | |
| 4 | 07.06.22 | 0.5 | 9.8 | 4.9 | 0 | No measurements of wind |
| 5 | 07.06.22 | 1 | 1 | 1 | 0.5 | |
| 6 | 07.06.22 | 0.17 | 4.4 | 0.8 | 0 | |
| 7 | 07.06.22 | 8.5 | 0.4 | 3 | 2.4 | |
| **8** | **08.06.22** | **1** | **0.5** | **0.5** | **0.3** | **Event 1** |
| **9** | **08.06.22** | **1** | **0.3** | **0.3** | **0.3** | **Event 2** |
| 10 | 09.06.22 | 6 | 0.2 | 1.3 | 1.2 | Over night |
| **11** | **09.06.22** | **0.25** | **2** | **0.5** | **0.3** | **Event 3** |
| 12 | 13.06.22 | 4 | 0.6 | 2.5 | 1.9 | Over night |
| 13 | 16.06.22 | 3 | 1 | 3 | 2.1 | Read on 19.6.22 |
| 14 | 20.06.22 | 0.5 | 0.2 | 0.1 | 0 | Not accurate |
| 15 | 21.06.22 | 1.25 | 0.8 | 1 | 1 | New rain event in the middle of reading |
| **16** | **22.06.22** | **1** | **2** | **2** | **1** | **Event 4** |
| 17 | 22.06.22 | 1 | 0.5 | 0.5 | 0.5 | Dripping effect of previous observation |
| 18 | 04.07.22 | 5 | 0.6 | 3 | 2.8 | Over night |
| **19** | **04.07.22** | **1** | **10** | **10** | **7.5** | **Event 5** |
| **20** | **04.07.22** | **1** | **13** | **13** | **10.3** | **Event 6** |
| **21** | **26.07.22** | **2** | **1.5** | **3** | **3.1** | **Event 7** |
| **22** | **26.07.22** | **0.5** | **2** | **1** | **0.8** | **Event 8** |

*Intensity I refers to $P_{REF}$

### 2.4.2 Interception and wind as variables for heterogeneity

Interception (IC) is defined as relative rain depth, encompassing locally bound losses or gains in water input. In the first step, it is estimated by the difference between throughfall TF in AV and areal precipitation in REF ($P_{REF}$).

In the second step, a geometric approach as suggested by Elamri et al. (2018b) is used to calculate the precipitation intercepted by a tilted impermeable surface of the solar panel. Elamri et al. (2018b) calculated the interception $IC_c$ from the product of the rain intensity I, and a constant defined per event that consists of the tilting angel of the solar panel $\beta_{PV}$ , the rain incidence angle $\alpha_R$ , the solar panels' azimuth $\Phi$ and the rain direction u. In Equation ( 4 ), the rain direction is set equal to the wind direction for simplicity.

$$IC_c = I(\cos\beta_{PV} - \tan\alpha_R \sin\beta_{PV} \cos(\Phi - u)) \qquad (4)$$

Therein, the rain incidence angle $\alpha_R$ can be deduced from the wind speed ws and the velocity of the falling rain drops $v_d$ as described by van Hamme (1992) in Equation ( 5 ) (Elamri et al., 2018b):

$$\tan\alpha_R = \frac{ws}{v_d} \qquad (5)$$

The rain drop velocity during a precipitation event, depends on their size which can be deduced from the rain intensity I. The relation between I and raindrop-size as established by Laws and Parsons (1943) and as reported by McCool et al. (2009) follows in Equation ( 6 ):

$$D_{50} = 1.238\, I^{0.182} \qquad (6)$$

$D_{50}$ represents the drop diameter at which 50 % of the rain volume consists of larger and 50 % consists of smaller raindrops. Gunn and Kinzer (1949) have measured the terminal velocities of distilled water droplets falling through stagnant air with an accuracy of 0.7 % such that the velocity of the falling rain drops $v_d$ could be derived from the estimated raindrop diameters per precipitation event for the computation of $IC_c$ [mm $h^{-1}$] per event. The resulting interception $IC_c$ [mm $h^{-1}$] then describes the transient storage effect of the solar panels. $IC_c$ was compared with the previously derived interception. Interception values were converted to interception depths in [mm] per precipitation event, to make the values comparable and more intuitive. Relevant fixed geometric parameters of the agrivoltaic structure can be found in Table 2 in section 2.1.1 Agrivoltaic system.

To account for the role of the wind in the heterogeneity within AV, the circular averages of wind directions were calculated for each precipitation event. First, a polar coordinate transformation was executed. The measurements in polar coordinates [0°, 360°) were converted to Cartesian coordinates described by cosines and sines in radians [π/180, 2π]. A wind direction was defined by two orthogonal vectors $\vec{u}$ and $\vec{v}$, describing the wind components towards the East and North direction, respectively. Taking their magnitudes into account by weighing their corresponding wind speeds, the average wind direction was expressed in radians. Computing the arctangent of them and reversing the conversion to degrees, gave the circular average of wind direction wd. Adding 360° to negative outputs corrected the range [-180°, 180°] to [0°, 360°) for interpretation (Grange, 2014).

In agriculture, the coefficient of variation $C_v$, is a measure of evaluating an irrigation system in its uniformity. It consists of the quotient of the standard deviation and the mean of the variable of interest. Low values indicate less variation, i.e., present a more uniform pattern and are therefore desirable. Values below 0.2 are considered acceptable in irrigation. This value was used as baseline for the evaluation of heterogeneity. As $C_v$ summarises the spatial variation of TF in one comparable single value, it was computed for each precipitation event and plot (Elamri et al., 2018b).

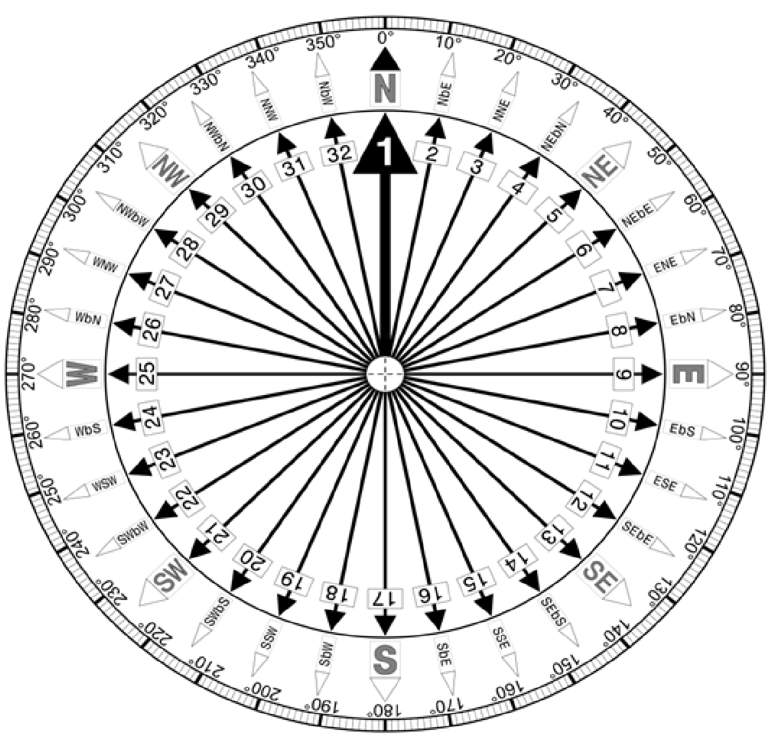


Figure 7: 32-point compass rose with associated directional abbreviations and corresponding degrees from north. (Smial, 2021; licensed under CC BY-SA 3.0)

The relation between the descriptive variables and the heterogeneity of water input, was described by Kendall's coefficient of correlation $\tau$. Five areas times eight precipitation events were assessed in their spatial heterogeneity in TF. Measured TF within AV was non-normal distributed (skewed to the right). Finally, because of ties present in the dataset, Kendall's $\tau_b$ was preferred over Spearman's r (Kendall, 1945).

### 2.4.3 Soil water retention characteristics

The soil water retention characteristics at the site were derived by fitting the measured data obtained from the undisturbed soil samples to the nonlinear soil-water retention model for unsaturated soils proposed by van Genuchten (1980). Equation ( 7 ) describes the soil water content $\theta_G$ [vol.-%] as a function of the pressure head h [cm] with four independent parameters accounting for the porosity, i.e., the structure of the soil, and its texture. As scaling parameter, $\alpha$ [$cm^{-1}$], relates to the inverse of the air entry pressure. The saturated soil water content $\theta_s$ and $\alpha$ describe the soil structure. The residual water content $\theta_r$ designates the pressure head at which no change in soil water content occurs. The shaping parameter n in $m = 1\text{-}1n^{-1}$ is based on the soil pore size distribution. Both account for the soil texture (van Genuchten, 1980; Wang et al., 2015):

$$\theta_G = \theta_r + \frac{(\theta_s - \theta_r)}{[1 + (\alpha h)^n]^m} \qquad (7)$$

The parameters were estimated with the program "SWRC Fit" (Seki, 2007). The resulting fitted soil water retention curves for the A and B horizons in both AV and REF were compared with idealised soil water retention curves of loam, clay loam, sandy loam and silty loam. Additionally, the $C_v$ was calculated for the parameters derived from the intact soil samples.

### 2.4.4 Soil water status

One week of continuous data of VWC measured by three TDR-sensors, served as exemplary visualisation of the soils' reaction to precipitation. For comparison, the rates of change (ROC) were calculated in daily steps. Instead of using absolute values, the response time to precipitation events were used. Hourly precipitation data were retrieved from the weather station in Heggelbach and were filled up with data from the weather station in Billafingen for when clear precipitation events were visible in the soil moisture data, but no precipitation was recorded at the site.

Since the data for the soil consists of three differently obtained data sets over different time frames, the previously fitted soil water retention curve was applied. The model was used to verify the results across the different data collection methods for soil moisture by converting biweekly VWC to corresponding soil water potential values and vice versa. A water potential of - 1.2 MPa (≈ 4 pF), was considered to be the threshold value for water stress deficit in winter wheat as suggested by Roohi et al. 2013.

### 2.4.5 Wheat plant water status during the phenological development stages

The most frequent BBCH-codes and the average code found in AV and REF were considered to determine the overall biweekly development stages of the wheat plants. The lowest and highest growth stages documented indicate the field's overall progression in development.
Measurements of leaf water potential (LWP) were split into sub-datasets to compare between AV and REF, predawn (PD) and midday (MD) measurements, and previously defined areas 1 - 5 (Figure 4). A two Sample t-test was applied to test the difference in the mean of LWP between the sample sets of REF and AV. To evaluate the significance of the variability between the defined areas within AV (AV 1 - 5), random and systematic factors for variability between sample subgroups needed to be distinguished. The mean square within each group was compared to the mean square between the defined groups. The focus was the maximum water deficit stress experienced by the plants during MD. For reference, LWP lower than - 2.2 MPa at MD was interpreted as water deficit stress, following the findings by Corso et al. (2020), who reported a 50 % loss of hydraulic conductivity in winter wheat leaves due to embolised vessels following cavitation due to dry conditions. In the case of PD measurements, Jiang et al. (2013) found negative effects on the plant growth in response to a LWP lower than - 1 MPa. The overall difference in PD and MD LWP per system and area over the observed time was calculated, as well as the diurnal variation between PD and MD.

### 2.4.6 Assessing the overall heterogeneity

Datasets regarding the water status are visually linked and compared to REF. A one-way Multivariate Analysis Of Variance (MANOVA) was applied to reject or confirm previously made observations in differences in mean water status. The MANOVA was built of one factor (area) with ten levels (REF 1 - 5 and AV 1-5) and four response variables (VWC in upper and lower soil, and LWP at PD and MD). A Linear Discriminant Analysis (LDA) was used as Post-Hoc Test to interpret the results of the model.

# 3 Results

## 3.1 Growth conditions during the season

The observed precipitation depths in REF over 22 events were mostly comparable to the values at the weather station in Heggelbach. Mean difference in precipitation measurements during the growing season amounts to 36.5 %, with REF receiving more precipitation than the weather station. Computation of the Kendall's rank of correlation still resulted in an agreement of $\tau_b = 0.66$ with significance ($p < 0.05$). These sums include five occasions when small amounts of precipitation were measured in REF but not at the station (Table 5). They account for almost half of the deviation and possibly illustrate measurement deficiencies of the tipping bucket (Sevruk, 1996). Removing them results in a remaining mean difference in precipitation of approx. 18 % and a stronger concordance of $\tau_b = 0.91$ with significance ($p < 0.05$). Hence, the measurements at the weather station in Heggelbach generally follow the occurring precipitation on the hill with the agrivoltaic system and could be used with restriction to interpolate the data set for when continuous data is necessary. According to the weather station in Heggelbach, total precipitation since the day of sowing (DAS) on the 27th of October amounted to 433 mm (Figure 8). March was the month with least precipitation while the following months each presented precipitation sums of approx. 70 mm or more. This year's monthly precipitation sums were lower than the recorded average at the weather station Billafingen but correspond in their relative values (Figure 2). The air temperature $T_{air}$ in Heggelbach also followed the average $T_{air}$ of several years in Billafingen.

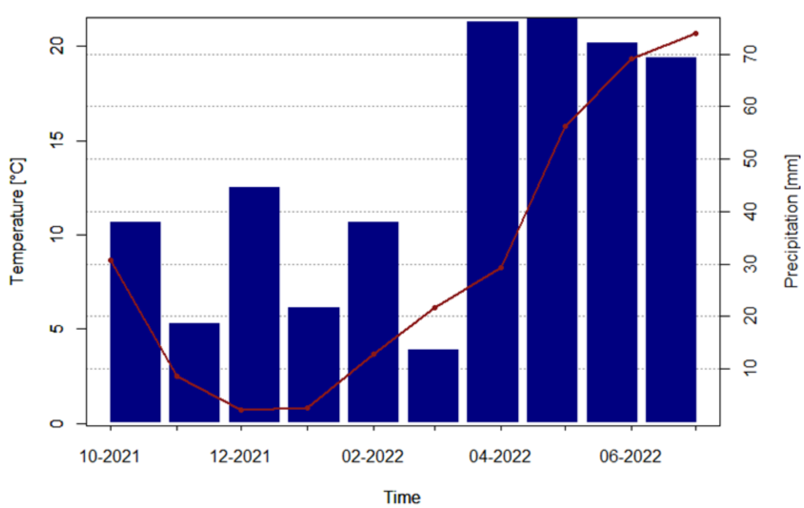


Figure 8: Basic meteorological data since the sowing of winter wheat in Heggelbach

Turning to the wind conditions, the weather station in Heggelbach indicates Northeast (NE) as most frequent wind direction (12.4 %), thereafter North-Northeast (NNE) with a frequency of 10.6 %. Figure 9 shows a histogram of 32 classes of wind directions based on the true-north azimuth. The length of the spokes indicates how frequently a class, this is wind direction, has occurred. The spokes are divided into colours indicating five classes of wind speed. NE as predominant wind direction in Heggelbach holds true in REF and AV. However, the distribution of the wind direction in AV has two peaks, South by West (SbW = 191.25°) and NNE (22.5°). As these directions approximately correspond with the setup of the agrivoltaic structure, with a SW orientation of 232.5°, the wind re-oriented within the agrivoltaic system. It created a tunnel effect, such that the wind mainly came from the NE or the opposite direction. This 'canyon' has not led to higher wind speeds but to more frequent higher wind speeds from those two directions. The highest wind speeds came from the Northwest in REF since there are no obstructions in the field. Generally, the observed wind speeds have been low to moderate. In REF the highest wind gusts were recorded at night-time on the 23rd and 27th of June with 14.6 m $s^{-1}$ and 14.9 m $s^{-1}$, respectively.

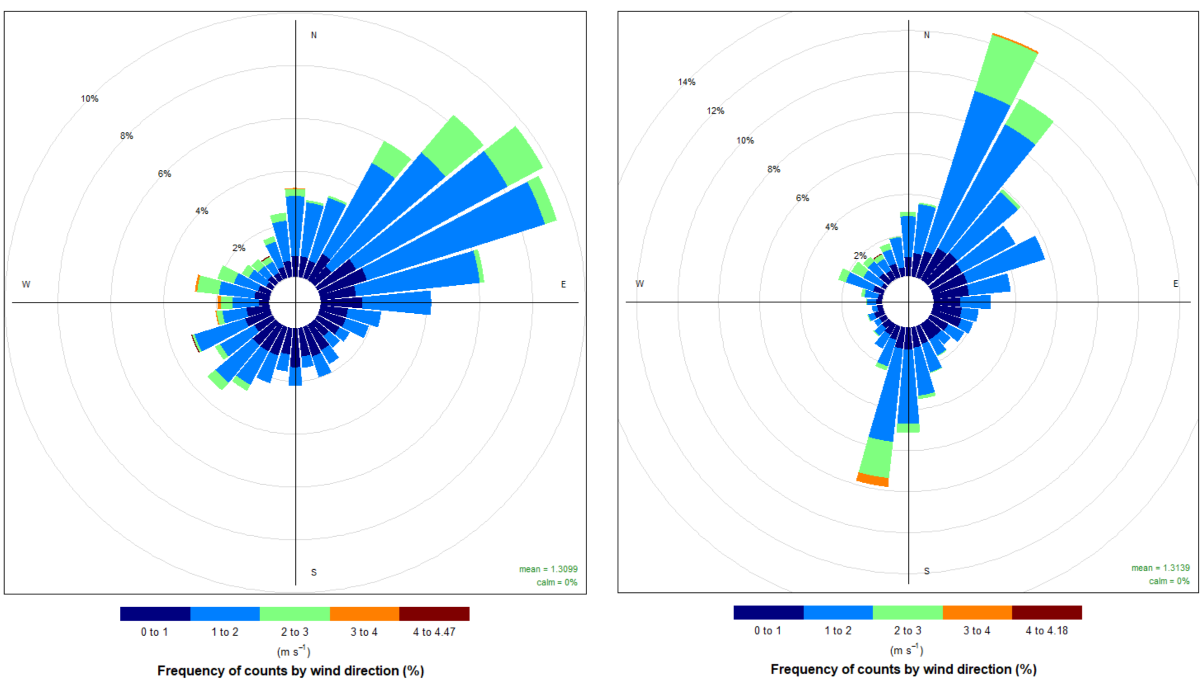


Figure 9: Wind rose of recorded wind in 190 cm above ground with spokes representing 32 wind directions and colours representing the frequency of five wind speed classes; left: REF, right: AV.

## 3.2 Estimation of areal precipitation and resulting interception losses

Cumulative areal precipitation within AV was 8 % less than in REF. Interception losses derived from measurements within AV range from 4 to 27 %, depending on the position of the plot (Table 6). The black dashed line depicts the cumulative mean of throughfall (TF) in AV, while the orange line shows the cumulative areal precipitation at REF ($P_{REF}$). Cumulative TF in area 4 between the solar panel rows matched areal precipitation $P_{REF}$. Area 3 experienced the greatest interception losses. As expected, since both area 3 and area 1 are underlying the strongest sheltering effect by the panels, rainfall measurements were less than $P_{REF.}$

In Table 6, negative values represent higher TF relative to the $P_{REF}$, since interception originally was defined as a loss. Negative values result from the redistribution of intercepted precipitation within AV due to the agrivoltaic structure. Hence, as expected area 5 under the dripping edge at the pillars had no interception losses but a gain in water input of 25 %. The difference in TF between area 5 and the remaining areas was significant ($p < 0.01$; $0.33 < \tau_b \leq 0.69$) for each case. As result, overall interception losses within the defined AV amount to 8 % relative to $P_{REF.}$ Including seven more recorded events with TF measurements of lower quality, would amount to interception losses of approx. 6 %.

Table 6: Cumulative throughfall TF and interception IC observed in AV over 8 events

| | Area 1 | Area 2 | Area 3 | Area 4 | Area 5 | Mean | $P_{REF}$ [mm] |
|---|---|---|---|---|---|---|---|
| Cumulative IC [mm] | 4.8 | 5.5 | 8.1 | 1.1 | -7.5 | 2.6 | |
| Relative IC [-] | 0.16 | 0.18 | 0.27 | 0.04 | -0.25 | 0.08 | 30.25 |
| $C_v$ [-] | 0.14 | 0.42 | 0.21 | 0.02 | 0.32 | 0.44 | |

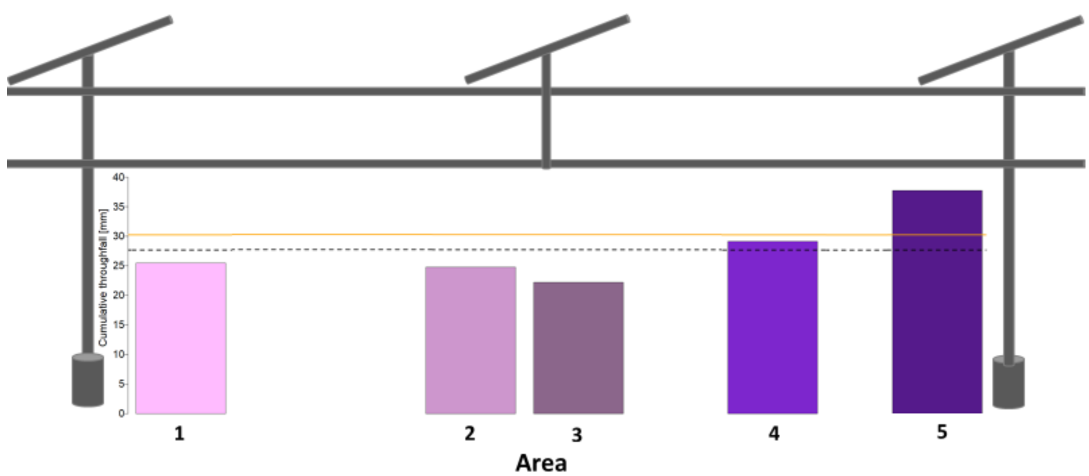


Figure 10: Cumulative TF of eight rain events from 8th June to 26th July with the black dashed line representing the mean in AV and the orange line the mean in REF (adapted from ©HILBER GmbH, 2016)

Two methods were applied to determine interception. The first method determines interception IC as the water loss or gain measured in throughfall (TF) at various positions in AV. In contrast, the geometric framework as suggested by Elamri et al. (2018b), interception $IC_c$ was calculated for eight events as a temporary storage on the panels before redistribution. In the latter method, the geometric approach has been limited to the calculation of the theoretical water depth intercepted by a solar panel. It therefore does not provide insight into the further apportion and distribution of IC and TF.
Table 7 presents IC and $IC_c$ and $\tau_b$ as measure of concordance between observed and calculated interception. Only IC in area 3 were significantly in concordance with the calculation ($\tau_b = 0.815$, $p < 0.05$). The absolute interception depths per rain event differ considerably from each other. Although area 1 is like area 3 located under a panel, it only weakly correlates with the calculated intercepted rain depth. Area 5 represents an area at the dripping edge, supposedly receiving much of the intercepted precipitation in the form of TF. The negative correlation confirms this; however, it is not statistically significant ($\tau_b$ = - 0.462, p = 0.162). Then again, area 2, which is also under a dripping edge, does not indicate a contrary relation.

A closer look at the redistribution of precipitation shows that single point measurements of TF differed considerably within a plot and with event (Figure 11). Within a plot, the individual measurements strongly influence the mean TF. Measurements in areas that are affected by the dripping edge (areas 2 and 5), expose considerable variations during the same event. Repeated point measurements revealed that the dripping edges can cause multiples of $P_{REF}$ to fall through within AV. During event 8 area 1 (gauge positions 1 - 5) received on average more TF than the other areas because the rain gauge in position 2 captured a main dripping edge.

Table 7: Calculated interception $IC_c$ compared to observed interception IC per area and event. Negative values correspond to higher observed throughfall TF than precipitation $P_{REF}$

| IC | **Event** | | | | | | | | |
|---|---|---|---|---|---|---|---|---|---|
| [mm] | **1** | **2** | **3** | **4** | **5** | **6** | **7** | **8** | $\tau_b$ |
| $IC_c$ | 0.2 | 0 | 0.2 | 0.9 | 1.2 | 2.7 | 1.1 | 1.2 | - |
| Area 1 | 0.50 | 0.25 | 0.50 | 0.70 | 0.40 | 2.80 | 0.80 | -1.20 | 0.302 |
| Area 2 | -0.50 | -0.45 | -0.10 | -0.40 | 0.60 | 7.20 | -0.50 | -0.30 | 0.491 |
| Area 3 | -0.10 | -0.25 | 0.20 | 0.30 | 1.80 | 3.20 | 2.00 | 0.80 | 0.815* |
| Area 4 | 0.20 | -0.05 | 0.00 | -0.40 | 0.50 | 0.70 | -0.40 | 0.40 | 0.491 |
| Area 5 | -0.10 | -0.25 | -0.20 | -1.20 | -2.00 | -1.20 | -2.00 | -0.60 | -0.462 |

*Correlation is significant at the 0.01 level

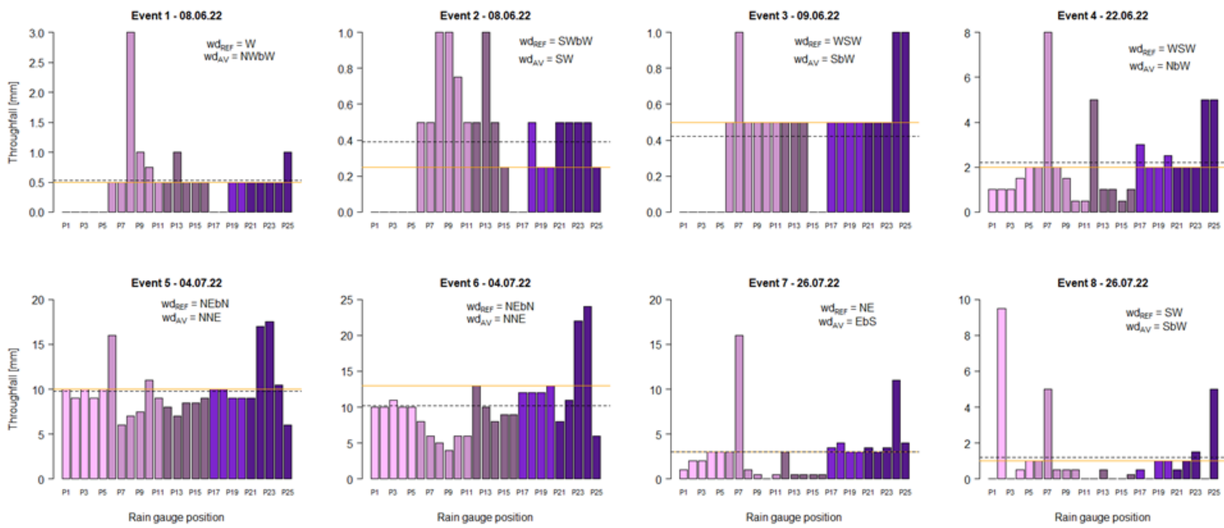


Figure 11: Throughfall TF recorded at 25 rain gauge positions during eight events with indication of the prevailing wind directions wd in REF and AV. The black dashed line indicates the mean TF in AV, the orange line indicates the mean TF in REF

The range of heterogeneity in TF is also visible in Figure 11. The horizontal orange line refers to $P_{REF}$, while the dashed line depicts mean areal TF in AV. Average wind direction wd during the events calculated for both REF and AV are included. Figure 7 gives an explanation on the labels used for the wd. During the events 1 - 3, which depict low intensity ($I_{REF}$) precipitation events (Table 9), the sheltered area 1 did not receive any TF with three differing wind exposures. In these cases, area 1 illustrates well the sheltered area caused by a solar panel while the neighbouring area 2 considerably exceeds the mean precipitation depths for those events (Elamri et al., 2018b). At the same time, during event 8 was also characterised by a low $I_{REF}$, area 1 received more TF than the other areas, including REF. Event 6 is striking because the lowest TF was observed in area 2, representing an area below a dripping edge. Mean areal TF values in AV exceeding the actual areal precipitation $P_{REF}$ of an event, could be explained by measurement inaccuracies or by an overrepresentation of the areas affected by the dripping edge.

Table 8: Characteristic variables per precipitation event and resulting coefficient of variation $C_v$ in throughfall TF

| Event | Time | IC [mm] | $wd_{REF}$ | $ws_{REF}$ [m s$^{-1}$] | $I_{REF}$ [mm h$^{-1}$] | $\overline{P}$ [mm] | SD [mm] | $C_v$* [-] |
|---|---|---|---|---|---|---|---|---|
| 1 | 08.06.2022 17:00 | 0 | W | 3.33 | 0.5 | 0.5 | 0.6 | 1.12 |
| 2 | 08.06.2022 18:00 | - 0.1 | SWbW | 1.75 | 0.25 | 0.4 | 0.3 | 0.83 |
| 3 | 09.06.2022 12:00 | 0 | WSW | 1.85 | 2 | 0.4 | 0.3 | 0.66 |
| 4 | 22.06.2022 7:00 | - 0.2 | WSW | 0.69 | 2 | 2.2 | 1.8 | 0.88 |
| 5 | 04.07.2022 16:30 | 0.25 | NEbN | 2 | 10 | 9.7 | 3 | 0.32 |
| 6 | 04.07.2022 17:30 | 2.5 | NEbN | 1.47 | 13 | 10.2 | 4.6 | 0.48 |
| 7 | 26.07.2022 6:30 | 0 | NE | 0.56 | 1.5 | 3 | 3.5 | 1.29 |
| 8 | 26.07.2022 11:00 | 0.2 | SW | 0.88 | 2 | 1.2 | 2.2 | 1.74 |

In summary, with coefficients of variation $C_v$ of 0.32 and 0.48, the least heterogeneous distributions in TF occurred during event 5 and 6, respectively, when the wind originally came from Northeast by North (NEbN = 33.75°) and $I_{REF}$ was highest. Most heterogeneous conditions occurred during the last event with the wind blowing from SW (Table 8).

Across these events, areas 2 and 5 have been the most variable areas in AV, with coefficients of variation of 0.42 and 0.32, respectively (Table 6). Those areas correspond to the dripping edges in the system. As expected, measurements in area 4, representing the open area between panel rows, almost did not vary during a precipitation event. Area 1, which is situated under a solar panel, and area 3, which is to be found under two solar panels with a small gap in between, have been moderately heterogeneous, with measurements in area 3 being slightly more variable, likely due to the dripping edge caused by the gap.

The position and extent of the dripping edge's effect depend on several factors, such as for this AV fixed parameters as the height and tilt of the solar panels (Table 2), and variables such as ws and wd (Elamri et al., 2018b). From Table 5 it can be deduced, that the events 5 and 6 show a similar redistribution of precipitation and are conditioned by similar wind conditions. In contrast, with the wind blowing from the same direction during the events 3 and 4, but the ws differing from each other, the redistributions of precipitation resulted to differ from each other. Table 9 shows the strength of relationships between for the heterogeneity of the water input and potentially relevant variables based on Kendall's rank correlation coefficient $\tau_b$ under the diagonal and Pearson's correlation coefficient r above the diagonal for comparison. Some corresponding coefficients are not alike, indicating non-linear relations, making Kendall's non-parametric measure for correlation more suitable. Unexpectedly, wind speed ws has weak to no correlations with either of the outcome variables throughfall TF, interception IC or coefficient of variation $C_v$. In contrast, both wind components $\vec{v}_{REF}$ and $\vec{u}_{REF}$, are moderately negative correlated to TF. These wind vectors describe the wind components towards East and towards North, respectively. Derived interception IC is most correlated with the intensity I, though they only have a weak negative correlation. Based on Kendall's rank correlation, heterogeneity encompassed as coefficient of variation $C_v$, is mostly correlated to interception IC and $\vec{v}_{REF}$, but only moderately.

Table 9: Correlation matrix based on eight precipitation events with Kendall's rank correlation coefficient $\tau_b$ under the diagonal and Pearson's correlation coefficient r above the diagonal for comparison

| | **ws** | $\vec{\mathbf{v}}_{\mathbf{REF}}$ | $\vec{\mathbf{u}}_{\mathbf{REF}}$ | **I** | **TF** | **IC** | $\mathbf{C_v}$ |
|---|---|---|---|---|---|---|---|
| **ws** | | -0.012 | 0.677 | -0.002 | -0.054 | -0.018 | -0.297 |
| $\vec{\mathbf{v}}_{\mathbf{REF}}$ | -0.071 | | 0.625 | -0.784 | -0.873 | 0.502 | 0.592 |
| $\vec{\mathbf{u}}_{\mathbf{REF}}$ | 0.357 | 0.571 | | -0.671 | -0.753 | 0.416 | 0.279 |
| **I** | 0.038 | -0.567 | -0.491 | | 0.969 | -0.83 | -0.639 |
| **TF** | -0.214 | **-0.714*** | **-0.714*** | 0.643 | | -0.734 | -0.619 |
| **IC** | -0.286 | 0.357 | 0.214 | **-0.491** | -0.357 | | 0.471 |
| $\mathbf{C_v}$ | -0.357 | **0.429*** | 0.286 | -0.34 | -0.143 | **0.5** | |

*Correlations significant at the 0.05 level

## 3.3 Soil water retention characteristics

The study site presented homogeneous soil conditions. With the the finger test, soil texture was determined to be silty loam (Lu) with the deeper soil having a little higher clay content. This corresponds to an approximated grain size distribution of 20 - 30 % clay, 10 - 30 % sand and 50 - 70 % silt across the field. The laboratory results of the generated soil water retention curve confirm that, as can be seen in Figure 12. Overall, the undisturbed ring soil samples behaved similar to the idealised curve for silty loam. This holds true for both A and B horizon.

A closer look at the fitted parameters of the curves shows little variation (Table 10). Also, within AV, the results per soil ring sample do not vary much, but the residual water content $\theta_r$ presents high coefficients of variation $C_v$ in both horizons, which could be explained by the low values and limited accuracy in the method to determine this parameter. The variation among samples is also higher for the parameter α. Both have to do with the soil structure, which allows the assumption of less reliability when drawing conclusions on the porosity from these results.

Table 10: Van Genuchten parameters of the fitted water retention curves

| | Horizon | $\theta_s$ | $\theta_r$ | $\alpha$ | n | $R^2$ |
|---|---|---|---|---|---|---|
| REF | A | 36.011 | 8.14E-19 | 0.0118 | 1.1519 | 0.988 |
| | B | 38.854 | 13.729 | 0.1839 | 1.1002 | 1.000 |
| AV | A | 40.813 | 1.15E-16 | 0.2182 | 1.1002 | 0.994 |
| | B | 37.971 | 1.85E-16 | 0.1354 | 1.0819 | 0.994 |
| $C_v$ in AV [-] | A | 0.06 | 2.17 | 0.83 | 0.02 | 0.02 |
| | B | 0.09 | 2.24 | 1.90 | 0.06 | 0.01 |

The fitted soil water retention curves obtained from the soil ring samples are illustrated in Figure 13. Standard deviations among samples in observed volumetric water content (VWC) per observed pressure head are shown as error bars. A rough indication of wilting point (WP), available water content (AWC), field capacity (FC) and air capacity (AC) are also given in Figure 13, to indicate differences. The exact values are given in Table 11. The soil moisture at field capacity $\theta_{FC}$, the amount of water that the soil can retain in its pores, was similar for all soils and is at around 32 vol.-%. The detected wilting point $\theta_{WP}$, the soil moisture level under which root water uptake is conventionally said to be inhibited, is higher for the B horizon, which was to be expected because of the higher estimated soil bulk density in the compacted plough pan (Table 11). The available water content $\theta_{AWC}$ for plants in the plough pan is correspondingly lower. For the same reason, air capacity AC is 3 vol.% higher in the A horizon of AV. Unexpectedly, AC in REF is lower in the same horizon of REF in comparison to the B horizon. The results for REF are to be considered with care since it was not possible to obtain more than two repetitions for either of the A or B horizon and measurements between the two diverged largely.

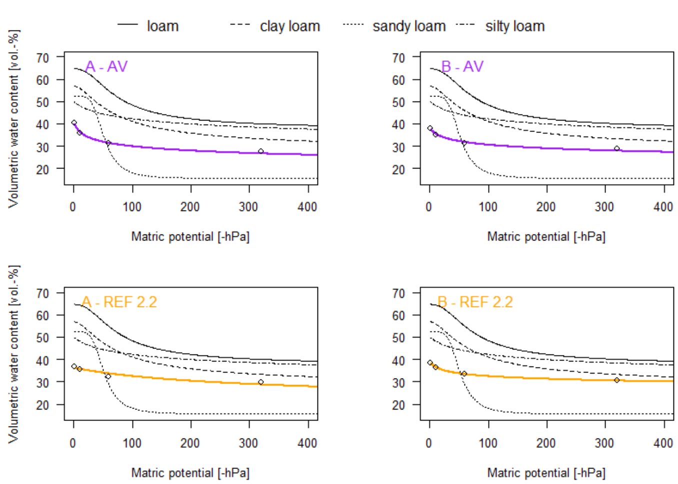


Figure 12: Fitted soil water retention curves in comparison with idealised curves; top: AV, bottom: REF; left: A horizon, right: B horizon

Table 11: Soil's water budget and key parameters of soil moisture

| System | Horizon | $\theta_{FC}$ [vol.-%] | $\theta_{AWC}$ [vol.-%] | $\theta_{WP}$ [vol.-%] | AC [vol.-%] | Density [g/cm$^3$] | Porosity [vol.-%] | N |
|---|---|---|---|---|---|---|---|---|
| AV | A | 31.34 | 13.79 | 17.55 | 9.03 | 1.54 | 40.37 | 7 |
| | B | 31.51 | 11.53 | 19.97 | 6.34 | 1.62 | 37.85 | 10 |
| REF | A | 32.28 | 16.14 | 16.14 | 4.34 | 1.45 | 36.62 | 2 |
| | B | 33.28 | 8.2 | 25.08 | 5.23 | 1.59 | 38.52 | 2 |

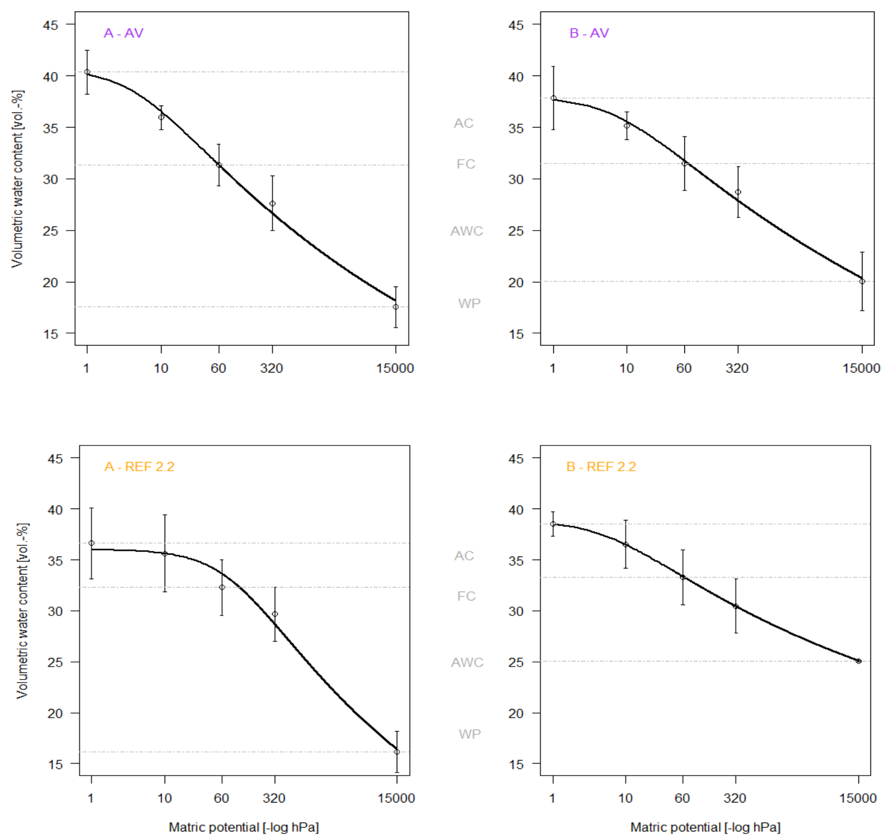


Figure 13: Fitted soil water retention curves in logarithmic scale with standard deviations at the observations; Top: AV, bottom: REF; Left: A horizon, right: B horizon

### 3.3.1 Dynamic soil water status in AV

The biweekly measurements of the bulk soil moisture in 0 - 30 cm and 30 - 60 cm depth on four occasions from beginning of May to end of June in AV and REF illustrate the tendencies of the soil water status (Figure 14). They cover the whole observed period of leaf water potential (LWP) measurements from wheat plant development stages tillering to grain filling and tillering to ripening, in AV and REF, respectively.

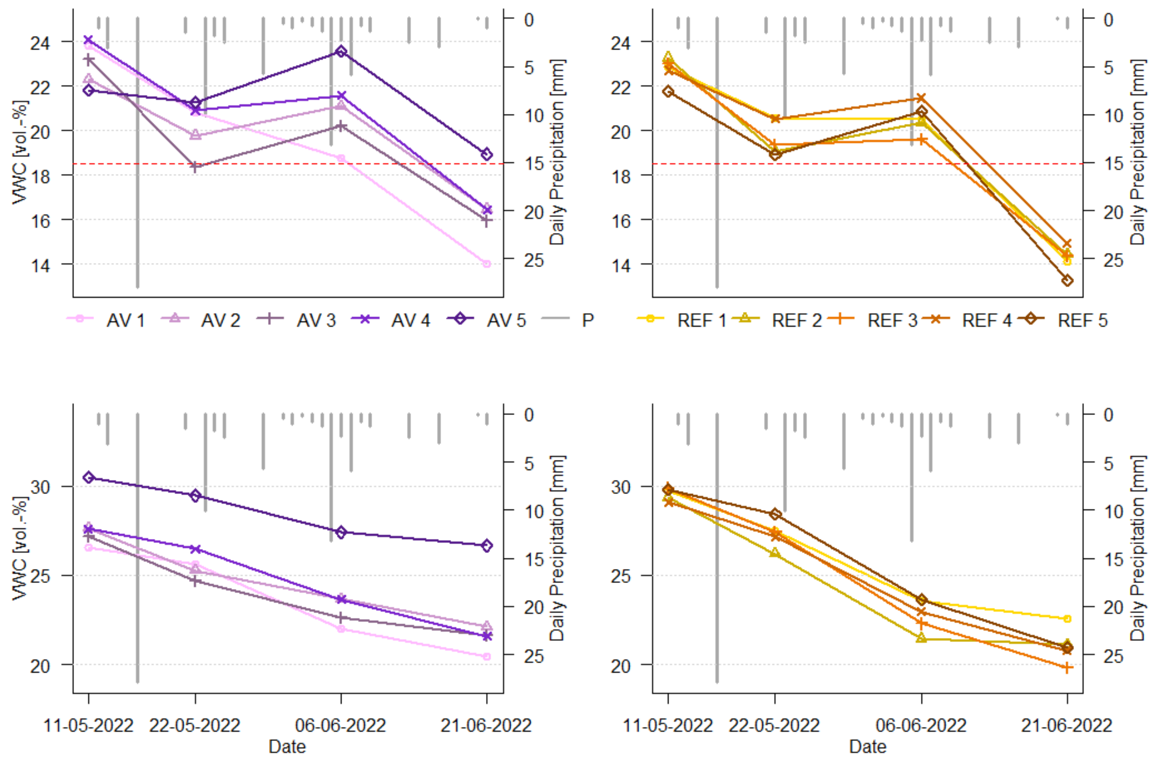


Figure 14: Mean volumetric water contents VWC per area obtained from biweekly destructive bulk soil samples. The red dashed line indicates 4 pF (≈ 18.5 vol.-%) of the A horizon.; Left: AV, right: REF; top: 0 - 30 cm depth, bottom: 30 - 60 cm depth

Overall, both systems and depths showed a gradual decline in soil moisture (Figure 14). The deeper soil layer was wetter but occurring precipitation did not refill the deeper soil water storage. In REF the soil drying process was almost double as fast than in AV. At the end of the measuring period the rate of change in REF was - 0.2 vol.-% per day. AV and REF encounter similar final bulk soil moisture values of just above 20 vol.-% in the deeper soil. The averaged measurements of the deeper soil in area 5 in AV (under the dripping edge) stand out, as it was consistently approx. 5 vol.-% wetter than the other areas in AV. Applying an imbalanced Welch Two-Sample t-test by treating the measurements of all other plots in AV as one sample group with the same mean suggests a significant difference between them and the measurements in area 5 at a significance level of 0.05 ($t(20.087) = 6.234$). Sill, AV 5 decreased at the same rate as other areas in AV.

In contrast to the deeper soil layer, the upper soil layer was temporarily recharged by precipitation events at the beginning of June (Figure 14). In Figure 14 it is prominent that the mean values of the areas in AV have a wide range in VWC. The difference is of 4.9 vol.-% between the lowest soil moisture value of 14 vol.-% in AV 1 (under a solar panel) and the highest value of 18.9 vol.-% in AV 5. AV 1 showed a decline at a rate of - 0.24 vol.-% similar to the upper soil of REF.

With the Welch Two Sample t-test, the null hypothesis of no difference for both upper and lower bulk soil in mean soil moisture between AV and REF could not be rejected, speaking for no significant difference in the soil water condition from beginning of May to end of June, which cover the period of LWP measurements from wheat plant development stages tillering to grain filling and ripening, in AV and REF, respectively.

Following to the biweekly measurement campaign, soil water status in AV was observed with half-hourly continuous data of the soil water potential with three tensiometers. The matric potential measurements in addition with soil temperature measurements covered the development stages of grain filling and grain filling to ripening, in AV and REF, respectively.

The period covers several smaller rain events with daily interruptions, a couple of more intense rain events and the longest dry spell of the growing season (two weeks). This is reflected in both soil temperature and water potential data (Figure 15).

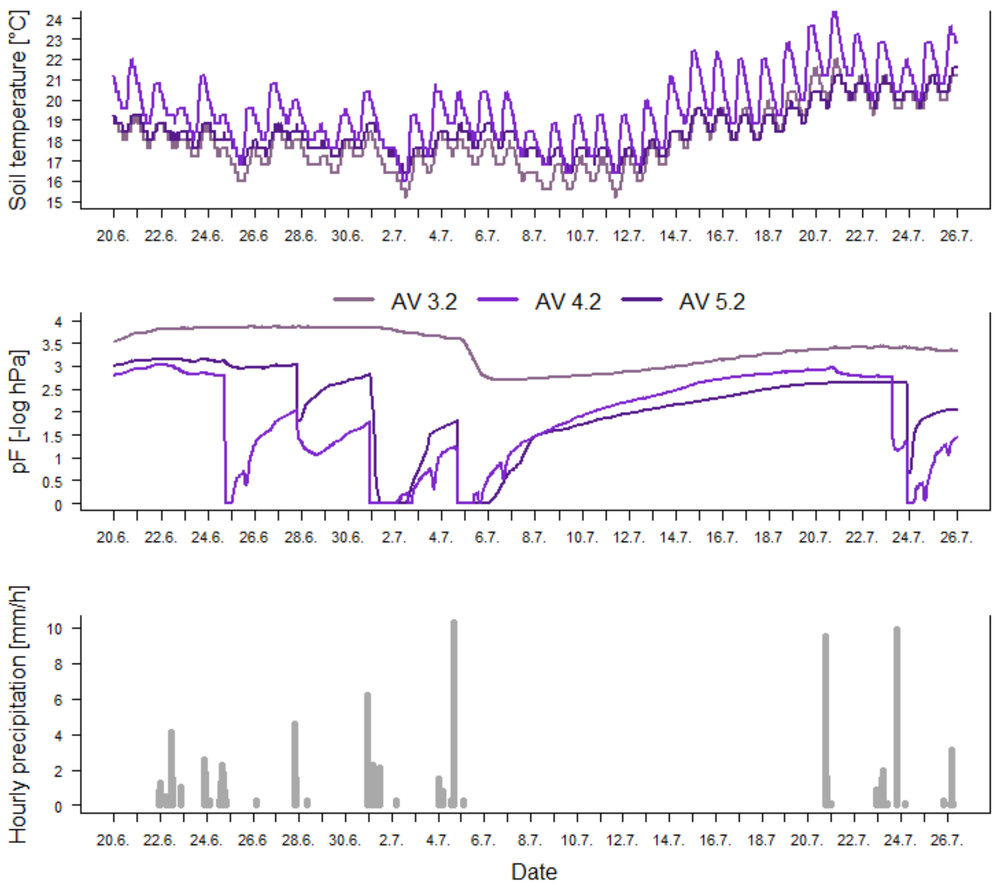


Figure 15: Time series of the three tensiometers installed in three plots in AV in 20 cm depth; top: soil temperature, centre: soil matric potential, bottom: recorded precipitation

During the dry and warm two weeks the soil temperature slowly increased. Plot AV 4.2 experiences stronger fluctuations in temperature from day to night was generally higher. During the time of the dry spell, the soil between the panels was up to 4°C, and on average 1.2°C warmer than the soil in AV 3.2. That plot has the lowest temperature, except for during the dry spell as AV 5.3 is the plot least affected by the dry conditions.

Before the beginning of the data collection of matric potential, it had rained only a couple of times during the previous two weeks (Figure 14). However, the soil water potential under the solar panel (AV 3.2) was with approx. - 3 200 hPa (≈ 3.5 pF) the most negative value and coincides with the grain filling stage. The soil remains at that potential throughout smaller precipitation events and only increases to approx. - 1 000 hPa (≈ 3 pF) after precipitation of in total 18.2 mm on the 4th of July (ripening in REF). In contrast to the inert behaviour of AV 3.2, the tensiometers in the other two plots showed immediate responses to some water inputs at steep rates, with the soil water potential in AV 4.2 recovering from days without rainwater input earlier than in AV 5.2. During the two-week dry spell, the soil water potential in AV 5.2 was slightly less negative than in AV 4.2.

Apart from the biweekly measurements of the bulk soil moisture, half-hourly continuous data of soil moisture sensors from the last week in July allowed to zoom into the dynamic soil water responses to precipitation events at the site. They cover the last observed period of leaf water potential measurements from wheat plant development stages which is the end of grain filling and the start of ripening, in AV and REF, respectively. It shows very irregular responses in both AV and REF (Figure 16). Overall, the soil moisture increases faster in AV than in REF, except for the second precipitation event (P > 6 mm) of this short period, when the reaction in REF is more pronounced.

During precipitation events of that week, there were alternating sensors that did not measure any change in VWC without any clear pattern. During the first event, of all sensors only the TDR-sensors in AV 1.1, AV 3.1, REF 3.1, and REF 4.1 reacted to the first event. Thereafter, the soil moisture in AV 2.1 showed a slow positive change in soil moisture after a relatively small rainwater input. While the sensors in AV 2.1 and AV 4.1 indicated an increase further on, the others do not. The sensor in AV 4.1 reacted earlier and the soil remained at a higher moisture state without further drying. In comparison, the sensor in AV 2.1 recorded a constantly slow decline. It is the two same sensors that indicate the last precipitation event while none of the other sensors, nor in REF, do. However, during the penultimate precipitation event, it is other sensors, AV 4.1 and 5.1, measuring a positive change in soil moisture.

The same irregular pattern for the changes in soil moisture holds true for the measurements in REF: The soils in REF 1.1, 2.1 and 5.1 barely show a response to the first stronger and second longer but lighter precipitation event. In contrast to AV, there was also no reaction at all with the last event. If the soil increases its volumetric water content in response to rainfall, it does so at the same instant and at the same initial rate in all plots of REF, while in AV the response time is shifted during the second event and at different rates during the last. Also, the drying process after precipitation events are more synchronous and regular in REF than in AV.

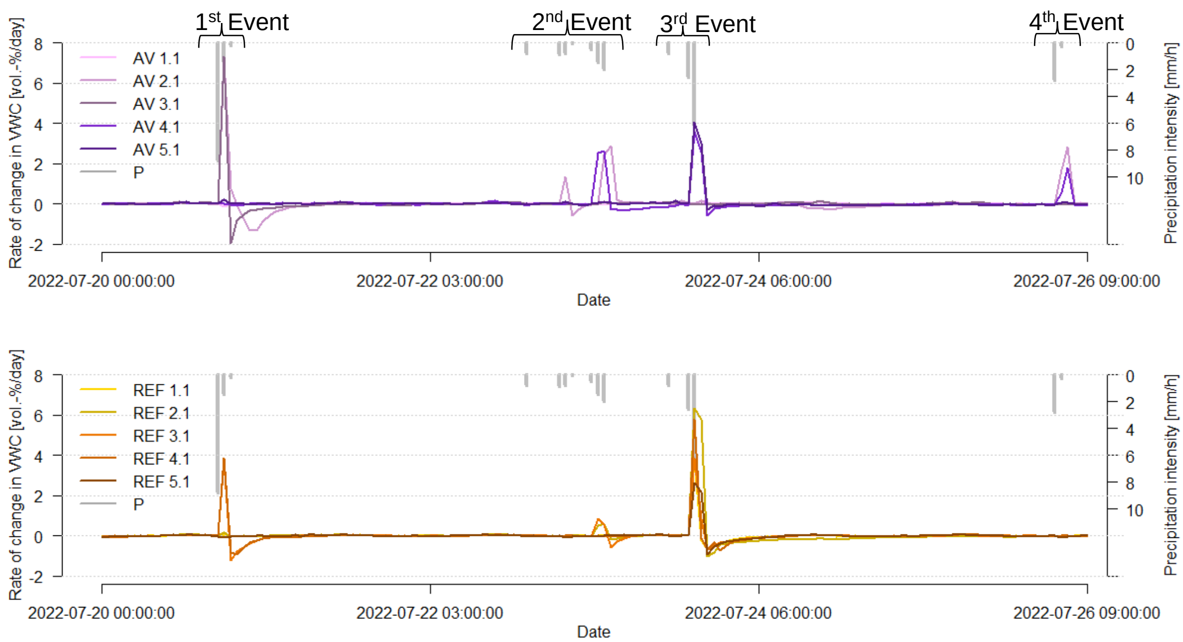


Figure 16: Rate of change ROC in volumetric water content VWC per day during the last week of July including four precipitation P events; top: AV, bottom: REF

### 3.3.2 Water deficit stress based on soil water status

The corresponding averaged soil matric potential of the defined areas AV 1 - 5 and REF 1 - 5 are shown in Figure 17. The soil water was regarded to present a water deficit for winter wheat at volumetric water contents (VWC) lower than 18.5 vol.-% as was suggested by Roohi et al. (2013). This corresponds to a matric potential in the present soil of 12 000 - hPa (4 pF). While the deeper soil (30 - 60 cm) remains below the chosen critical value for water deficit stress of 4 pF, the upper soil (0 - 30 cm) surpasses it in REF on the final sampling day. The area under the panel (AV 1) is the only area in AV that reaches similarly high soil matric potentials like the areas in REF. AV 5 is the only area that does not surpass 4 pF during these six weeks.

Looking at the conitnuation of the time series of the soil water status with original soil matric potential measurements (Figure 15), the measured matric potential in 20 - 30 cm depth do not resemble the converted pF-values based on the bulk volumetric water contens of the upper 30 cm. The measured initial values of AV 3.2, AV 4.2 and AV 5.2 as shown in Figure 15 are lower than the converted final mean values in Figure 17 and the converted final individual values for the corresponding plots. Accordingly, the tensiometers did not indicate water deficit stress at that moment, nor in the further progress of the soil measurements. This includes the dry spell of two weeks during the first half of July.

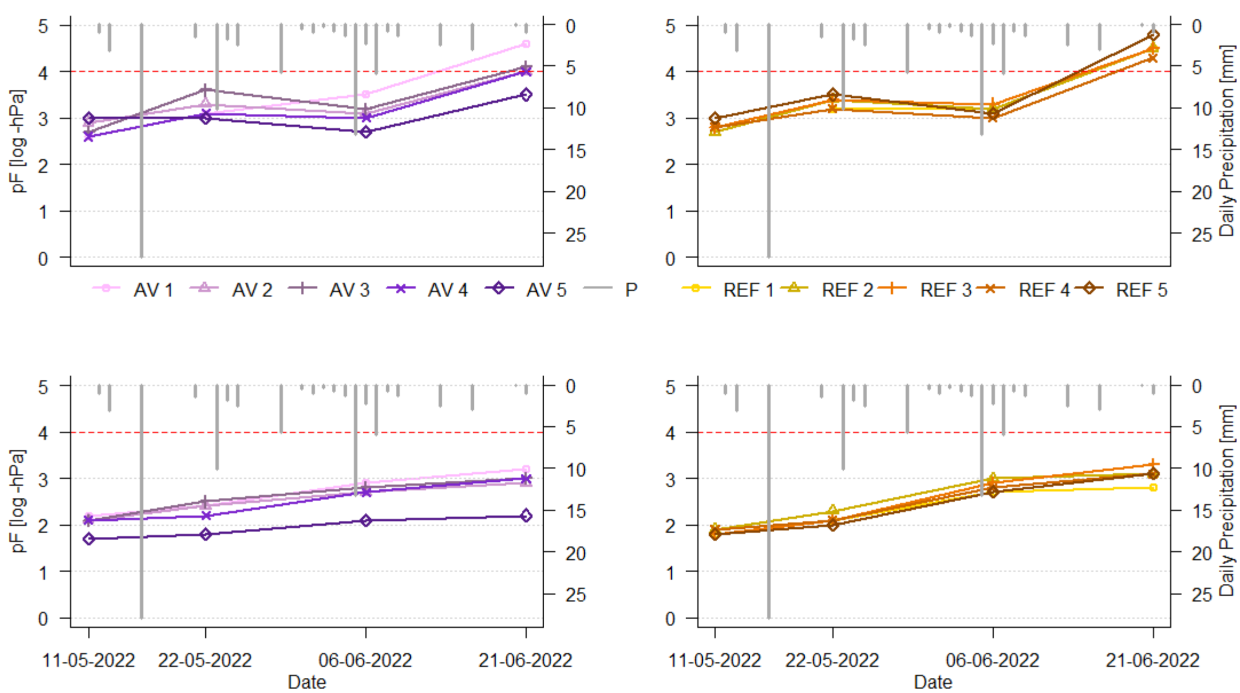


Figure 17: Estimate of the soil water status' in matric potential (pF) derived from bulk soil moisture measurements and the established soil water retention curves for the A and B horizon. Water stress of 4 pF for winter wheat is indicated as dashed red line.; left: AV, right: REF; top: 0 - 30 cm, bottom: 30 - 60 cm

## 3.4 Environmental plant physiology

Plants in REF tended to have more negative leaf water potentials (LWPs), i.e., some of the measured leaves in REF were less hydrated than the majority (Figure 18). Still the means of the predawn (PD) measurements were almost identical, as is indicated by the red squares in Figure 18. For the midday (MD) measurements, the LWP had a wider range in AV and the mean LWP was more negative in REF. Applying a two sample t-test to the MD measurements showed that the difference between the means of 90 LWP measurements at MD in AV and REF each, was statistically significant ($t(144) = 4.336$, $p < 0.001$) with a moderate effect size of approx. $d = 0.7$ (Cohen, 1992). Furthermore, with the Welch Two Sample t-test it can be assumed at a significance level $p < 0.05$ that the LWP measurements in REF have a lower mean (more negative) than in AV.

Computing the coefficient of variation $C_V$ in REF and AV of each measurement day resulted in a similarly wide range of variation in the PD measurements of both AV and REF (Figure 18). The sample means $C_V$ in the PD measurements are approx. identical ($C_V = 0.33$) as can be seen in the third boxplot in Figure 18. In contrast, the means of $C_V$ per measurement day of MD LWP in REF and AV differed in two regards. Mean $C_v$ for LWP at MD was higher in AV and more consistent than in REF. A Welch two-samples t-test showed that at a significance level of $\alpha = 0.05$ the difference in means in $C_v$ per measurement day was statistically significant, with $t(5.6) = 2.49$, $p = 0.049$ and a large effect size of $d = 1.58$ (Cohen, 1992).

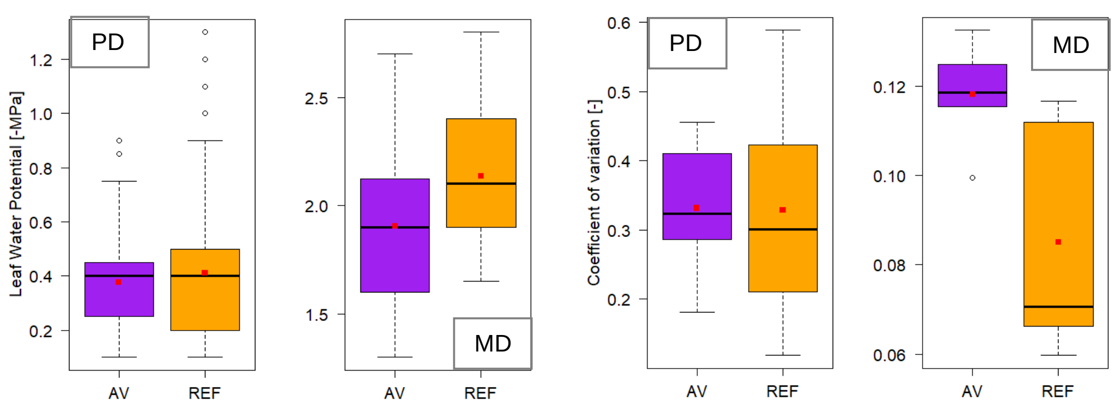


Figure 18: Boxplots of leaf water potential LWP and coefficient of variation $C_V$; left: four boxplots of LWP for predawn PD and midday MD measurements comparing between AV and REF, right: four boxplots of coefficients of variation $C_V$ of LWP calculated for PD and MD per measurement day comparing between AV and REF

Table 12: Computed coefficient of variation $C_V$ for midday leaf water potential LWP in AV for each measurement day and area

| Mean $C_V$ [-] of midday LWP in REF | | | | | | | |
|---|---|---|---|---|---|---|---|
| | 12.05.22 | 25.06.22 | 26.05.22 | 08.06.22 | 19.06.22 | 03.07.22 | Mean |
| REF 1 | 0.14 | 0.15 | 0.06 | 0.05 | 0.02 | 0.06 | 0.11 |
| REF 2 | 0.16 | 0.20 | 0.07 | 0.05 | 0.02 | 0.15 | 0.16 |
| REF 3 | 0.13 | 0.21 | 0.07 | 0.05 | 0.05 | 0.16 | 0.15 |
| REF 4 | 0.09 | 0.17 | 0.09 | 0.10 | 0.13 | 0.14 | 0.15 |
| REF 5 | 0.04 | 0.15 | 0.07 | 0.06 | 0.06 | 0.11 | 0.13 |
| **REF** | 0.11 | 0.07 | 0.06 | 0.07 | 0.12 | 0.14 | **0.11** |
| **Mean $C_V$ [-] of midday LWP in AV** | | | | | | | |
| | 12.05.22 | 25.06.22 | 26.05.22 | 08.06.22 | 19.06.22 | 03.07.22 | Mean |
| AV 1 | 0.21 | 0.10 | 0.15 | 0.06 | 0.12 | 0.18 | 0.21 |
| AV 2 | 0.12 | 0.10 | 0.13 | 0.14 | 0.12 | 0.18 | 0.12 |
| AV 3 | 0.03 | 0.05 | 0.11 | 0.14 | 0.01 | 0.17 | 0.03 |
| AV 4 | 0.09 | 0.07 | 0.08 | 0.19 | 0.13 | 0.20 | 0.09 |
| AV 5 | 0.10 | 0.06 | 0.11 | 0.11 | 0.09 | 0.19 | 0.10 |
| **AV** | 0.12 | 0.10 | 0.12 | 0.13 | 0.12 | 0.18 | **0.12** |

Across ‘repetitions’ of the areas defined by differing throughfall (AVx.1-3), the $C_v$ ranged between 18 % and 20 % during PD measurements. In contrast, MD measurements were more variable with a range of 41 - 55 %.

In Figure 19, it becomes apparent that regular daily precipitation governed the evolution of LWP. The longest period without precipitation was for four days, from the 26th to 28th of May, when the wheat plants in REF were in the development stage of tillering and those in AV were in the stage of stem elongation. On the day before, in sum it rained 27.9 mm. Before the rain events on the 25th of May, the wheat plants were in modest water stress in both REF and AV, made visible in the graphs for MD measurements by the red dashed line indicating the critical value for water stress. The critical value of - 2.2 MPa was exceeded during midday, being more pronounced and less variable among plots in REF (Corso et al., 2020). After the day with highest precipitation in that period, and after the successive dry spell of four days, the LWP of wheat plants was at less negative values in all plots. In the case of REF, during booting, the observation did not exceed the threshold value for water stress. In the middle of anthesis and after regular low daily precipitation depths of < 2.3 mm and two larger precipitation events of 13.2 mm and 5.8 mm, the measured MD LWP in REF was at the threshold level. In contrast, in AV the same measurement was well below that threshold with greater differences between areas. In area AV 4, which is located between the solar panels, the measured wheat plant showed the highest negative LWP while the identified development stage was the end of heading. The measurement during grain filling in both systems was conditioned by eight days of no leaf water potential in both systems were found to be above the threshold again. AV 1 and AV 3 exposed values well over the threshold for water stress. Measured leaf water potentials in REF were more pronounced than in AV. The variability among the areas in AV become more evident just before the beginning of ripening in REF, or the end of grain filling in AV, after it had rained almost every day. AV 1 of all areas in AV, still presented stress at the most negative water potential of - 2.2 MPa. In AV 3 - 5 the wheat plants were under the threshold, with AV 5 presenting the least negative observation. In REF, all plants were found to experience water deficit stress at the end of the measurement campaign. Looking at the PD measurements in the top section of Figure 19 and considering a threshold value for PD LWP of - 1 MPa in winter wheat, this growing season the plants never experienced water stressed that would have detrimental effects on their growth (Jiang et al., 2013).

The midday LWP in AV differed more in their ROC in comparison with the mostly consistent rates in REF. The changes in midday LWP are more consistent over all areas in REF than in AV. On average, the plots AV 1.1 and REF 1.1, have undergone the overall largest difference in PD LWP over time. In general, the areas of AV and REF have undergone similar magnitudes of variation with respect to predawn measurements. Based on the midday measurements, plants in areas of AV showed a larger mean difference than those in REF. In both systems, areas 1 and 5 show a smaller, and the central areas 2 - 4 show a larger variation in midday leaf water potential over time. More specifically, plot REF 3.1 and AV 4.1 have shown the largest difference over time with 1.4 MPa and 1.5 MPa, respectively.
Diurnal changes in LWP have been largest in (REF 3.3) with a difference between PD and MD of 2.5 MPa. Nine plots in REF experienced larger diurnal variations than 2 MPa, in AV it was four plots.

Apart from the observations made on day 210 after sowing (DAS), the wheat plants in REF were always slightly ahead in development (Table 13). Especially as the season progressed, it became visually evident that the plants in REF were more advanced in their development than in AV. They also started the process of ripening earlier. The development stages pre-anthesis progresses slowly in Heggelbach. Afterwards, the wheat plants progressed quickly through their plant development cycle. The plant development stages booting to early grain filling are meant to be especially vulnerable to water stress. AV went unnoticed through the phase of booting, but it took place after the second measurement. In this time frame, water stress increased with each measurement and did not recede until after early grain filling (Sun et al., 2006; Marrou et al., 2013a; Morgun et al., 2020).

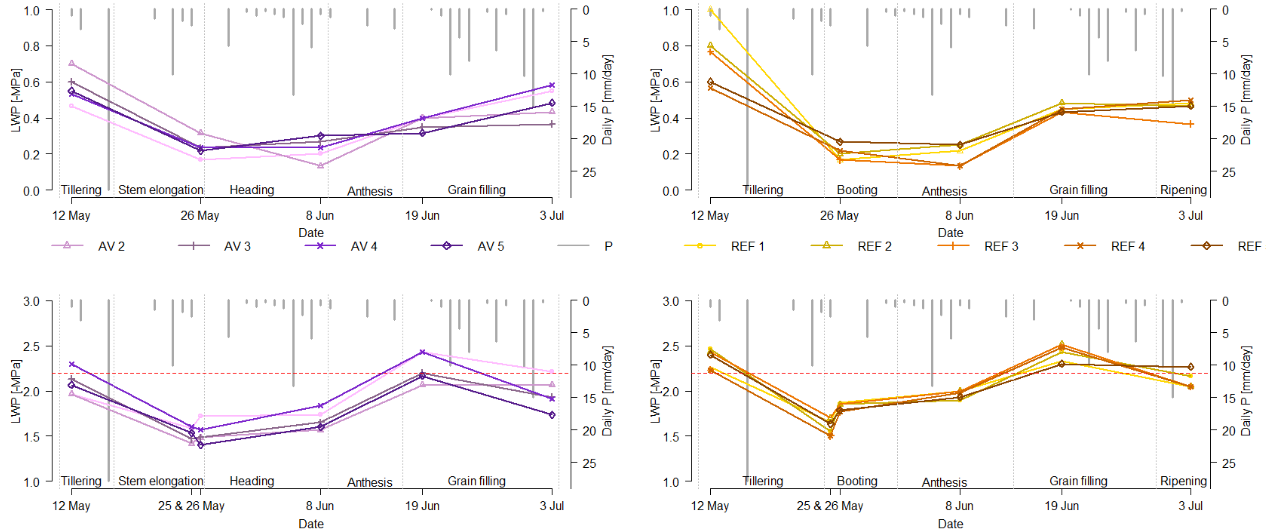

Figure 19: Averaged LWP during different plant development stages. The red dashed line indicates the critical threshold for water stress in MD LWP; left: AV, right: REF; top: PD, bottom: MD

Table 13: Biweekly BBCH from 12th May (210 days after seeding DAS) to 4th July 2022 (251 DAS)

| | 198 DAS | | 210 DAS | | 224 DAS | | 236 DAS | | 251 DAS | |
|---|---|---|---|---|---|---|---|---|---|---|
| | REF | AV | REF | AV | REF | AV | REF | AV | REF | AV |
| Most frequent | 21 | 21 | 39 | 43 | 65 | 59 | 75 | 73 | 83 | 77 |
| Range | 13 - 26 | 12 -24 | 37 - 53 | 37 - 47 | 58 - 65 | 51 - 67 | 71 - 77 | 71 -77 | 77 - 85 | 75 - 85 |

## 3.5 Overall heterogeneity of the water state within the agrivoltaic system

The here considered heterogeneity in AV comprises the spatial variability in soil and plant water status. In Figure 22 the overall soil water status in the time period of the 11th of May to the 21st of June 2022 is represented as mean volumetric water content (VWC) of the first 30 cm of the soil. In Figure 21 the overall plant water status in the time period of the 12th of May to the 3rd of July 2022 is represented as mean midday (MD) leaf water potential (LWP). They also depict the 25 positions of the rain gauges in a colour scale that shows their placement regarding measured cumulative throughfall (TF) with respect to the cumulative areal precipitation in REF $P_{REF}$ of 30 mm, and the minimum and maximum value measured.

The TF depths in AV correspond well to the mean VWC per area in Figure 22. However, even though most TF was measured in area 5, the VWCs in area 4, where TF almost equaled $P_{REF}$, are barely different to the VWCs in area 5. The differences in VWC become apparent between area

5 under the dripping edge and area 1 under the solar panel. Area 3 under the central inner dripping edge exhibits the most inconsistent mean values in VWC.

When looking at the MD LWP, the TF depths in AV do not correspond clearly to the mean LWP per area in Figure 21Figure 22. This is especially visible in areas 2 and 3, where the mean MD LWP is on the higher end of the spectrum and TF for those areas on the lower end. For MD LWP, area 2 exposes the most variable mean values ($C_V = 0.56$). The strongest differences between areas can be seen when comparing the area between solar panels (area 4) and under a panel (area 1) with the designated areas of the dripping edge (areas 2, 4 and 5).

Comparing the mean values for VWC in 0 - 30 cm depth in the areas of AV to those in REF shows that VWC is generally lower in REF, with exception of area 1. The mean MD LWPs in REF are generally more negative than in AV. Also, both variables show a smaller range of values in REF than in AV.

A MANOVA produced the following outcome: Pillai's Trace = 0.48, $F(36, 440) = 1.66$, $p < 0.05$. It indicates at least one statistically significant difference in between the areas regarding their means of VWC in upper and lower soil, and LWP at PD and MD. However, the effect of the variables was not large (Partial Eta Squared = 0.13). Performing a Linear Discriminant Analysis did not help in finding the statistically significant associations between areas and the dependent variables. Comparing the boxplots of all areas and tested variables let only area AV 5 stand out in VWC in 30 - 60 cm depth. Running an individual one-way Analysis Of Variances (ANOVA), to compare the effect of the area on the lower VWC, resulted in a statistically significant difference between at least two areas ($F(9,110) = 2.154$ $p < 0.05$). Tukey's HSD post hoc tests were applied, and significant differences ($p < 0.05$) were detected between the areas AV 5 and AV 1 as well as AV 5 and AV 3. Those differences are also visible in Figure 22.

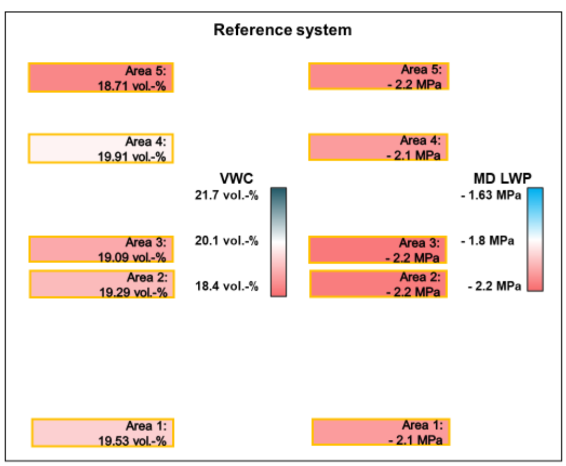


Figure 20: Mean values of VWC in 0 - 30 cm depth and MD LWP in REF

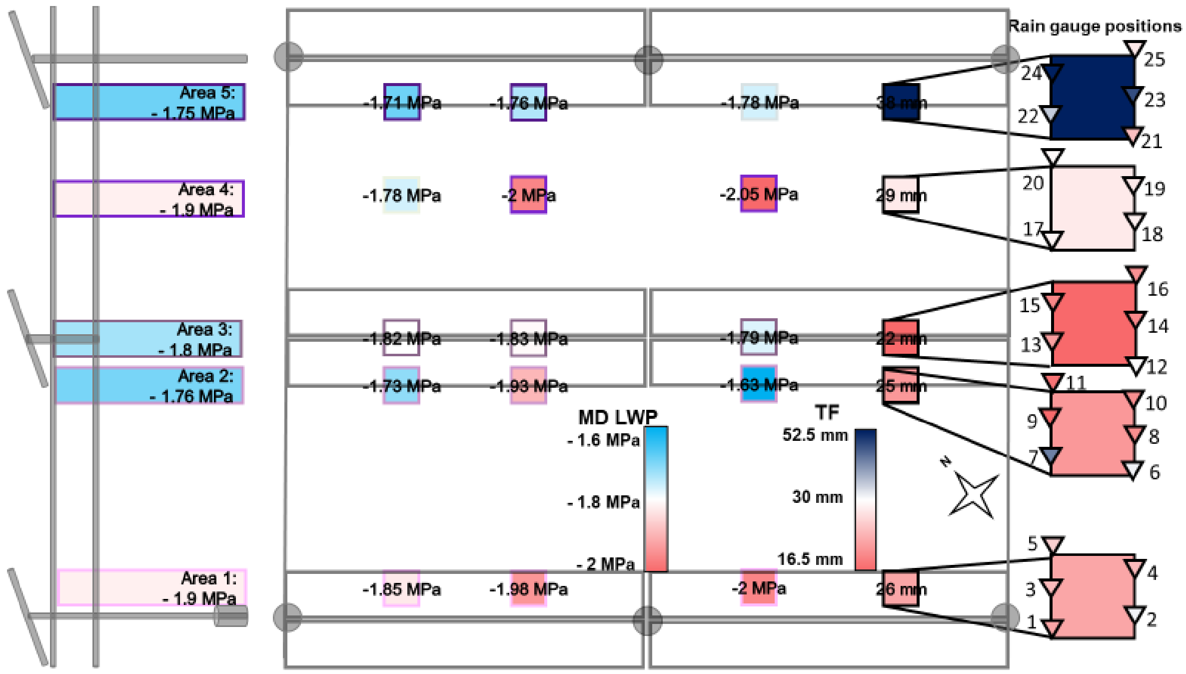


Figure 21: Mean midday LWP over the growing season per plot & area in AV and cumulative throughfall TF per defined area including rain gauge positions 1 - 25. In the colour scale for TF, cumulative $P_{REF}$ = 30 mm is represented in white (adapted from ©HILBER GmbH, 2016)

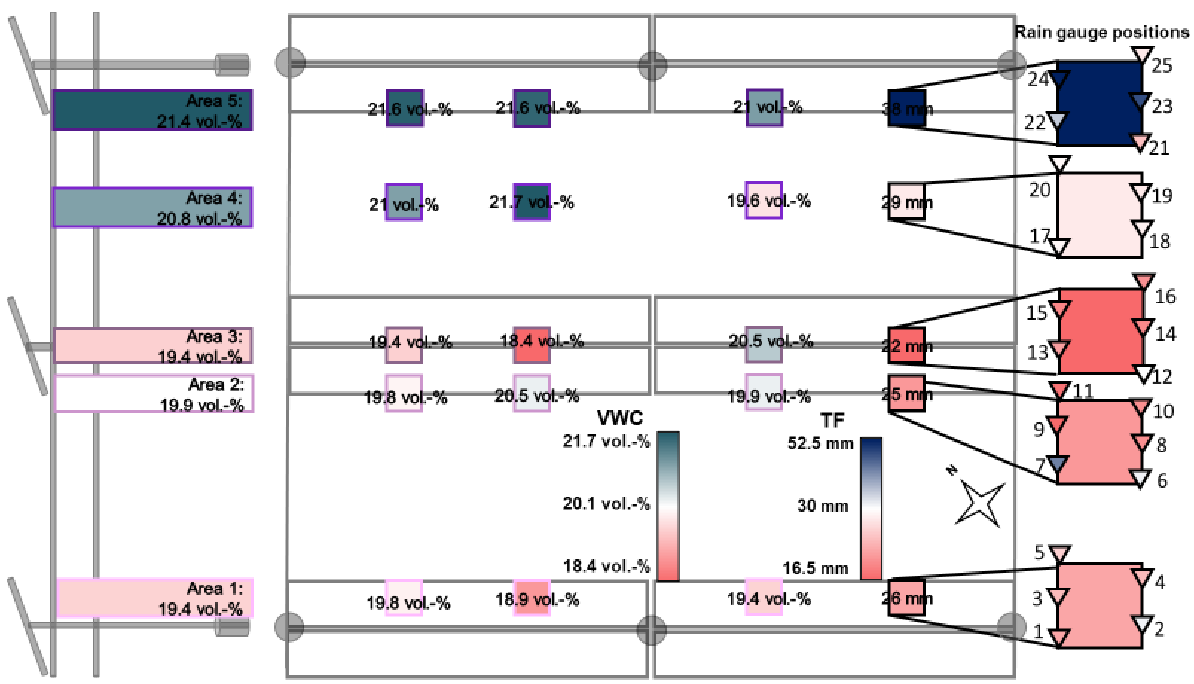


Figure 22: Mean VWC in the upper soil over the growing season per plot & area in AV and cumulative throughfall TF per defined area including rain gauge positions 1 - 25. In the colour scale for TF, cumulative $P_{REF}$ = 30 mm is represented in white (adapted from ©HILBER GmbH, 2016)

# 4 Discussion

## 4.1 Assessing the heterogeneity

The conceptual transfer of interception (IC), throughfall (TF) and stemflow from a context of vegetative forest canopies to an agrivoltaic construction may be debatable seeing that the pathways would differ in their magnitudes and not all established relations, such as regarding biogeochemical cycles, would hold true. While a forest canopy exhibits an irregular pattern of gaps over several branch layers, an agrivoltaic construction constitutes a regular pattern of open stripes and obstructing solar panel rows (Guswa and Spence, 2012). However, it gave a starting point from which to examine the systematic heterogeneity in water distribution based on the modified water fluxes and storages in an AV.

Stemflow is an inevitable component of intercepted precipitation. Within an agrivoltaic system it emanates from the necessity to erect a stable mounting structure for the solar panels. So far, this component of the water balance in an agrivoltaic system has not played a role in assessing the heterogeneity it may contribute to, nor in the utility it could bring to the water management in an agrivoltaic system. In the case of the agrivoltaic system at hand, a part of intercepted precipitation runs down steel pillars and infiltrates uncultivated, green strips along the arable field. In other cases, the mounting structure could contribute to a managed redistribution of the precipitation by harnessing the concentrated water inputs for cultivation. For some crops, such as cereal crops, this might be incommensurable with the field management plan, while for other crops that already rely on a drip irrigation, it may be easier to incorporate the 'stemflow' into the design of the agrivoltaic system. Quantifying this local water flux and its potential contribution to the water uptake of plants nearby and to deep percolation, may give further insights into the various environmental modifications induced by setting up an agrivoltaic system (Levia and Germer, 2015). Area 5 could be a first indication of the influence of local repeated increased water input (Figure 14). Further research is also needed in economic aspects with the purpose of weighing the option of irrigation systems in AVs. The incorporation of irrigation systems could control the heterogeneity within an agrivoltaic system, in this way reducing differences in crop quality and optimising water productivity. How beneficial an irrigation system would be to the farmer depends on the site, the agrivoltaic system design and the cultivated crop.

The assessment of heterogeneity in AV was limited to the events observed. On the base of those events, the moderate Kendall's rank correlation $\tau_b$ between IC and the coefficient of variation ($C_V$), which also exhibited the highest coefficient among the considered variables, supports the statement for the IC to be a driver and measure of heterogeneity (Elamri et al. 2018b).

No extreme event was recorded, thus there has been a bias towards smaller events. So there is no knowledge on the extent to which the agrivoltaic system could redistribute extreme precipitation depths and which consequences for the crops would follow compared to an open field (Levia and Germer, 2015).

Not all defined areas (AV 1 - 5) represented the areas of differing water input they were originally intended to represent (Figure 21). Area 2, which was selected due to the above located dripping edge, had an unexpectedly low water input. It showed TF values corresponding to other areas affected by sheltering. Hence, the positioning of area 2 and therein comprised rain gauges 6 - 11, must have been mispositioned. Since area 2 varied most in TF, it may partially have represented the intended dripping edge (rain gauge position 7) and the neighbouring sheltered area. This illustrates the degree of heterogeneity within AV and the necessity for a high spatial resolution in measurements. IC was found to be correlated with the $C_v$ of TF, but it was not possible to find a clear relation based on the limited number of precipitation events.

It has been shown that it is difficult to compromise the heterogeneity of one agrivoltaic system in one single value, since it can present both almost homogeneous and extremely heterogenous water distributions. Aim of future studies should entail measuring and controlling the maximum possible heterogeneity. Relevant variables to keep in mind are the wind direction, the modified drop size distribution (DSD), the stomatal conductance, interception, throughfall, and stemflow along the mounting structure (Sudmeyer and Speijers, 2007; Elamri et al., 2018b; Abdalla et al., 2022).

### 4.1.1 Confounding variables

The collection of biweekly data, including leaf water potential (LWP), was done in a manner that minimised the confounding variable of fluctuating shade for when drawing conclusions on the heterogeneity in the system based on the relation between the location and the water status. Measurements were carried out in a differently defined order each time, such that the influence of biased light conditions during the day could be blocked. However, even though the variability in water status could be distinguished from confounding effects of shade in this way, the five defined areas as determining factor, do not allow to pinpoint a clear explanatory environmental variable that influences the plant development. The five areas are defined by several variables such as rain and wind shelter, availability of nutrients or soil, of which not all were examined (Wery, 2005). Certainly, no notable inhomogeneities in soil were detected, but spatial variations in soil density could not be excluded due to the lower reliability of the fitted parameters describing the soil structure (Table 10). Areas 2 and 3 could be subject to repeated soil compaction due to agricultural machines considering that they also presented the lowest water status in the absence of intercepting solar panels in REF (Figure 20).

Even though the heterogeneity in light availability was not of interest here, a combined analysis including measurements of radiative and water fluxes could give interesting insights about the timely effect the wandering shade may have on crop processes, such as transpiration (Marrou et al., 2013a). This again links to the interconnected relations of light and water as resources driving stomatal conductance and thus photosynthesis activity. Their interlinked heterogeneities require repeated data of high spatial resolution, ideally on stand, plant, and leaf level to understand interdependencies over several temporal scales and lags (Sudmeyer and Speijers, 2007; Mamun et al., 2022).

### 4.1.2 Root systems against heterogeneity

Another aspect to consider in heterogeneous environments like AVs that was not considered here nor in other studies, is the root systems of different crops and variants. A coping mechanism of plants in reduced light conditions is a lower root:shoot ratio (RSR) to balance the overall plant growth (Seidlova et al., 2009; Marrou et al., 2013b). Less roots imply the plants will devote more energy to above ground biomass seeking for more radiation while devoting less energy to roots in the search for nutrients, and thus water. Elamri et al. (2018a) and Armstrong et al. (2016) found heterogeneous soil moisture to be of limited significance as it was potentially diminished by an active root system and lateral diffusion (Guswa and Spence, 2012). However, if the RSR of a crop adapts a lower value in response to limited light availability, spatial differences could become more significant. The implications for the root water uptake in heterogeneous soil water conditions vary vastly among crops (Cernusak et al., 2016). A closer monitoring of the root development in AVs could help in understanding morphological adaptions to reduced light availability, heterogenous soil water conditions and their interrelationship (Yadav et al., 2018). How does the imposed shade affect a crops' root development? And how will an adapted root system perform in heterogeneous soil water conditions? Root systems and root growth behaviour could be criteria for the suitability of a crop in an AV next to the shade tolerance. The deeper soil (30 - 60 cm) was shown to be more inert in their soil water status as it remained relatively unaffected by spatially heterogeneous environmental conditions caused by both modifications in radiation and water fluxes (Figure 14). Crops that either develop heterogeneous root systems in the surface soil or deep root systems, may be unaffected by spatial and temporal heterogeneous soil water conditions in the upper soil of an AV (Guswa and Spence, 2012; Armstrong et al., 2016; Elamri et al., 2018a). Elamri et al. (2018a) looked at these relations with lettuce, where solely the upper soil plays a relevant role. Generally, the root development under modified microclimatic conditions, including changes to the radiation and evapotranspiration processes, is a research gap that needs further investigations (Steduto et al., 2007; Cernusak et al., 2016; Cai et al., 2021).

### 4.1.3 Approaches to address heterogeneity

The severity of heterogeneity depends on the climate, the design of the agrivoltaic system as intercepting structure, and the cultivated crop (Jackson, 2000; Dupraz et al., 2011; Guswa and Spence, 2012; Levia and Germer, 2015; Hassanpour Adeh et al., 2018). For the design of an agrivoltaic system (tilt of solar panels, orientation, height, panel edges) or the assessment of a potential site, it will be necessary to consider environmental factors such as the dominant wind direction at the location as they will influence the redistribution of precipitation in the facility (Elamri et al., 2018b; Hassanpour Adeh et al., 2018). The design of the agrivoltaic system as an artificial structure in an agricultural landscape needs to be planned accordingly to enhance beneficial impacts and mitigate adverse heterogeneities (Armstrong et al., 2016). Even small considerations, such as the design of the panel edges may mitigate erosion and damages to young crops (Smegal et al.; Elamri et al., 2018b). Further research is needed to assess the severity of erosion of the upper soil caused by the dripping edge at agrivoltaic sites with high inclination.

Similar to the frameworks presented by Trommsdorff et al. (2021) and Laub et al. (2022), crops and their suitability for cultivation in agrivoltaic systems could be re-evaluated considering their water requirements and ability to adapt to heterogenous conditions. Such a framework should ensure that the agricultural productivity in dependence on water conditions will play a role when designing a site-specific agrivoltaic system (Cassel et al., 2000; Mamun et al., 2022).

## 4.2 Assessing the water status in AV

The determination of timely occurrences of dry spells as part of assessing the soil and plant water deficit, was based on continuous precipitation data from the weather stations in Heggelbach and Billafingen. Even though precipitation at REF and the weather station in Heggelbach were in significant concordance, the data analysis revealed precipitation events that were not recorded at the station in Heggelbach. This may be because tipping bucket gauges used at the site, are prone to random errors. Mechanical or electronical malfunctions may have resulted in missing hourly precipitation depths. Clogging was witnessed and resolved once during the measurement campaign. However, precipitation measurements were not corrected. Considering the data at hand, adjusting the precipitation values based on a physical model might distort the results unreasonably as uncertainties in regards to the sources of error cannot fully be explained yet (Sevruk, 1996).

Also, rather less intense precipitation events were observed which tend to increase systematic discrepancies between actual and measured precipitation with a tipping bucket gauge (Sevruk, 1996). Indeed, Table 5 shows that precipitation at the weather station tends to underestimate precipitation measured with the manually read cone rain gauges in REF. Unlike what is recommended by the 'Deutscher Wetterdienst' (DWD) for precipitation measurements of the highest class, the weather station in Heggelbach is located at a relatively steep slope such that it might be exposed to irregular wind conditions (Löffler, 2012). Missing measured precipitation values at the station in Heggelbach could also indicate the occurrence of spatially distributed thunderstorm cells in the hilly area. Considering that the weather station was only installed recently, this increases the uncertainty of the data and complicates its correction. For the assessment of the water status at REF and AV, the discrepancies have been deemed not relevant enough to apply a correction. Especially because of the short time series, which only provides a limited insight into potential error sources, no correction factor was applied, meaning the reported absolute precipitation depths may be inaccurate. The combined use with the precipitation data from the weather station in Billafingen was considered appropriate for the purpose of documenting the relative water inputs during the growing season.

### 4.2.1 Surface water balance

The observations regarding the soil water status are mainly limited to the upper 30 cm of the arable soil. The determined VWCs for the bulk soil of 0 - 30 cm and 30 - 60 cm could have aided in estimating the actual evapotranspiration $ET_a$ from a simplified root zone water balance that assumes deep percolation DP to equal zero in dry conditions and neglects capillary rise (Baser et al., 2004; Plaut, 2005; Marrou et al., 2013a; Elamri et al., 2018b; Alghory and Yazar, 2019):

$$\Delta S = P - E - T - DP$$

The change of storage ΔS only encompasses the change of soil moisture in the root zone due to evaporation E and transpiration T. However, for this assumption to be acceptable, dry conditions of two weeks were required. Dry conditions without precipitation input have never lasted longer than four days with one exception in July. However, collected soil moisture data in root depth did not cover the only occurring two-week dry spell recorded in July (Figure 15 and Figure 17).

### 4.2.2 Assessment of a water deficit based on the soil water status

The continuous data of VWC obtained with the aid of the TDR-sensors did not deliver a reliable source of the soil water status. Due to the sensor installation in wet conditions, they did not represent the actual soil water status during the only longer dry spell in July and never reached the same soil moisture level. This led to uncertainties too great to draw reliable conclusions from. As a solution, the rate of change (ROC) was computed but also showed inconsistencies. After uninstalling the sensors, the surrounding soil and the sensors were inspected for irregularities such as rocks or damages but did not deliver a possible explanation.

The measurements of the soil water potential with three tensiometers indicated that no water deficit stress was induced in the upper root zone in 20 cm depth of the plots AV 3.2, 4.2, and 5.2. In contrast, the indirect matric potential calculated from the bulk VWCs showed the inset of water deficit stress at the end of June, if referred to the critical value of - 12 000 hPa (4 pF ≈ 18.5 vol.-%) as suggested by Roohi et al. (2013) or if referred to the calculated wilting point (4.2 pF) in the A horizon of AV. According to Plaut et al. (2005) and Morgun et al. (2020), water deficit stress in winter wheat can be induced at a soil moisture level of below 30 - 33 % of the $\theta_{FC}$. At the site, this corresponds to a soil moisture of 10.3 vol.-%, or 5.7 pF, none of which were reached. Considering the soil water status, in a stricter sense, winter wheat had not experienced a severe water deficit stress in AV nor in REF during the plant development stages in 2022. The only considerable dry spell of two weeks in July coincided with the ripening stage of winter wheat, when the root water uptake is already becoming redundant to the crops' final development stage.

The biweekly bulk measurements in 30 - 60 cm soil depth revealed a significant difference between the area under a dripping edge and the other areas (Figure 14). A reason could be the increased TF combined with a decreased root water uptake from deeper soils as water was readily available in the surface soil at the dripping edge. The assessment of the water deficit stress in plants based on the bulk soil water status is only a rough approximation of a plants' water status as it fails to represent the various water gradients across the rhizosphere. Evaluating the actual plant water status requires not only to look at the soil water status, but again a detailed look into the root system and hydraulic conductivities to understand which soil water pool was accessed by the plant (Wallace et al., 1983; Cernusak et al., 2016).

### 4.2.3 Assessment of a water deficit based on the plant water status

The assessment of the plant water status through the leaf water potential (LWP) at midday (MD) revealed that the winter wheat plants were not exposed to longer severe water deficit stress. However, a higher variability of MD LWP in AV was evident compared to REF (Figure 18). Since MD LWP is a proxy for maximum daily water deficit stress in plants, this result speaks for the winter wheat plants in AV having experienced water stress to different degrees depending on their location on the same day.

In addition, the biweekly documentation of LWP may not be frequent enough to represent the history of water stress during the growing season (Karamanos and Papatheohari, 1999). Especially in an AV a higher resolution of LWP measurements not only in space but also in time would be recommendable to gain a better understanding on the modified water status in context of the developing stages, since a temporal lag in the water balance is suspected (Marrou et al., 2013a; Elamri et al., 2018a). This would also aid the validation of models, such as the one in development by Chopard et al. (2021), which simulates daily LWP at predawn (PD) to facilitate a dynamic strategy of irrigation and tracking of the solar panels. It should be ensured that PD measurements are conducted with highest possible care. During the measurement campaign with regular rain, it became evident that if the LWP approached zero, the reading of the measurement from the Scholander pressure bomb became increasingly inaccurate despite adjusting the rate valve that controls the rate at which the chamber is pressurised.

### 4.2.4 Soil water potential vs. volumetric water content

The last measurement of the volumetric water contents (VWC) overlapped in time with the measurements of the matric potential by the tensiometers. Using the established water retention curve to compare the soil water status depicted by the different methods did not show consistent results for the three plots. Inaccuracies in the conversion from measured VWC to matric potential are to be expected and could be attributed to hysteresis (Blume et al., 2011). However, the approximation fails to verify the plots exhibiting lowest or highest water potential given by the tensiometer measurements. One explanation for the discordance between the two different methods, could be that the point measurements of matric potential do not accurately represent the bulk soil moistures of 0 - 30 cm and vice versa. The misalignment could also be attributed to the fitted parameters of the van Genuchten equation that was used to derive the corresponding VWC or matric potentials. Compaction of the soil samples during collection could have led to an overestimation of the VWC at considered pressure heads in the van Genuchten model. Indeed, the estimated matric potential of the bulk soil moisture (0 - 30 cm) derived from the soil retention curve tends to be higher than the directly measured matric potential.

Preferential flow or stagnation of water are influencing factors that could explain the rapid increase in matric potential in response to precipitation events. Possibly for that reason, the tensiometers in plots AV 4.2 and AV 5.2 reached 0 pF and stopped working at that point. Because the ploughing pan was found to be at 22 cm depth only after installment of the tensiometers at a 20 cm depth and the soil texture was found to be silty loam, stagnating water in that soil layer is likely to have influenced the measurements (Audu et al., 2022).

Next to the measured matric potential, the data collected by the tensiometer revealed furthermore on average 1.2 °C higher soil temperatures and stronger diurnal fluctuations in soil temperature in plot AV 4.2 than in the plots under the solar panel and the dripping edge (Figure 15). AV 4.2 should compare to REF as it is situated between panel rows. This confirms observations made at the site by Weselek et al. (2021a).

Overall, it must be noted that only edaphic induced water stress was looked at, even though the atmospheric water demand also contributes to the water stress experienced by crops and is expected to change in AVs (Marrou et al., 2013b; Armstrong et al., 2016; Hassanpour Adeh et al., 2018). Marrou et al. (2013b) found the atmospheric water demand to be reduced in the solar panel's shade, leading to a reduction in $ET_a$. In the light of climate change, the atmospheric demand is attributed an increasingly important role as driver for water deficit stress in plants and should be further investigated if agrivoltaics is to be a measure of climate adaption. However, primary role was given to soil-plant interactions since they are more correlated to the temporal scale of one growing season (Novick et al., 2016; Yuan et al., 2019).

## 4.3 AV as a measure for climate adaption

The Deutscher Bauernverband (2022) has stated in its press release that the overall quality of the cereal has suffered from dry periods in 2022. Some regions have experienced little precipitation since March 2022 onwards, while others have not. The high variability in quality was attributed to the regional distribution of precipitation (Deutscher Bauernverband, 2022). In Heggelbach, only two dry spells were evident before harvesting this year: The whole month of March and two weeks in July presented little and no precipitation, respectively. During March 2022, the winter wheat in AV and REF had not passed the vegetative developing stage of tillering (BBCH 20 - 29) yet. Tillering is considered to be vulnerable to water deficit stress but less relevant for the grain yield (Trimble, 2005; Sun et al., 2006; Yadav et al., 2018). The measurement campaign had not yet started at that point. By the beginning of the dry spell in July, the measurement campaign had ended since the wheat plants were mostly already in the stage of ripening. Posterior measurements were not intended due to the inset of senescence in the leaves, that makes measurements regarding plant physiology, water status and productivity redundant. Thus, this year's investigations were governed by rather wet conditions, which limits the ability to make any judgements on the effect AV has on the water status and development of winter wheat in dry conditions compared to REF.

While in temperate regions like Heggelbach the main limiting factor for crop growth is light availability, or more precisely, PAR, in (semi-)arid regions, where excessive radiation may cause stress to the plants, it is water availability (Beck et al., 2012; Armstrong et al., 2016; Hassanpour Adeh et al., 2018). Agrivoltaics as an adaption measure against climate change in arid areas has therefore been pointed out repeatedly (Beck et al., 2012; Hassanpour Adeh et al., 2018; Barron-Gafford et al., 2019; Fraunhofer Institute for Solar Energy Systems ISE, 2022). In this study, despite the rather wet conditions that lasted during the growing season in 2022, the reduction of water deficit stress for winter wheat in some locations of AV relative to REF was reflected in both soil and plant water status. The illustrated difference could be of significance in drier years or regions.

AVs may exhibit more benefits in water limited regions, however the presence of the solar panels and their associated dripping edges poses a higher risk for erosion, especially on dry, bare soil. The potential eroding effect an AV may have on such soil should therefore not be depreciated. A way to mitigate this risk, would be the inclusion of erosion modules in the simulation of modified water fluxes in AVs. This could entail looking more closely at relevant variables such as the modified raindrop size distribution (DSD) in an AV (Laws and Parsons, 1943; McCool et al., 2009)

# 5 Conclusion

Since its first proposal by Goetzberger and Zastrow (1982), the concept of agrivoltaics has come a long way. The proof-of-concept has been provided in various settings worldwide. Not only has the implementation of agrivoltaics confirmed expected beneficial synergies within the water-energy-food nexus but also, they have substantiated issues that need to be addressed for an optimised application of agrivoltaics. One of these issues consists in the inherent heterogeneity of the agrivoltaic system. To date, the heterogeneity in water distribution caused by agrivoltaic systems is not understood sufficiently for it to be avoided or controlled.

The presented study contributes to a better understanding of the heterogeneous water distribution within an elevated, rainfed agrivoltaic system by making use of the concept of interception, throughfall and 'stemflow'. While areas affected by interception and throughfall were identified, the latter water flux remains an unknown variable in the context of agrivoltaic systems. Depicting varying throughfall and interception with a high spatial resolution of measurements in an uncontrolled setting over eight precipitation events showed the degrees to which the rainwater input was modified by the agrivoltaic construction. The heterogeneity in throughfall was moderately concordant to the wind coming from the South and the interception depth. However, the collected throughfall data did not sufficiently the various outcomes in heterogeneity of throughfall. A higher temporal solution in throughfall measurements would contribute to a further understanding of variables driving the heterogeneity.

The differences in soil and plant water statuses between the agrivoltaic and the reference systems were made evident by looking at the volumetric soil water content, the soil matric potential and the leaf water potential. Significant differences were limited to the volumetric water content in 30 - 60 cm depth between the area under a dripping edge and sheltered areas underneath solar panels, signalising larger differences in soil moisture within the agrivoltaic system than compared to the reference system. Closer investigations on the root development of plants in spatially heterogeneous soil conditions, could assist in assessing whether this could be significant for crops.

Leaf water potential as a selected measure of the plant water status was a reliable method to monitor the water deficit stress and revealed differences between areas corresponding to the observed differences in soil water status, though to no significance. However, a significantly higher mean in coefficient of variation for each measurement day, indicated a stronger variability in midday leaf water potential within the agrivoltaic system than compared to the reference system. During the growing season in 2022, no water deficit stress was observed that affected the winter wheat during a crucial development stage. Therefore, the potential benefits in dry conditions for winter wheat to be cultivated in the agrivoltaic system are still unverified.

This work has been conducted in response to the concerns raised by the farmers in Heggelbach and addresses issues observed in their facility. Therefore, the reported spatial heterogeneities in interception, throughfall, soil and plant water status may be limited in their transferability. The results are at least constrained to agrivoltaic installations with a clear height (Category I) and to hilly locations with a maritime climate and winter wheat as cultivated crop (DIN Deutsches Institut für Normung e. V., 2021). They exemplify the spatial heterogeneity in Heggelbach to emphasise the necessity of individually examining existing and potential agrivoltaic sites with the aim to optimise the water distribution and suggest solutions to site-specific requirements and circumstances. By doing so, this study gives a starting point from which to further optimise agrivoltaic systems. An interdisciplinary exchange of lessons learned that incorporates considerations on water management in rainfed agrivoltaic systems in both dry and wet conditions is advocated for.

## References


Abdalla, M., Ahmed, M.A., Cai, G., Wankmüller, F., Schwartz, N., Litig, O., Javaux, M., Carminati, A., 2022. Stomatal closure during water deficit is controlled by below-ground hydraulics. Annals of botany 129 (2), 161–170.

Alghory, A., Yazar, A., 2019. Evaluation of crop water stress index and leaf water potential for deficit irrigation management of sprinkler-irrigated wheat. Irrig Sci 37 (1), 61–77.

Amaducci, S., Yin, X., Colauzzi, M., 2018. Agrivoltaic systems to optimise land use for electric energy production. Applied Energy 220, 545–561.

Armstrong, A., Ostle, N.J., Whitaker, J., 2016. Solar park microclimate and vegetation management effects on grassland carbon cycling. Environ. Res. Lett. 11 (7), 74016.

Audu, V., Ruf, T., Vogt-Kaute, W., Emmerling, C., 2022. Changes in microbial biomass and activity support ecological intensification of marginal land through cultivation of perennial wheat in organic agriculture. Biological Agriculture & Horticulture 38 (3), 202–215.

Barron-Gafford, G.A., Pavao-Zuckerman, M.A., Minor, R.L., Sutter, L.F., Barnett-Moreno, I., Blackett, D.T., Thompson, M., Dimond, K., Gerlak, A.K., Nabhan, G.P., Macknick, J.E., 2019. Agrivoltaics provide mutual benefits across the food–energy–water nexus in drylands. Nat Sustain 2 (9), 848–855.

Baser, I., Sehirali, S., Orta, H., Erdem, T., Erdem, Y., Yorgancilar, Ö., 2004. Effect of different water stresses on the yield and components of winter wheat. Cereal Research Communications 2004 (32), 218–223.

Beck, M., Bopp, G., Goetzberger, A., Obergfell, T., Reise, C., Schindele, S., 2012. Combining PV and food crops to agrophotovoltaic. Optimization of orientation and harvest. In: EU PVSEC Proceedings (Editor), Combining PV and Food Crops to Agrophotovoltaic - Optimization of Orientation and Harvest, München, pp. 4096–4100.

Blume, H.-P., Stahr, K., Leinweber, P., 2011. Bodenkundliches Praktikum. Eine Einführung in pedologisches Arbeiten für Ökologen, insbesondere Land- und Forstwirte, und für Geowissenschaftler. Spektrum Akademischer Verlag, Heidelberg.

Brady, N.C., Weil, R.R., 2002. The Nature and Properties of Soils. Soil water characteristics and behaviour. Pearson, Prentice Hall, NJ.

Bundschuh, B., Hintemann, T., Boer, H. de, 2022. Stationskarte. Billafingen. https://www.wetter-bw.de/Agrarmeteorologie-BW/Wetterdaten/Stationskarte. Accessed August 14, 2022.

Cai, G., Carminati, A., Abdalla, M., Ahmed, M.A., 2021. Soil textures rather than root hairs dominate water uptake and soil-plant hydraulics under drought. Plant Physiol 187 (2), 858–872.

Cassel, D.K., Nielsen, D.R., 1986. Field Capacity and Available Water Capacity. In: A. Klute, (Keine Angabe) (Editors), Methods of Soil Analysis - Part 1. Physical and Mineralogical Methods. American Society of Agronomy, Inc., Soil Science Society of America, Inc., Madison, Wisconsin USA, pp. 901–924.

Cassel, D.K., Wendroth, O., Nielsen, D.R., 2000. Assessing Spatial Variability in an Agricultural Experiment Station Field: Opportunities Arising from Spatial Dependence. Agronomy Journal 92 (4), 706–714. /10.2134/agronj2000.924706x.

Cernusak, L.A., Barbour, M.M., Arndt, S.K., Cheesman, A.W., English, N.B., Feild, T.S., Helliker, B.R., Holloway-Phillips, M.M., Holtum, J.A.M., Kahmen, A., McInerney, F.A., Munksgaard, N.C., Simonin, K.A., Song, X., Stuart-Williams, H., West, J.B., Farquhar, G.D., 2016. Stable isotopes in leaf water of terrestrial plants. Plant, cell & environment 39 (5), 1087–1102.

Chopard, J., Bisson, A., Lopez, G., Persello, S., Richert, C., Fumey, D., 2021. Development of a Decision Support System to Evaluate Crop Performance under Dynamic Solar Panels. In: AIP Conference Proceedings (Editor), AIP Conference Proceedings, pp. 1–7.

Cohen, J., 1992. A Power Primer. American Psychological Association 1992 (112), 155–159.

Cook, L.M., McCuen, R.H., 2013. Hydrologic Response of Solar Farms. J. Hydrol. Eng. 18 (5), 536–541.

Corso, D., Delzon, S., Lamarque, L.J., Cochard, H., Torres-Ruiz, J.M., King, A., Brodribb, T., 2020. Neither xylem collapse, cavitation, or changing leaf conductance drive stomatal closure in wheat. Plant, cell & environment 43 (4), 854–865.

Deutscher Bauernverband, 2022. Bauernverband - Erntebilanz 2022. Rukwied: Wiederum unterdurchschnittliche Ernte, Berlin.

DIN Deutsches Institut für Normung e. V., 2021. 91434:2021-05. Agri-photovoltaic systems – 27.160, 65.020.01. Beuth Verlag GmbH, Berlin. https://dx.doi.org/10.31030/3257526. Accessed October 23, 2022.

Dinesh, H., Pearce, J.M., 2016. The potential of agrivoltaic systems. Renewable and Sustainable Energy Reviews 54, 299–308.

Donovan, L., Linton, M., Richards, J., 2001. Predawn plant water potential does not necessarily equilibrate with soil water potential under well-watered conditions. Oecologia 129 (3), 328–335.

Dupraz, C., Marrou, H., Talbot, G., Dufour, L., Nogier, A., Ferard, Y., 2011. Combining solar photovoltaic panels and food crops for optimising land use: Towards new agrivoltaic schemes. Renewable Energy 36 (10), 2725–2732.

Elamri, Y., Cheviron, B., Lopez, J.-M., Dejean, C., Belaud, G., 2018a. Water budget and crop modelling for agrivoltaic systems: Application to irrigated lettuces. Agricultural Water Management 208, 440–453.

Elamri, Y., Cheviron, B., Mange, A., Dejean, C., Liron, F., Belaud, G., 2018b. Rain concentration and sheltering effect of solar panels on cultivated plots. Hydrol. Earth Syst. Sci. 22 (2), 1285–1298.

Fischer, H., 2010. Das aktuelle Laborkochbuch. Institut für Bodenkunde und Standortslehre der Universität Hohenheim, Hohenheim.

Fraunhofer Institute for Solar Energy Systems ISE, 2022. Agri-Photovoltaik: Chance für Landwirtschaft und Energiewende. Ein Leitfaden für Deutschland | Stand April 2022, Freiburg i. Br.

Goetzberger, A., Zastrow, A., 1982. On the Coexistence of Solar-Energy Conversion and Plant Cultivation. International Journal of Solar Energy 1 (1), 55–69.

Grange, S.K., 2014. Technical note: Averaging wind speeds and directions.

Gunn, R., Kinzer, G.D., 1949. The terminal velocity of fall for water droplets in stagnant air. Journal of Meteorology 1949 (6), 234–248.

Guswa, A.J., Spence, C.M., 2012. Effect of throughfall variability on recharge: application to hemlock and deciduous forests in western Massachusetts. Ecohydrol. 5 (5), 563–574.

Hassanpour Adeh, E., Selker, J.S., Higgins, C.W., 2018. Remarkable agrivoltaic influence on soil moisture, micrometeorology and water-use efficiency. PloS one 13 (11), e0203256.

Hernandez, R.R., Easter, S.B., Murphy-Mariscal, M.L., Maestre, F.T., Tavassoli, M., Allen, E.B., Barrows, C.W., Belnap, J., Ochoa-Hueso, R., Ravi, S., Allen, M.F., 2014. Environmental impacts of utility-scale solar energy.

IPCC, 2022. Climate Change 2022: Mitigation of Climate Change. Working Group III contribution to the Sixth Assessment Report of the Intergovernmental Panel on Climate Change, Cambridge, UK and New York, NY, USA.

Jackson, N.A., 2000. Measured and modelled rainfall interception loss from an agroforestry system in Kenya. Agricultural and Forest Meteorology 2000 (100), 323–336.

Jiang, J., Huo, Z., Feng, S., Kang, S., Wang, F., Zhang, C., 2013. Effects of deficit irrigation with saline water on spring wheat growth and yield in arid Northwest China. J. Arid Land 5 (2), 143–154.

Karamanos, A.J., Papatheohari, A.Y., 1999. Assessment of Drought Resistance of Crop Genotypes by Means of the Water Potential Index. Crop Sci. 39 (6), 1792–1797.

Kendall, M.G., 1945. The treatment of ties in ranking problems. Biometrika 33 (3), 239–251.

Knipfer, T., Bambach, N., Hernandez, M.I., Bartlett, M.K., Sinclair, G., Duong, F., Kluepfel, D.A., McElrone, A.J., 2020. Predicting Stomatal Closure and Turgor Loss in Woody Plants Using Predawn and Midday Water Potential. Plant physiology 184 (2), 881–894.

Krug, K., 2022. Hofgemeinschaft Heggelbach. https://hofgemeinschaft-heggelbach.de/. Accessed October 22, 2022.

Lancashire, P.D., Bleiholder, H., van Boom, T. den, Langelüddeke, P., Stauss, R., Weber, E., Witzenberger, A., 1991. A uniform decimal code for growth stages of crops and weeds. Ann Applied Biology 119 (3), 561–601.

Laub, M., Pataczek, L., Feuerbacher, A., Zikeli, S., Högy, P., 2022. Contrasting yield responses at varying levels of shade suggest different suitability of crops for dual land-use systems: a meta-analysis. Agron. Sustain. Dev. 42 (3), 1–13.

Laws, J.O., Parsons, D.A., 1943. The relation of raindrop-size to intensity. Trans. AGU 24 (2), 452.

Lecoeur, J., Wery, J., Turc, O., 1992. Osmotic adjustment as a mechanism of dehydration postponement in chickpea (Cicer arietinum L.) leaves. Plant Soil 144 (2), 177–189.

Lecoeur, J., Wery, J., Turc, O., Tardieu, F., 1995. Expansion of pea leaves subjected to short water deficit: cell number and cell size are sensitive to stress at different periods of leaf development. J Exp Bot 46 (9), 1093–1101.

Levia, D.F., Germer, S., 2015. A review of stemflow generation dynamics and stemflow-environment interactions in forests and shrublands. Rev. Geophys. 53 (3), 673–714.

Li, F., Meng, P., Fu, D., Wang, B., 2008. Light distribution, photosynthetic rate and yield in a Paulownia-wheat intercropping system in China. Agroforest Syst 74 (2), 163–172.

Li, H., Jiang, D., Wollenweber, B., Dai, T., Cao, W., 2010. Effects of shading on morphology, physiology and grain yield of winter wheat. European Journal of Agronomy 33 (4), 267–275.

Li, X., Cai, J., Li, H., Bo, Y., Liu, F., Jiang, D., Dai, T., Cao, W., 2012. Effect of Shading from Jointing to Maturity on High Molecular Weight Glutenin Subunit Accumulation and Glutenin

Macropolymer Concentration in Grain of Winter Wheat. Journal of Agronomy and Crop Science 198 (1), 68–79.

Lipiec, J., Doussan, C., Nosalewicz, A., Kondracka, K., 2013. Effect of drought and heat stresses on plant growth and yield: a review. International Agrophysics 27 (4), 463–477.

Lopes, M.S., Rebetzke, G.J., Reynolds, M., 2014. Integration of phenotyping and genetic platforms for a better understanding of wheat performance under drought. Journal of experimental botany 65 (21), 6167–6177.

Mamun, M.A.A., Dargusch, P., Wadley, D., Zulkarnain, N.A., Aziz, A.A., 2022. A review of research on agrivoltaic systems. Renewable and Sustainable Energy Reviews 161, 112351.

Marrou, H., Dufour, L., Wery, J., 2013a. How does a shelter of solar panels influence water flows in a soil–crop system? European Journal of Agronomy 50, 38–51.

Marrou, H., Guilioni, L., Dufour, L., Dupraz, C., Wery, J., 2013b. Microclimate under agrivoltaic systems: Is crop growth rate affected in the partial shade of solar panels? Agricultural and Forest Meteorology 177, 117–132.

McCool, D.K., Williams, J.D., Morse, J.R., 2009. Raindrop Characteristics in the Pacific Northwest, Reno, Nevada.

Meier, U., 2001. BBCH Monografie. Entwicklungsstadien mono- und dikotyler Pflanzen, Berlin.

METER Group AG, 2019. 5TM Manual. METER Group AG, München.

Morgun, V.V., Stasik, O.O., Kiriziy, D.A., Sokolovska-Sergiienko, O.G., Makharynska, N.M., 2020. Effects of drought at different periods of wheat development on the leaf photosynthetic apparatus and productivity. Regul. Mech. Biosyst. 10 (4), 406–414.

Mu, H., Jiang, D., Wollenweber, B., Dai, T., Jing, Q., Cao, W., 2010. Long-term Low Radiation Decreases Leaf Photosynthesis, Photochemical Efficiency and Grain Yield in Winter Wheat. Journal of Agronomy and Crop Science 196 (1), 38–47.

Nakhforoosh, A., Grausgruber, H., Kaul, H.-P., Bodner, G., 2014. Wheat root diversity and root functional characterization. Plant Soil 380 (1-2), 211–229.

Novick, K.A., Ficklin, D.L., Stoy, P.C., Williams, C.A., Bohrer, G., Oishi, A.C., Papuga, S.A., Blanken, P.D., Noormets, A., Sulman, B.N., Scott, R.L., Wang, L., Phillips, R.P., 2016. The increasing importance of atmospheric demand for ecosystem water and carbon fluxes. Nature Clim Change 6 (11), 1023–1027.

Olszewski, J., Pszczółkowska, A., Kulik, T., Fordoński, G., Płodzień, K., Okorski, A., Wasielewska, J., 2008. Rate of Photosynthesis and Transpiration of Winter Wheat Leaves and Ears Under Water Deficit Conditions. Polish Journal of Natural Science 23 (2), 326–335.

Passioura, J.B., 1980. The Transport of Water from Soil to Shoot in Wheat Seedlings. Journal of experimental botany 1980 (120), 333–345.

Pinheiro, C., Chaves, M.M., 2011. Photosynthesis and drought: can we make metabolic connections from available data? Journal of experimental botany 62 (3), 869–882.

Plaut, Z., 2005. Plant Water Stress: Exposure during Specific Growth Stages. In: S.W. Trimble (Editor), Encyclopedia of Water Science. Marcel Dekker, New York, pp. 843–845.

Qiao, X., Sai, L., Chen, X., Xue, L., Lei, J., 2019. Impact of fruit-tree shade intensity on the growth, yield, and quality of intercropped wheat. PloS one 14 (4), e0203238.

R Core Team, 2022. R: A Language and Environment for Statistical Computing [Computer software manual]. R Foundation for Statistical Computing, Vienna, Austria.

Reyer, F., 2022. Termine und Infos für die Datenerhebung an der APV in Heggelbach. E-Mail, Heggelbach. Accessed June 10, 2022.

Richter, D., 1995. Ergebnisse methodischer Untersuchungen zur Korrektur des systematischen Meßfehlers des Hellmann-Niederschlagmessers. Berichte des Deutschen Wetterdienstes. Deutscher Wetterdienst (DWD), Offenbach / Main.

Roohi, E., Tahmasebi Sarvestani, Z., A. M. Modarres-Sanavy, S.A.M., Siosemardeh, A., 2013. Comparative Study on the Effect of Soil Water Stress on Photosynthetic Function of Triticale, Bread Wheat, and Barley. J. Agr. Sci. Tech 2013 (15), 215–228.

RStudio Team, 2022. RStudio: Integrated Development Environment for R. R Studio, PBC, Boston, MA.

Schmidhalter, U., 1997. The gradient between pre-dawn rhizoplane and bulk soil matric potentials, and its relation to the pre-dawn root and leaf water potentials of four species. Plant Cell Environ 20 (7), 953–960.

Schopfer, P., Brennicke, A., 2010. Pflanzenphysiologie. Springer Berlin Heidelberg, Berlin, Heidelberg.

Seidlova, L., Verlinden, M., Gloser, J., Milbau, A., Nijs, I., 2009. Which plant traits promote growth in the low-light regimes of vegetation gaps? Plant Ecol 200 (2), 303–318.

Seki, K., 2007. SWRC fit – a nonlinear fitting program with a water retention curve for soils having unimodal and bimodal pore structure.

Sevruk, B., 1996. Adjustment of tipping-bucket precipitation gauge measurements. Atmospheric Research 42 (1-4), 237–246.

Smegal, J., Lukachko, A., Straube, J., Trainor, T. Quantitatively evaluating the effectiveness of different drip edges profiles, 14th Canadian conference on building science and technology, pp. 89–99.

Smial, 2021. Compass Card B+W. Accessed 2 Sept 2022. https://id.wikipedia.org/wiki/Penamaan_titik_utama_kompas#/media/Berkas:Compass Card B+W.svg. Accessed.

Steduto, P., Hsiao, T.C., Fereres, E., 2007. On the conservative behavior of biomass water productivity. Irrig Sci 25 (3), 189–207.

Strub, J., Richter, D., Schwanitz, D., 1999. Hydrologischer Atlas von Deutschland. 2 Hydro-Meteorologie. 2.5 Mittlere korrigierte jährliche Niederschlagshöhe. Deutscher Wetterdienst (DWD), Institute of Hydrology, Freiburg i. Br.

Sudmeyer, R.A., Speijers, J., 2007. Influence of windbreak orientation, shade and rainfall interception on wheat and lupin growth in the absence of below-ground competition. Agroforest Syst 71 (3), 201–214.

Sun, H.-Y., Liu, C.-M., Zhang, X.-Y., Shen, Y.-J., Zhang, Y.-Q., 2006. Effects of irrigation on water balance, yield and WUE of winter wheat in the North China Plain. Agricultural Water Management 85 (1-2), 211–218.

tagesschau, 2022. Anhaltende Dürre wirkt sich negativ auf Ernte aus. Norddeutscher Rundfunk. https://www.youtube.com/watch?v=mZzZuMmckZM. Accessed August 29, 2022.

Topp, G.C., Davis, J.L., Annan, A.P., 1980. Electromagnetic determination of soil water content: Measurements in coaxial transmission lines. Water Resources Research 1980 (16), 574–582. 10.1029/WR016i003p00574.

Trimble, S.W. (Ed.), 2005. Encyclopedia of Water Science. Marcel Dekker, New York.

Trommsdorff, M., Kang, J., Reise, C., Schindele, S., Bopp, G., Ehmann, A., Weselek, A., Högy, P., Obergfell, T., 2021. Combining food and energy production: Design of an agrivoltaic system applied in arable and vegetable farming in Germany. Renewable and Sustainable Energy Reviews 140, 1–13.

Turner, N.C., 1981. Techniques and experimental approaches for the measurement of plant water status. Plant and Soil 1981 (58), 339–366.

van Genuchten, M.T., 1980. A Closed-form Equation for Predicting the Hydraulic Conductivity of Unsaturated Soils. Soil Science Society of America Journal 44 (5), 892–898.

van Hamme, T., 1992. La pluie et le topoclimat. Hydrologie Continentale 1992 (7), 51–73.

Wallace, J.S., Clark, J.A., McGowan, M., 1983. Water relations of winter wheat: 3. Components of leaf water potential and the soil-plant water potential gradient. J. Agric. Sci. 100 (3), 581–589.

Wang, D., Zhang, Y., Sun, Y. (Eds.), 2018. A Criterion of Crop Selection Based on the Novel Concept of an Agrivoltaic Unit and M-matrix for Agrivoltaic Systems. IEEE, Piscataway, NJ.

Wang, Y., Shao, M., Han, X., Liu, Z., 2015. Spatial Variability of Soil Parameters of the van Genuchten Model at a Regional Scale. Clean – Soil, Air, Water 2015 (43), 271–278.

Waraich, E.A., Ahmad, R., 2010. Physiological Responses to Water Stress and Nitrogen Management in Wheat (Triticum aestivum L.): Evaluation of gas exchange, water relations and water use efficiency. Fourteenth International Water Technology Conference 2010 (14), 731–747.

Weil, R.R., Brady, N.C., 2017. The Nature and Properties of Soils. Pearson, Columbus.

Wery, J., 2005. Differential effects of soil water deficit on the basic plant functions and their significance to analyse crop responses to water deficit in indeterminate plants. Aust. J. Agric. Res. 56 (11), 1201.

Weselek, A., Bauerle, A., Hartung, J., Zikeli, S., Lewandowski, I., Högy, P., 2021a. Agrivoltaic system impacts on microclimate and yield of different crops within an organic crop rotation in a temperate climate. Agron. Sustain. Dev. 41 (5).

Weselek, A., Bauerle, A., Zikeli, S., Lewandowski, I., Högy, P., 2021b. Effects on Crop Development, Yields and Chemical Composition of Celeriac (Apium graveolens L. var. rapaceum) Cultivated Underneath an Agrivoltaic System. Agronomy 11 (4), 733.

Weselek, A., Ehmann, A., Zikeli, S., Lewandowski, I., Schindele, S., Högy, P., 2019. Agrophotovoltaic systems: applications, challenges, and opportunities. A review. Agron. Sustain. Dev. 39 (4).

wetter-bw.de, 2022. Agrarmeteorologie-BW/Wetterdaten/Stationskarte. https://www.wetter-bw.de/Agrarmeteorologie-BW/Wetterdaten/Stationskarte. Accessed October 17, 2022.

Yadav, D., Singh, C., Singh, H., 2018. Impact of Shading on Wheat Crop in Poplar Based Agroforestry Practice of Northern Plain of Uttar Pradesh, India. Int.J.Curr.Microbiol.App.Sci 7 (2), 2955–2962.

Yuan, W., Zheng, Y., Piao, S., Ciais, P., Lombardozzi, D., Wang, Y., Ryu, Y., Chen, G., Dong, W., Hu, Z., Jain, A.K., Jiang, C., Kato, E., Li, S., Lienert, S., Liu, S., Nabel, J.E., Qin, Z., Quine, T., Sitch, S., Smith, W.K., Wang, F., Wu, C., Xiao, Z., Yang, S., 2019. Increased atmospheric vapor pressure deficit reduces global vegetation growth. Science Advances 2019 (5), 1–12.

Zadoks, J.C., Chang, T.T., Konzak, C.F., 1974. A decimal code for the growth stages of cereals. Weed Research 14 (6), 415–421.

Zhang, X., Pei, D., Hu, C., 2003. Conserving groundwater for irrigation in the North China Plain. Irrig Sci 21 (4), 159–166.

Zotarello, L., Dukes, M.D., Romero, C.C., Migliaccio, K.W., Morgan, K.T. Step by Step Calculation of the Penman-Monteith Evapotranspiration (FAO-56 Method), 1–10. Accessed.

# A Appendix

## A.1 List of Symbols

| Name | Unit | Symbol |
|---|---|---|
| Actual evapotranspiration | [mm] | $ET_a$ |
| Air temperature | [°C] | $T_{air}$ |
| Areal precipitation | [mm] | $\overline{P}$ |
| Azimuth | [°] | $\Phi$ |
| Change of soil moisture storage in the root zone | [mm] | $\Delta S$ |
| Coefficient of determination | | $R^2$ |
| Coefficient of variation | | $C_v$ |
| Deep percolation | [mm] | DP |
| Density | [g/cm³] | d |
| Difference | | $\Delta$ |
| Evaporation | [mm] | E |
| Evapotranspiration | [mm] | ET |
| Field capacity | [vol.-%, mm] | FC |
| Gravitational potential | | $\psi_G$ |
| Interception | [mm $h^{-1}$] | IC |
| Interception depth | [mm] | $IC_d$ |
| Kendall's coefficient of correlation tau b | [-] | $\tau_b$ |
| Leaf area index | [-] | LAI |
| Logarithm of the absolute value of matric potential in soil water | [-log hPa] | pF |
| Lower module height | [m] | l |
| Matric potential | [hPa, MPa, cm] | $\psi_M$ |
| Module length | [m] | L |
| Number (of samples) | | N |
| Photosynthetically Active Radiation | [µmol $m^{-2}$ $s^{-1}$] | PAR |
| Precipitation | [mm] | P |
| Pressure head | [cm] | h |
| Pressure potential | | $\psi$ |
| Relative Humidity | [-] | RH |

| | | |
|---|---|---|
| Relative photosynthetically active radiation | [-] | %PAR |
| Row distance between pillars | [m] | B |
| Scaling parameter in the van Genuchten equation | [$cm^{-1}$] | $\alpha$ |
| Soil moisture derived from the van Genuchten model | [vol.-%] | $\theta_G$ |
| Soil moisture derived from gravimetric method | [vol.-%] | $\theta_{VWC}$ |
| Soil moisture derived from TDR method | [vol.-%] | $\theta_{TDR}$ |
| Soil-plant-atmosphere-continuum | | SPAC |
| Standard deviation | | SD |
| Temperature | [°C] | T |
| Throughfall | [mm] | TF |
| Tilting angle | [°] | $\beta_{PV}$ |
| Transpiration | [mm] | T |
| Residual water content | [vol.-%] | $\theta_r$ |
| Saturated soil water content | [vol.-%] | $\theta_s$ |
| Soil moisture | [vol.-%] | $\theta$ |
| Wind direction | [°] | wd |
| Wind speed | [m $s^{-1}$] | ws |

## A.2 List of Abbreviations

| Name | Abbreviation |
|---|---|
| Analysis of variances | ANOVA |
| Agrivoltaic system | AV |
| Above sea level | a. s. l. |
| Biologische Bundesanstalt für Land- und Forstwirtschaft, Bundessortenamt und Chemische Industrie | BBCH |
| Days after sowing | DAS |
| Deutsches Institut für Normung | DIN |
| Deutscher Wetterdienst | DWD |
| Landwirtschaftliches Technologiezentrum Augustenberg | LTZ |
| Silty loam | Lu |
| Soil-plant-atmosphere-continuum | SPAC |
| Multivariate analysis of variances | MANOVA |
| Midday | MD |
| North | N |
| Northeast | NE |
| North-Northeast | NNE |
| Northwest | NW |
| Predawn | PD |
| Photovoltaic | PV |
| Raindrop size distribution | DSD |
| Root:shoot ratio | RSR |
| Reference system | REF |
| South | S |
| Southeast | SE |
| South by West | SbW |
| Southwest | SW |
| Volumetric water content | VWC |

## A.3 Eight precipitation events

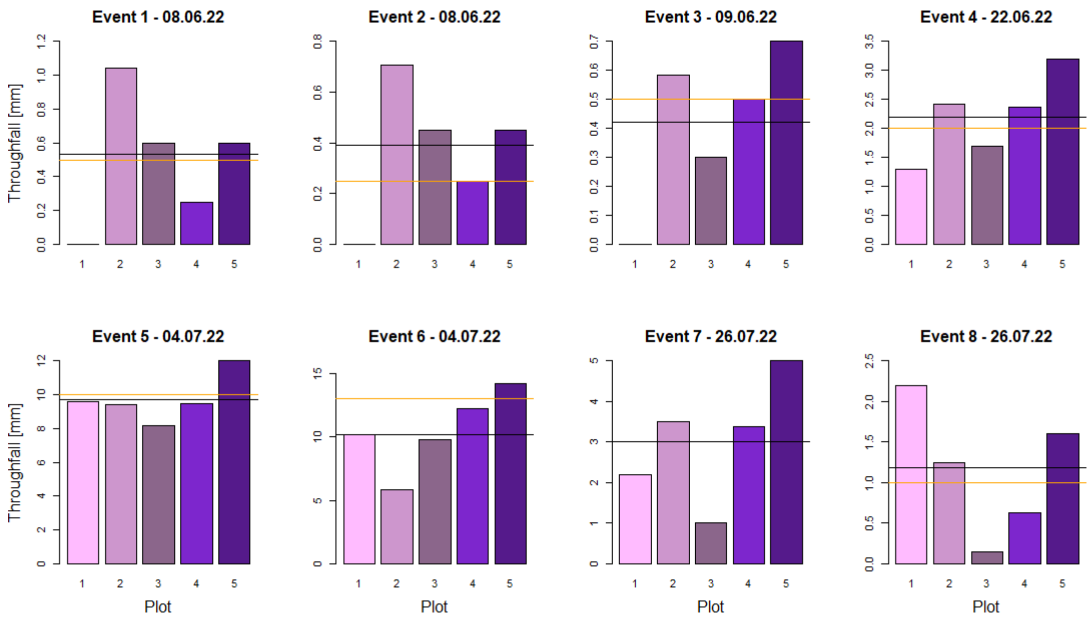


Figure 23: Mean throughfall TF per event and areas that are distinguishably affected by precipitation due to the agrivoltaic system. The black line refers to the mean in AV and the orange line refers to $P_{REF}$.

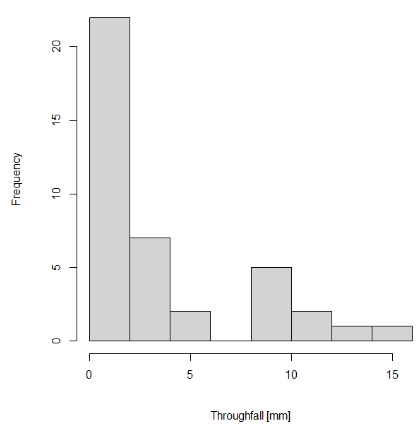


Figure 24: Histogram of throughfall TF measurements in AV showing non-normality

## A.4 Fifteen precipitation events

Table 14: Coefficient of variation $C_v$ in throughfall for seven more precipitation events of lower data quality

| Event | Time | $P_{REF}$ [mm] | $wd_{REF}$* | $C_v$ [-] |
|---|---|---|---|---|
| 9 | 23.05.2022 17:00 | 8.0 | SbW | 0.44 |
| 10 | 07.06.2022 12:30 | 1.0 | SbW | 0.88 |
| 11 | 07.06.2022 20:00 | 3.0 | SEbE | 0.96 |
| 12 | 09.06.2022 03:00 | 1.3 | WbN | 0.80 |
| 13 | 13.06.2022 03:00 | 2.5 | N | 0.63 |
| 14 | 21.06.2022 21:45 | 1.0 | WbS | 0.65 |
| 15 | 04.07.2022 01:00 | 3.0 | NNE | 0.48 |

*For events 9 - 11 $wd_{REF}$ is retrieved from the weather station of Heggelbach

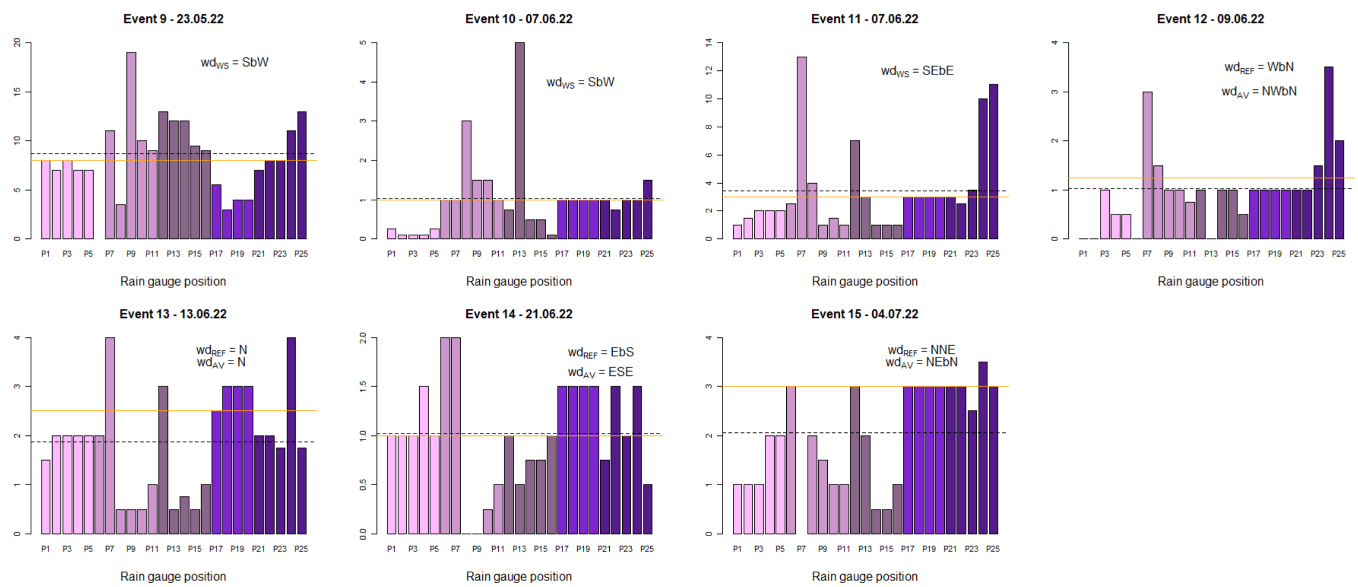


Figure 25: Throughfall TF recorded at 25 rain gauge positions for events 9 -15 of lower data quality with indication of the prevailing wind directions wd in REF and AV. The black dashed line indicates the mean TF in AV, the orange line indicates the mean TF in REF.

## A.5 Volumetric water content

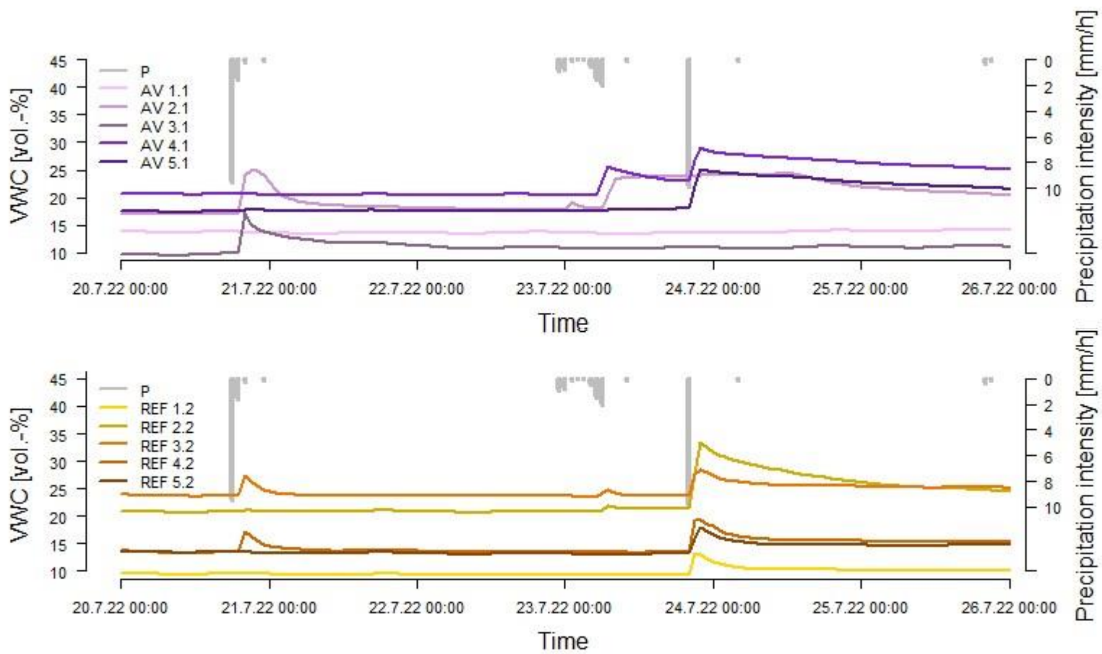


Figure 26: Absolute volumetric water content VWC in 20 cm depth in AV and REF during the last week of July with hourly precipitation data from Billafingen; top: AV, bottom: REF

## A.6 Relative rate of change in leaf water potential

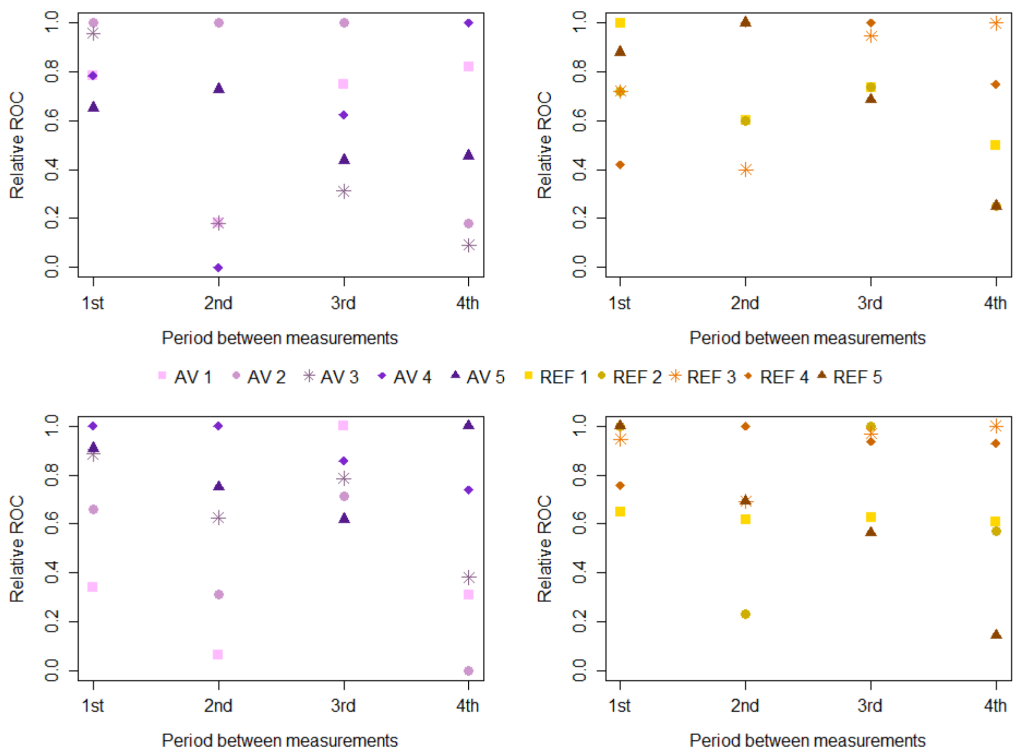


Figure 27: Relative rate of change ROC in mean leaf water potential LWP per area relative to maximum change in system and time; left: AV, right: REF, top: predawn PD, bottom: midday MD

# Ehrenwörtliche Erklärung

Hiermit erkläre ich, dass die Arbeit selbständig und nur unter Verwendung der angegebenen Hilfsmittel angefertigt wurde.

Freiburg i. Br., 26. Oktober 2022